SUPPORTING INFORMATION

Modulation of protein-protein interactions during amyloid assembly using tethered small molecules

Emma E. Cawood, Nicolas Guthertz, Jessica S. Ebo, Theodoros K. Karamanos, Sheena E. Radford*, Andrew J. Wilson*

Supplementary Figures

A   FTMap data from lowest energy structure

B   FTMap data from all structures

C

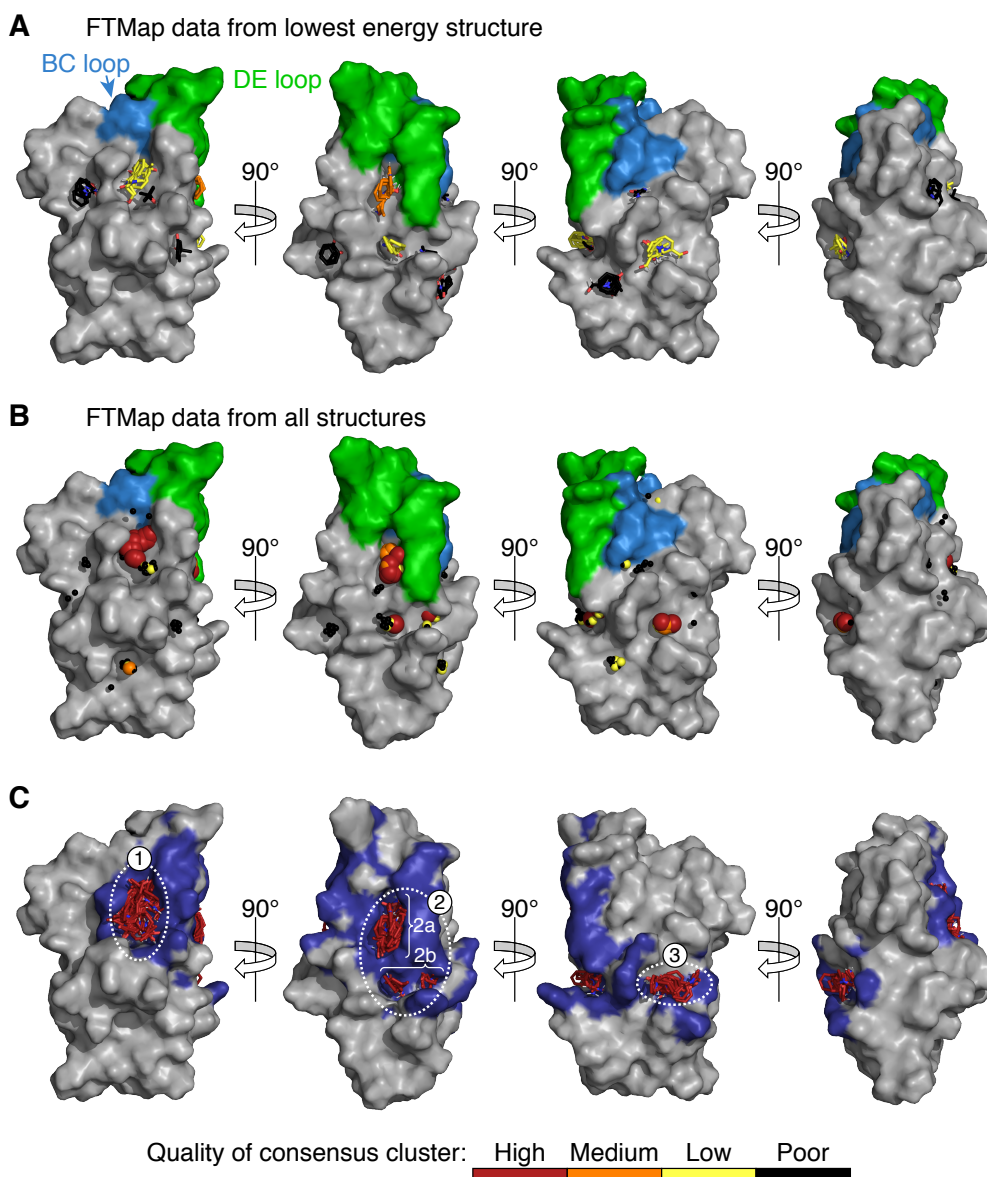Quality of consensus cluster: High   Medium   Low   Poor

Figure S1. Identification of ligandable pockets of ΔN6 using computational solvent mapping. Consensus clusters of solvent molecules from the FTMap server[1] are shown either as sticks (**A**, **C**) or single spheres (at the cluster's center of mass) (**B**) and are colored and/or scaled in size based on the cluster quality. The criteria for quality classification can be found in Table S2. Data from the lowest energy solution structure of ΔN6 (out of an NMR ensemble with 30 structures; PDB 2XKU[2]) are shown in **A**, while the data from all structures in the NMR ensemble are in **B** (overlaid on the lowest energy structure). Across the NMR ensemble, the highest quality consensus clusters are found adjacent to the BC (blue surfaces in **A**, **B**) and DE (green surfaces) loops. If only the high-quality clusters (red) are considered, then three main pockets (1-3) can be identified (**C**). Site 2 can be split into two subsites (2a, 2b) as indicated. All atoms in ΔN6 which are within 2 Å of a high-quality consensus cluster (for at least one structure in the NMR ensemble) are shown in dark blue.
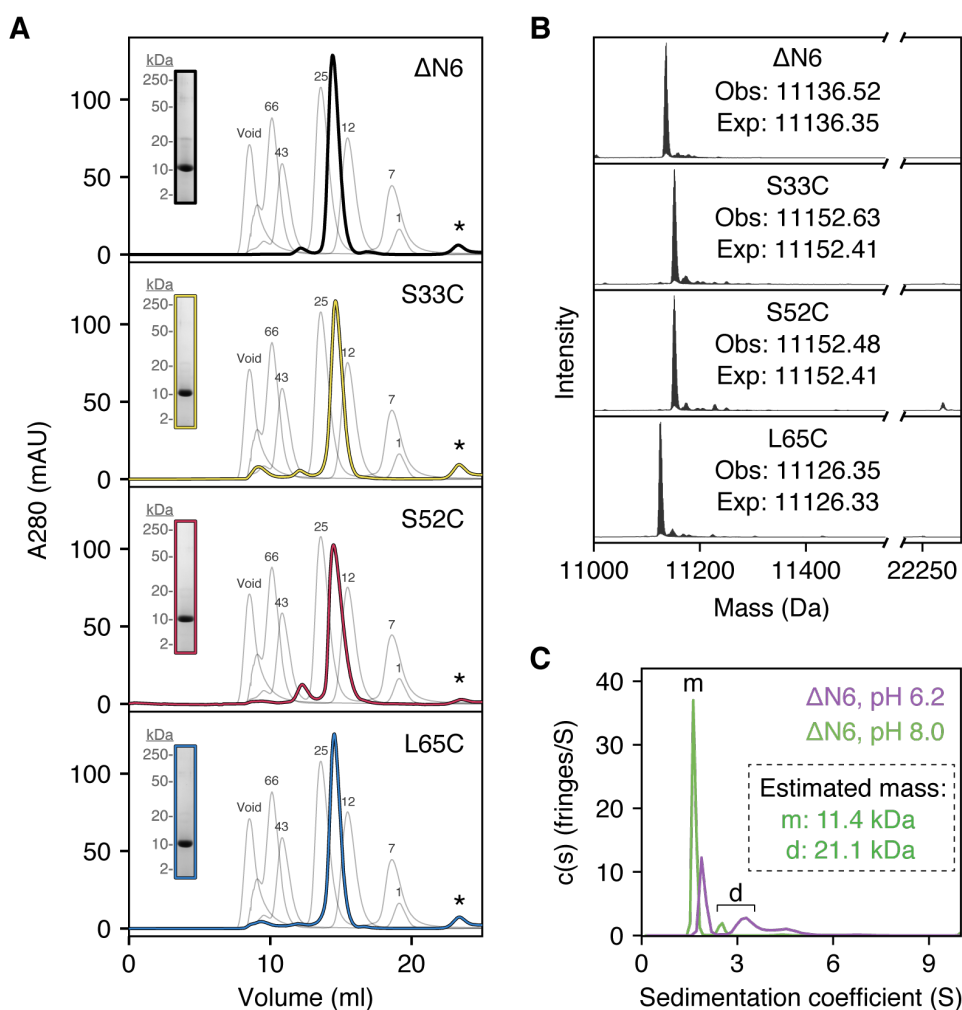
Figure S2. Characterization of the identity (**A**, **B**), purity (**A**, **B**), and oligomeric state (**A**, **C**) of the protein samples used in this study. **A:** Analytical size exclusion chromatography traces from purified ΔN6 cysteine variants, compared to ΔN6 itself. Samples (150 μM, 300 μL) were incubated with a 10-fold molar excess of dithiothreitol (DTT) for 30 min prior to loading onto a Superdex 75 10/300 GL size exclusion chromatography column (pre-equilibrated with 100 mM Tris-HCl, pH 8.0). Comparison of the traces to standards (gray traces) of known molecular weight (listed above each peak in kDa) indicated that all four proteins were predominantly monomeric. SDS-PAGE (inset) showed that all proteins were > 95% pure. The peaks highlighted by asterisks did not contain material which could be detected by Coomassie staining and were assumed to contain oxidized DTT. **B:** Deconvoluted electrospray ionization mass spectra provide further information concerning the identity and purity of the target proteins. Values for observed (Obs) and expected (Exp) average masses are quoted in daltons. **C:** Continuous sedimentation coefficient distributions ($c(s)$) obtained for ΔN6 (150 μM) show that this protein is 90% monomeric at pH 8.0 (with a best-fit frictional ratio of 1.23), and estimated molecular masses from SEDFIT[3] confirmed that the two peaks observed in the $c(s)$ distribution are from monomeric (m) and dimeric (d) ΔN6. At pH 6.2, ΔN6 is more aggregation-prone, which is reflected in a reduction in the area of the monomeric peak. The best-fit frictional ratio for the pH 6.2 data was 0.98, implying that significant exchange occurred during sedimentation[4]. Consequently, the molecular mass estimates from the pH 6.2 dataset are unlikely to be accurate and peak areas can be used only to estimate (rather than accurately quantify) oligomer populations.
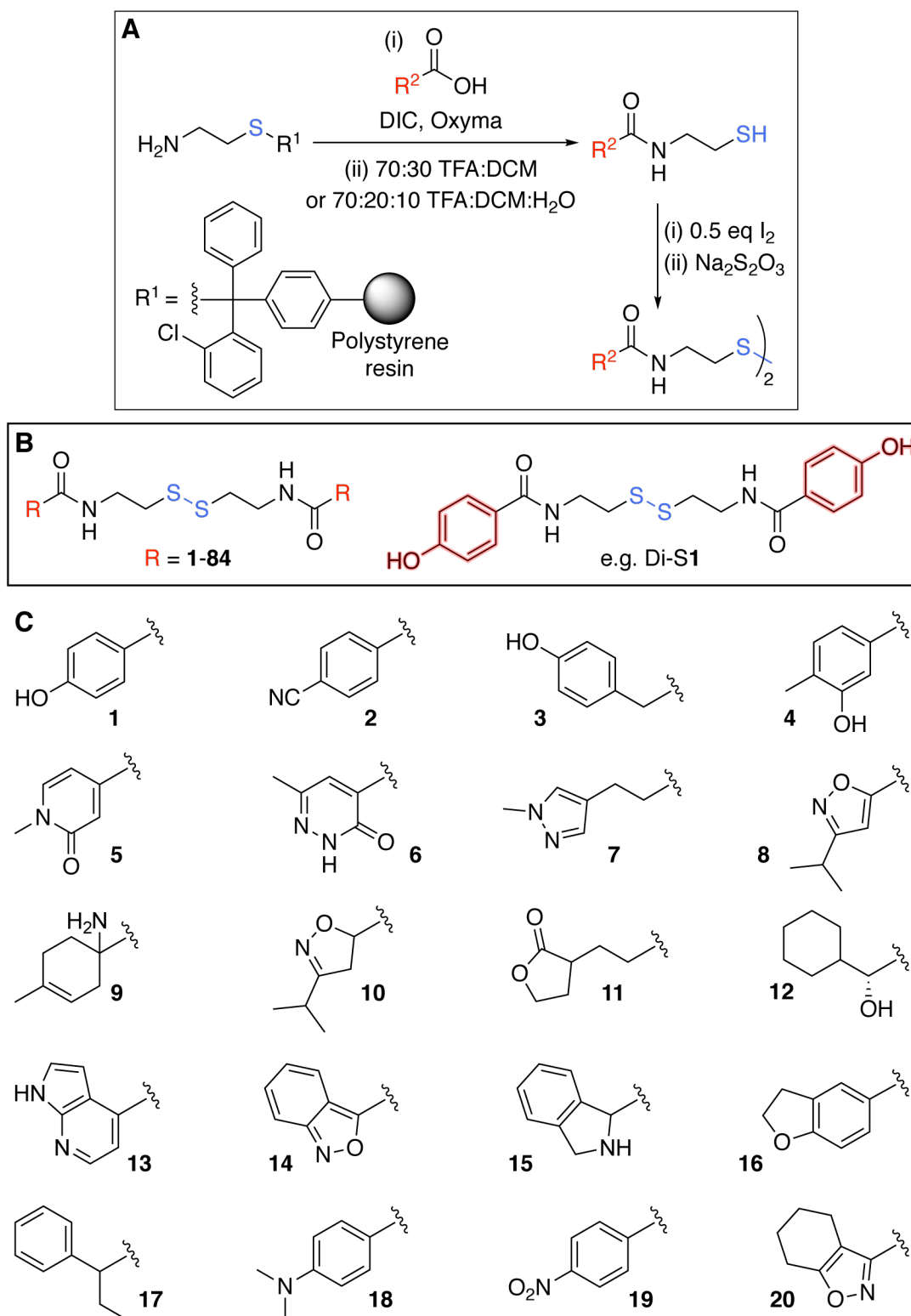
Figure S3. A: Synthetic route by which symmetrical disulfides were prepared using solid phase resin. **B:** General structure (left) and an example (right) of the symmetrical disulfides used for disulfide tethering. All symmetrical disulfides (given the prefix Di-S) are numbered based on the identity of the R group. **C:** Structures of the 76 R groups (assigned numbers between 1 and 84) found in the disulfide library. All R groups contained 7-16 non-hydrogen atoms. *Figure continued over the page.*
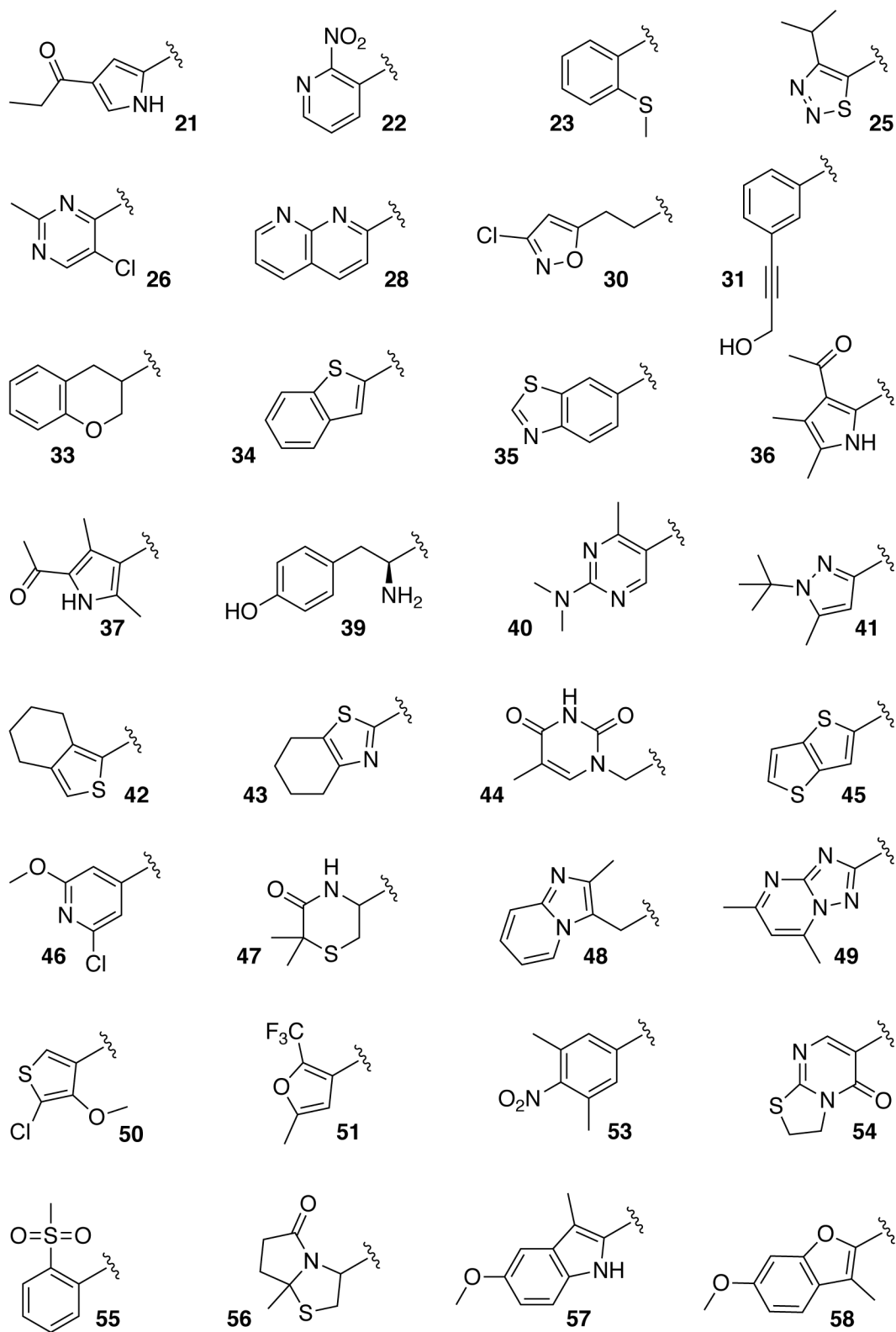
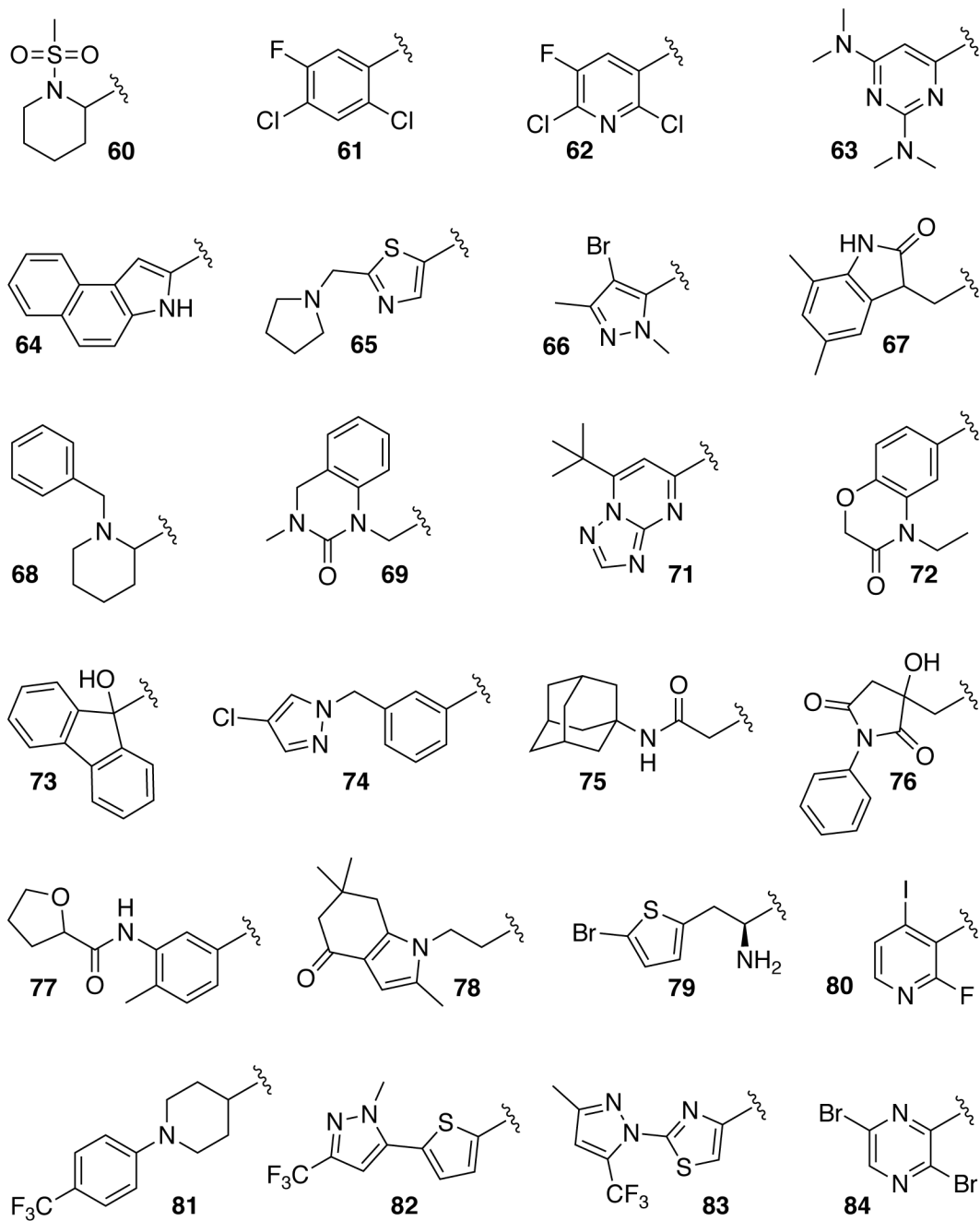**Figure S3. C:** Continued from previous page. *Figure continues over the page.*

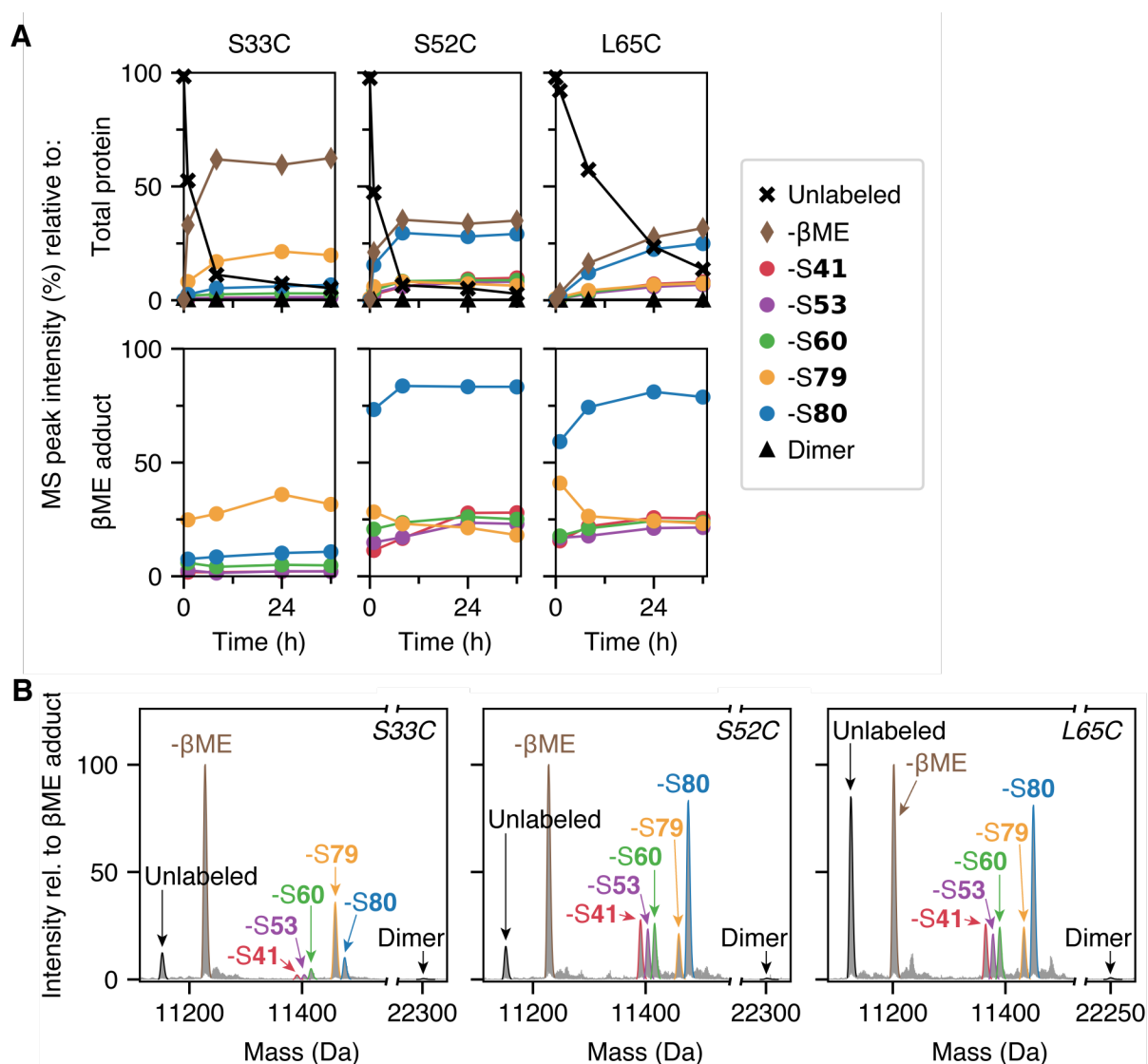**Figure S3. C:** Continued from previous page.

Figure S4. A: Changes in the intensity of various protein species over time during disulfide tethering for a representative fragment cocktail at pH 6.2. In the top panels, peak intensities were normalized so their sum at each time point was 100. This shows that while the S33C and S52C screening mixtures have equilibrated by 8 h, the L65C mixture is still undergoing changes in the intensity of protein-fragment adducts. However, if the amount of unlabeled monomer (black crosses) and dimer (black triangles) is not considered, and the protein-fragment adduct intensities are instead normalized relative to the βME adduct (bottom panels in **A**), then it is clear that the relative populations are no longer changing for any of the cysteine variants after 8 h, and in the case of L65C, it is only the overall redox state of the system that is still changing. **B:** Deconvoluted mass spectra acquired for each sample from part **A** at 24 h.
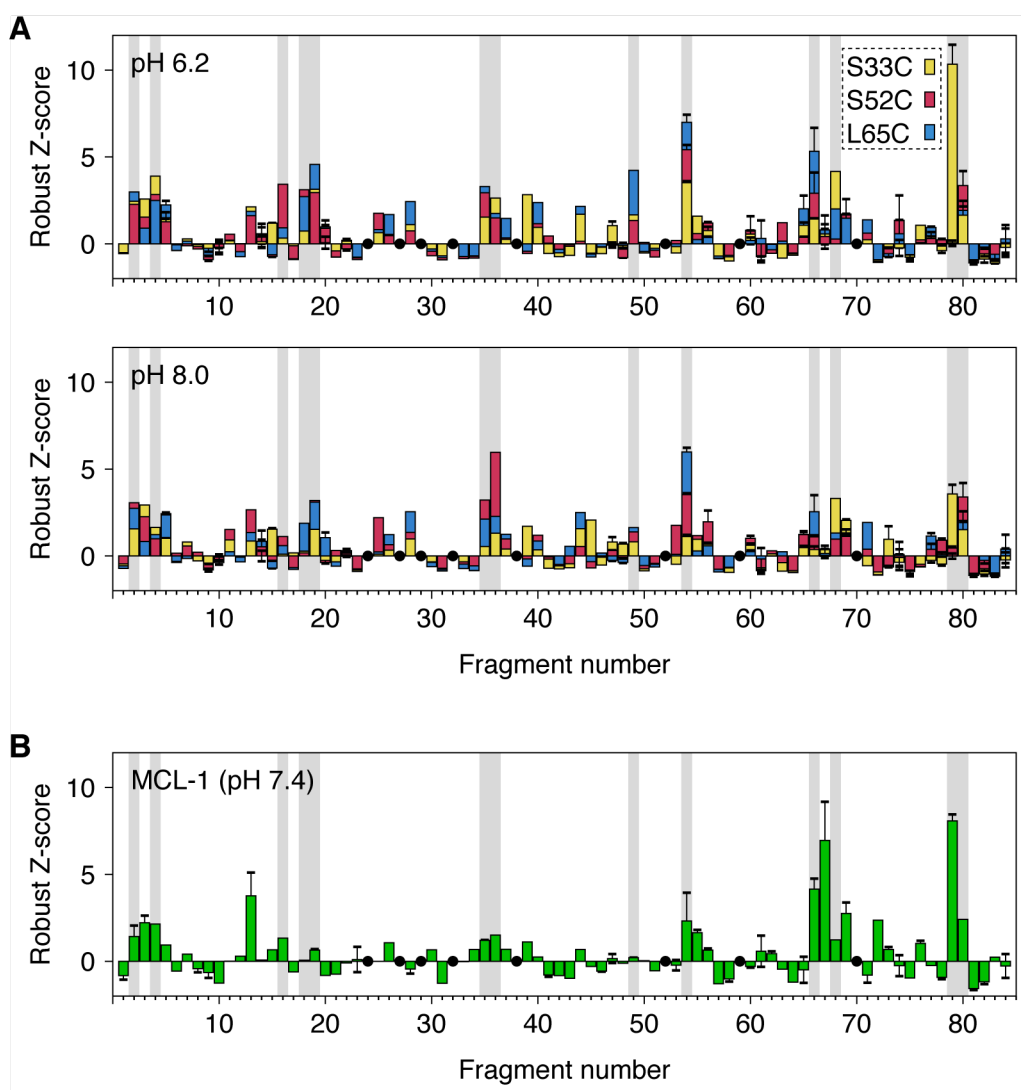
Figure S5. All screening data for the 76-member disulfide fragments against all three ΔN6 cysteine variants (**A**) compared with a control protein, MCL-1 (**B**). The data for ΔN6 obtained at pH 6.2 (conditions under which ΔN6 is aggregation-competent[2]) and pH 8.0 (where ΔN6 forms only monomer and dimers – see Figure S2C) differ significantly from the MCL-1 data acquired at pH 7.4, indicating that specific protein-fragment interactions were being detected. Fragments which performed particularly well against at least one ΔN6 cysteine variant (RZ score ≥ 3 at either pH 6.2 or 8.0) are highlighted in gray in both **A** and **B**, for ease of comparison. For fragments which were screened in more than one cocktail, the mean RZ score ± one standard deviation is shown. All screening was performed in 25 mM sodium phosphate (pH 6.2-8.0), 2% v/v DMSO. Black circles are shown for fragments which were synthesized but not included in the screening library due to poor purity. The ΔN6 and MCL-1 screening data are directly compared in Figure S6.
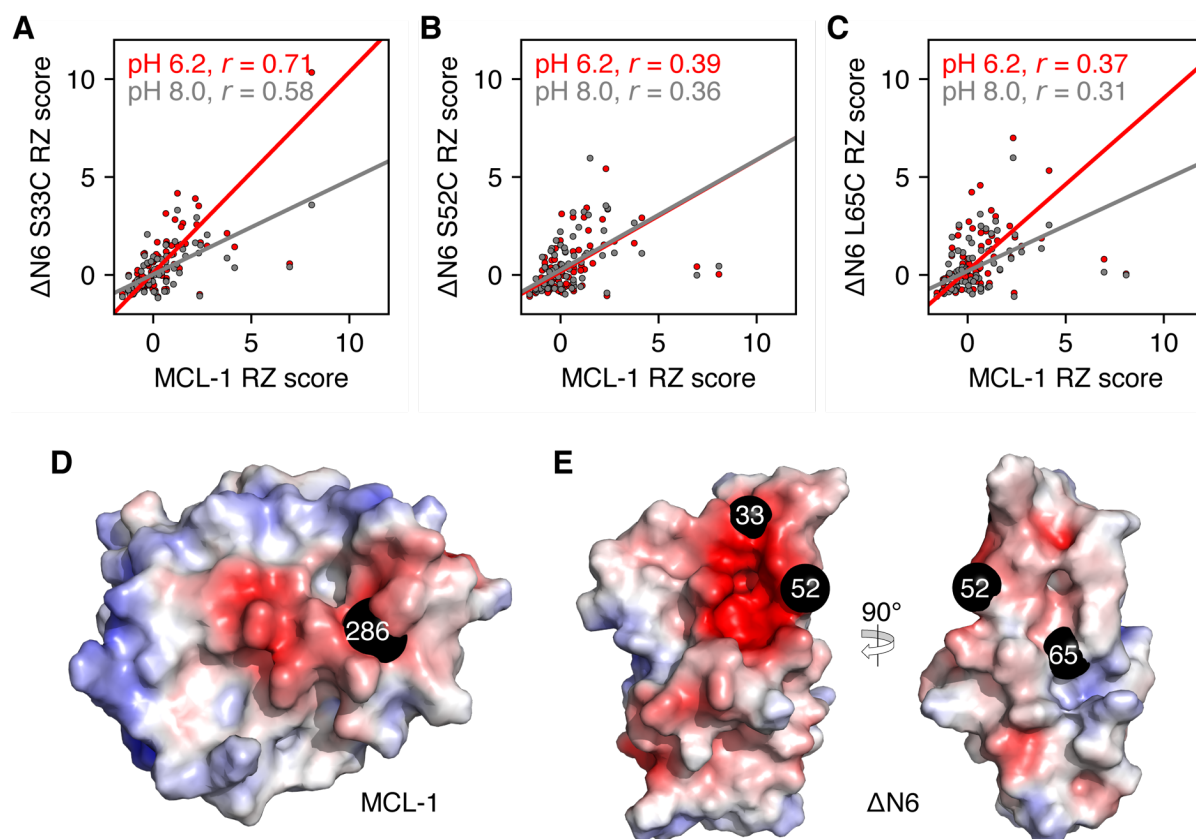
Figure S6. Comparison of the disulfide tethering screening data for ΔN6 cysteine variants (S33C, S52C, and L65C) with that of a control protein, MCL-1 (**A**-**C**). Screening was performed in 25 mM sodium phosphate, 2% v/v DMSO – the buffer was prepared to have a pH of 7.4 for MCL-1 and a pH of 6.2 (red) or 8.0 (gray) for the ΔN6 cysteine variants. The orthogonal linear regression lines for each ΔN6 and MCL-1 combination are shown in either red or gray, depending on the pH at which the ΔN6 screening was performed. The correlation between the screening data obtained for MCL-1 with the S52C and L65C ΔN6 variants is poor, with Pearson correlation coefficients (*r*) between 0.3-0.4 under all conditions. The poor correlation indicates that the RZ score of a given fragment depends on the identity of the protein, and therefore that these values are affected by non-covalent protein-fragment interactions. By contrast, there is a moderate correlation between the screening data obtained for the S33C ΔN6 variant and MCL-1, particularly for the S33C data obtained at pH 6.2, where the linear regression line has a slope of 1.0, with *r* = 0.71; this may reflect similarities between the regions of MCL-1 and ΔN6 surrounding these tethering residues (i.e., the native cysteine residue at position 286 for MCL-1 and the introduced cysteine residue at position 33 for ΔN6). Indeed, electrostatic surface potentials show that both tethering residues are located in acidic regions of the respective proteins (**D**, **E**), and as the highest RZ-scoring fragment for both S33C ΔN6 and MCL-1 (Di-S**79**) has a free amine that will be positively charged under the screening conditions, it is likely that electrostatic interactions were a key driving force behind the observed distribution of protein-fragment adducts for S33C ΔN6 and MCL-1. While residue 52 of ΔN6 is also adjacent to an acidic pocket, it is also close to the hydrophobic pocket where residue 65 is located, and so fragments tethered to residue 52 are likely to be able to access both pockets. The surfaces shown in **D**-**E** were colored by the electrostatic surface potential of each atom (± 5 kT/e; red: negative, blue: positive, white: neutral) in MCL-1 (**D**; PDB 5W8F[5]) and ΔN6 (**E**; PDB 2XKU[2]) using APBS[6]. Black spheres are shown at the gamma residue of the sidechain in the wildtype structures.
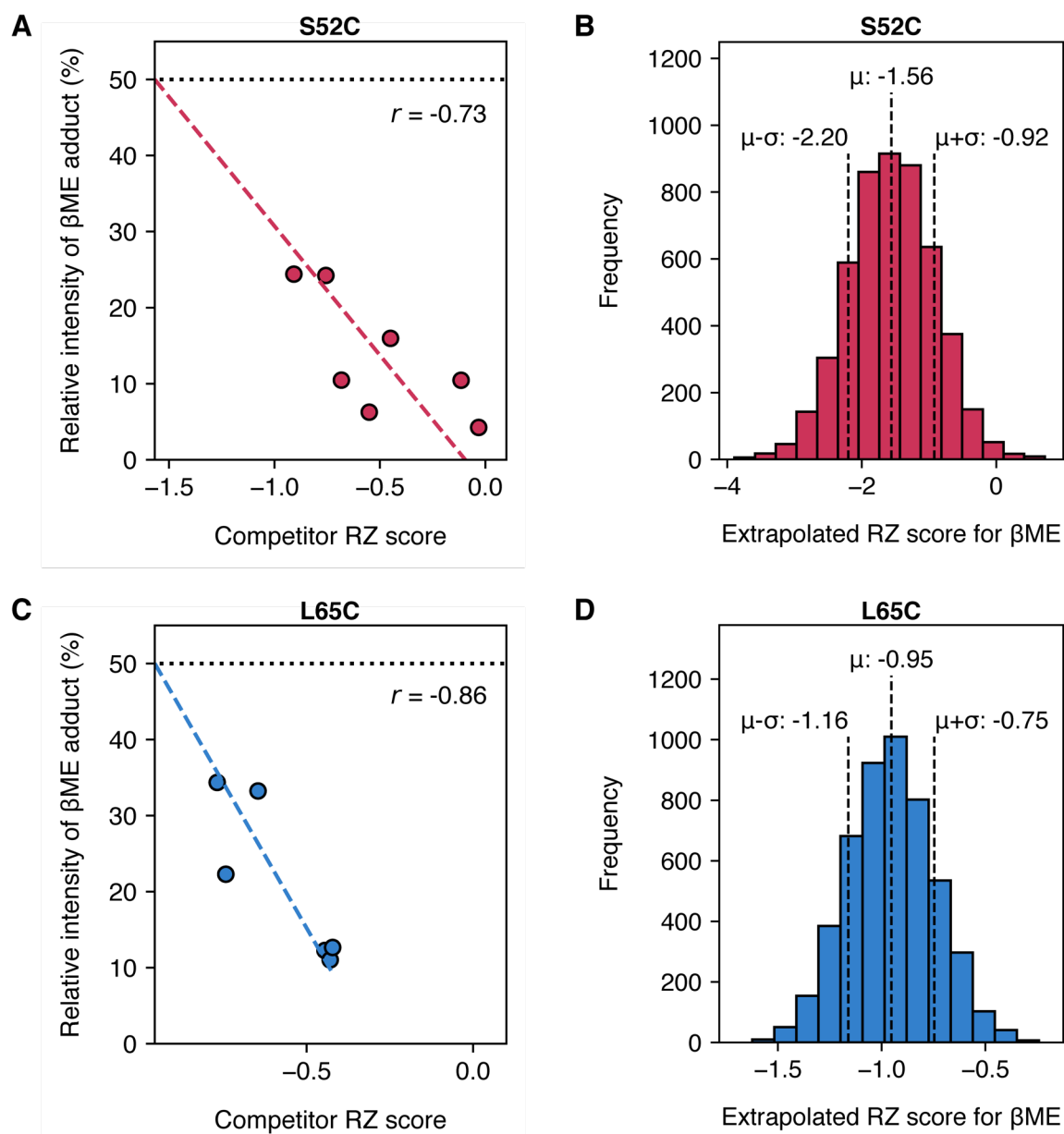
Figure S7. Calculation of RZ scores for βME in the presence of S52C (**A**, **B**) or L65C (**C**, **D**) at pH 6.2. As βME was used as a reducing agent in the disulfide tethering screen, the RZ score of this compound could not be calculated in the same way as for the other fragments discussed in this paper. Instead, the ability of the disulfide analogue of βME to outcompete fragments with known RZ scores was assessed. S52C and L65C ΔN6 variants (5 μM) were combined with a 1:1 mol/mol mixture of oxidized βME (2,2'-disulfanediylbis(ethan-1-ol)) and a low RZ scoring disulfide fragment (the "competitor") (25 μM each) in 25 mM sodium phosphate, pH 6.2, 2% v/v DMSO. Samples were incubated for 24 h at ambient temperature (~18 °C), and the relative intensity of the βME adduct peak was determined by mass spectrometry ($I_{βME}/[I_{βME}+I_{competitor}]*100$). RZ scores for βME were estimated by orthogonal linear regression analysis (dotted red/blue lines) between competitor RZ score and the relative intensity of the βME adduct peak (**A**, **C**), to identify the competitor RZ score at which the intensity of the protein-βME adduct is equal to the protein-competitor adduct (i.e., 50% intensity; dotted black lines). The error (standard deviation, σ) of the extrapolated value (μ) was calculated using a Monte Carlo method with 5000 steps (**B**, **D**).
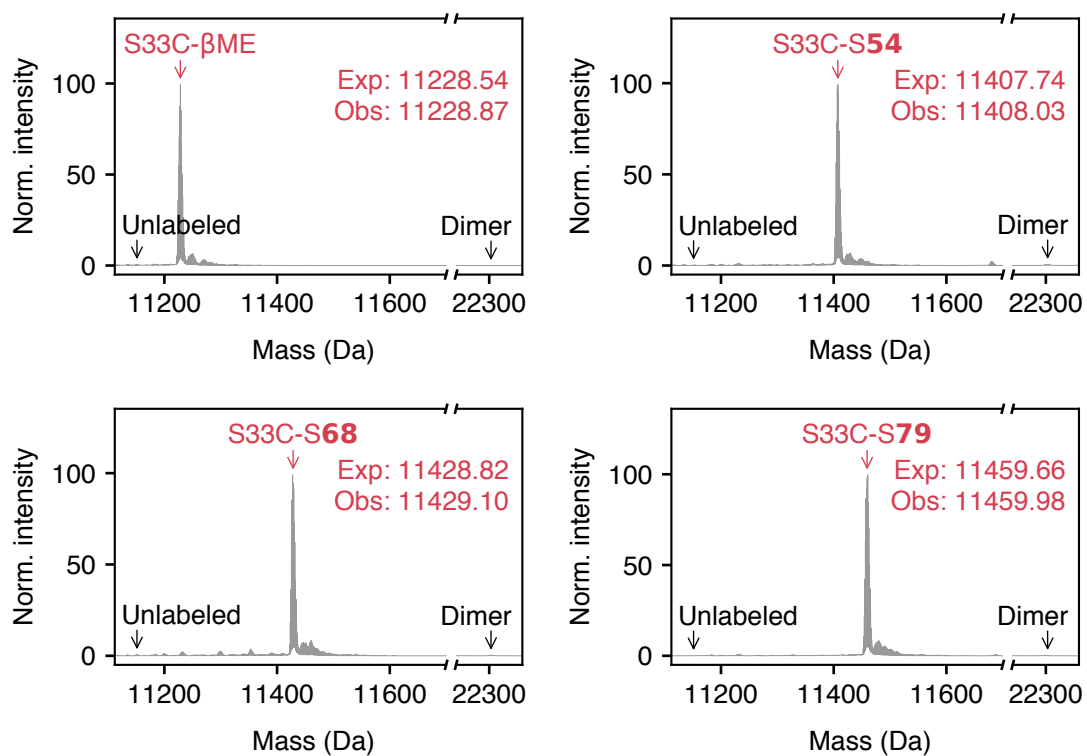
Figure S8. Deconvoluted electrospray ionization mass spectra of individual S33C-fragment adducts which are discussed in the main text and which are associated with Figure S11. The expected (Exp) and observed (Obs) average molecular masses of the protein-fragment adducts are listed in daltons. The masses of the unlabeled monomeric protein and dimeric protein are indicated on the mass spectra, to show that these species were not present after fragment labeling.

Figure S9. Deconvoluted electrospray ionization mass spectra of individual S52C-fragment adducts which are discussed in the main text and which are associated with Figure S12. The expected (Exp) and observed (Obs) average molecular masses of the protein-fragment adducts are listed in daltons. The masses of the unlabeled monomeric protein and dimeric protein are indicated on the mass spectra, to show that these species were not present after fragment labeling.
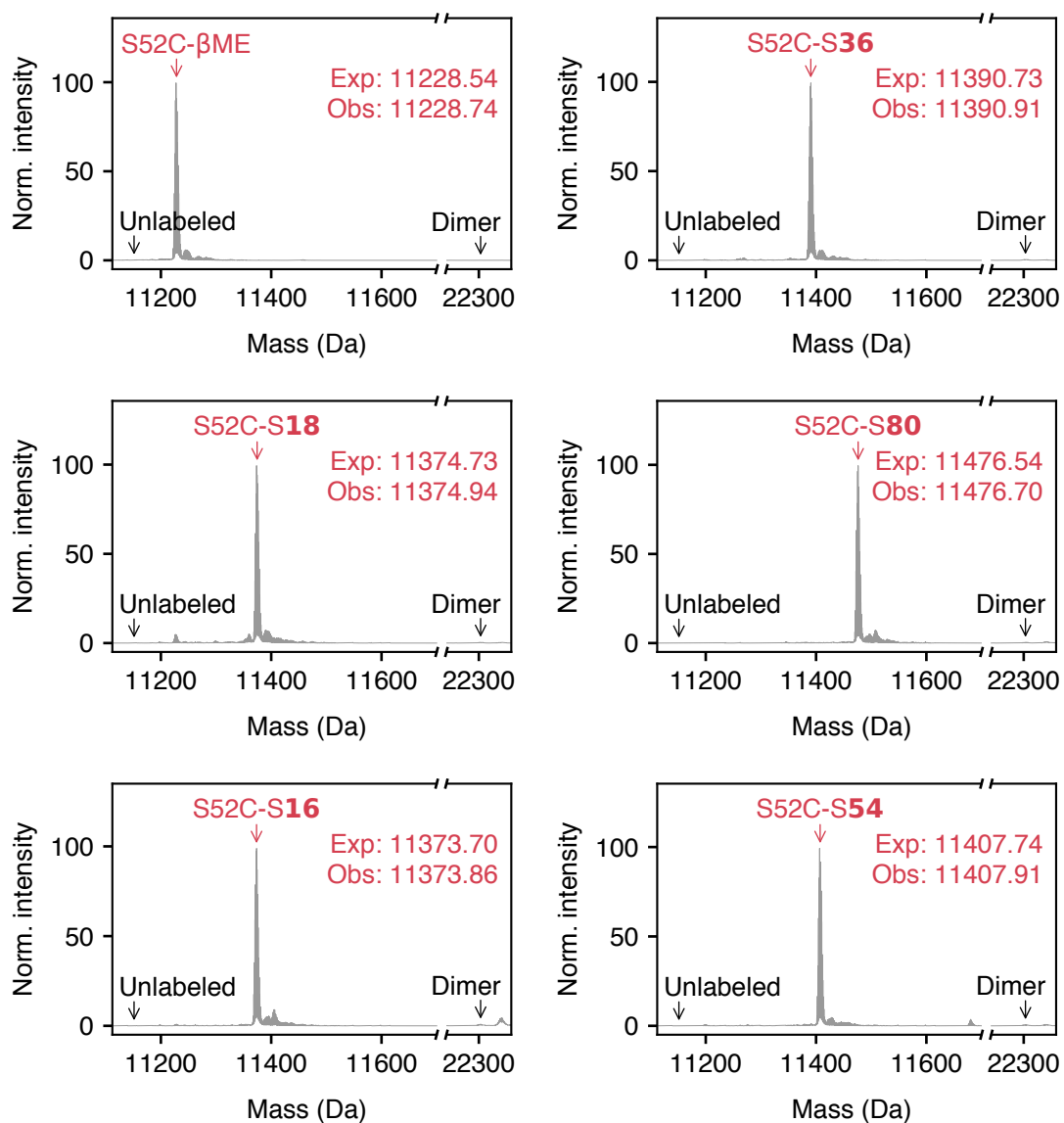
Figure S10. Deconvoluted electrospray ionization mass spectra of individual L65C-fragment adducts which are discussed in the main text and which are associated with Figure S13. The expected (Exp) and observed (Obs) average molecular masses of the protein-fragment adducts are listed in daltons. The masses of the unlabeled monomeric protein and dimeric protein are indicated on the mass spectra, to show that these species were not present after fragment labeling.
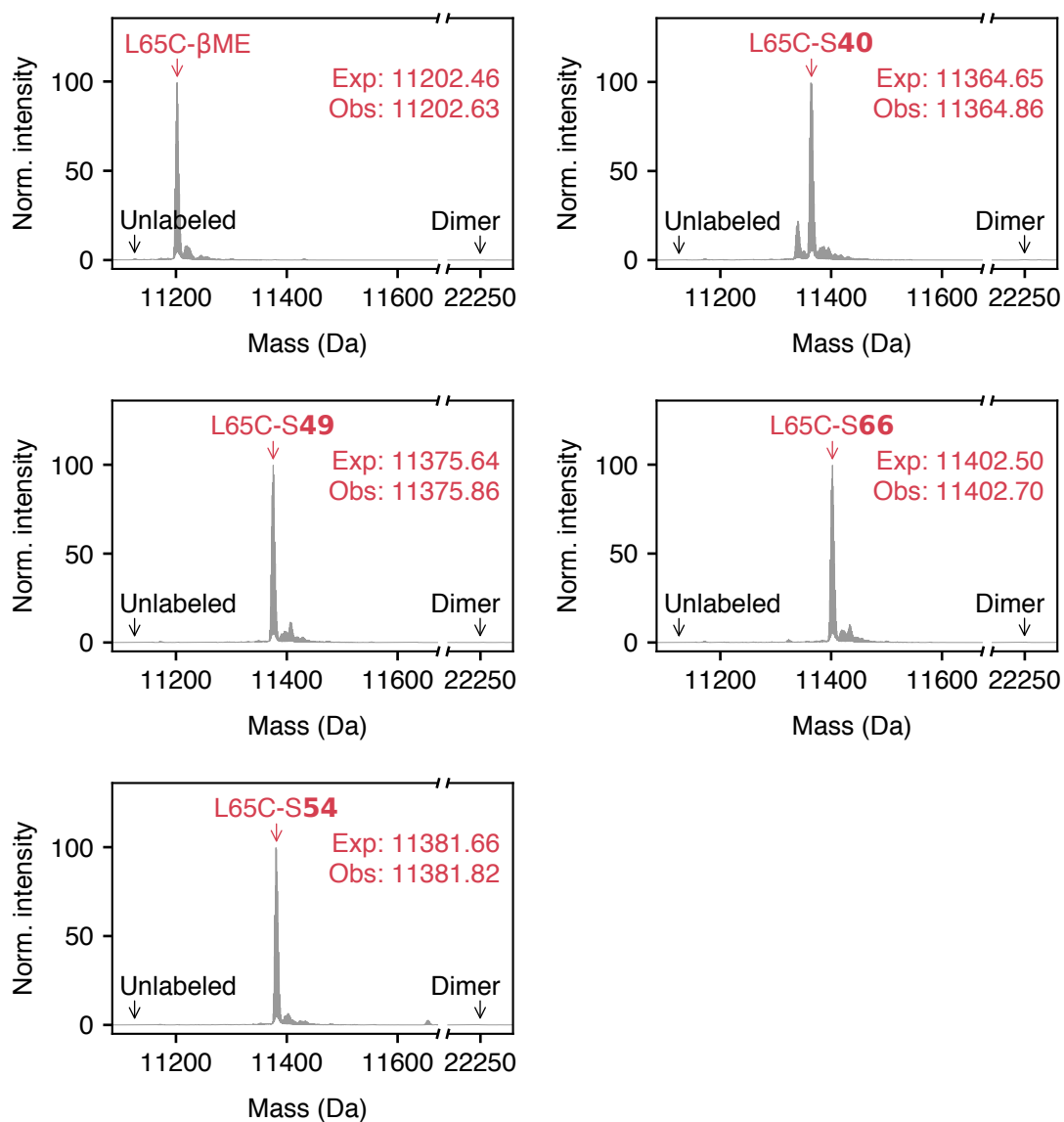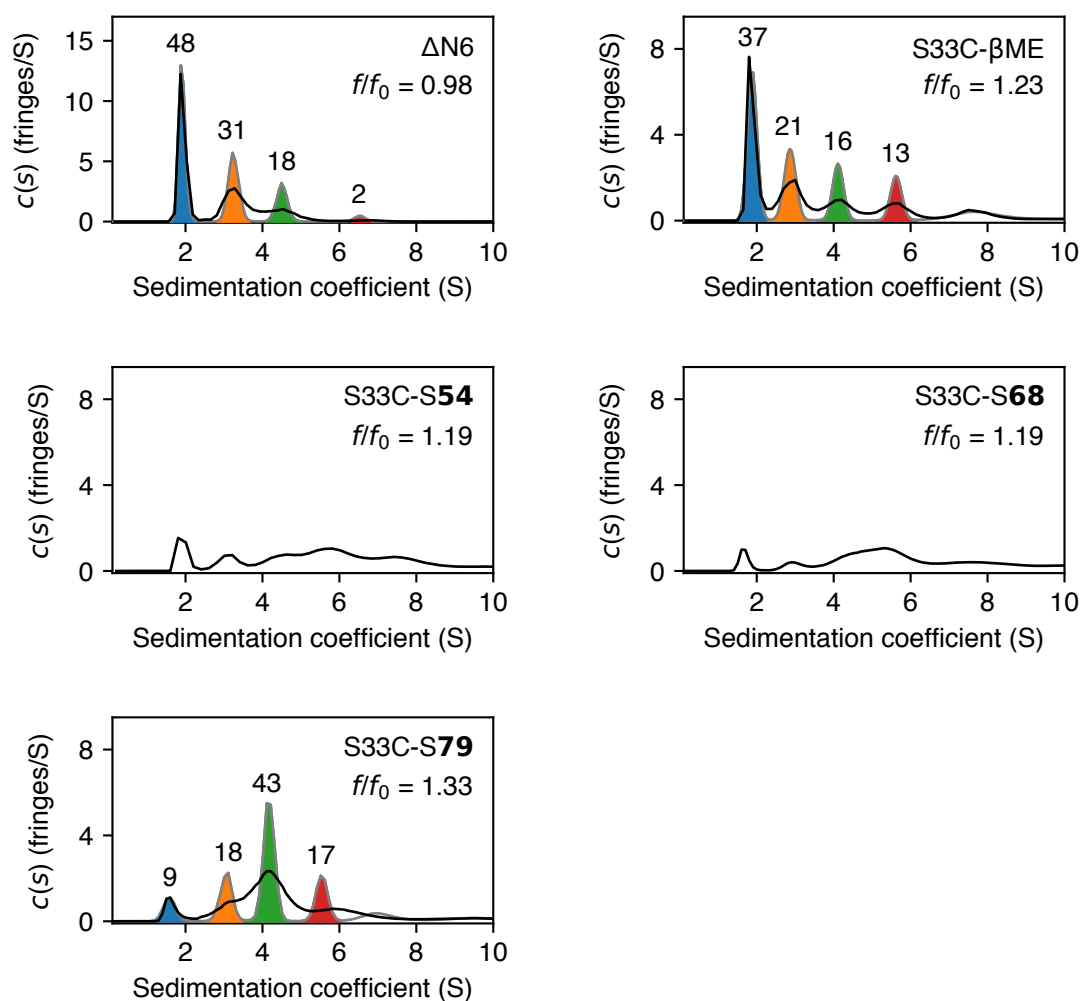
Figure S11. SV-AUC $c(s)$ distributions (black lines) for representative S33C-fragment adducts, compared with ΔN6 alone. Only the S33C-βME and S33C-S**79** adducts produced $c(s)$ distributions where the position and number of peaks allowed confident assignment to monomer (blue), dimer (orange), tetramer (green), and hexamer (red) oligomerization boundaries. To gain more accurate estimates of oligomer populations from these data, additional processing was performed with Bayesian prior expectations[7] to generate distributions (gray) with baseline-resolved peaks for the monomeric, dimeric, tetrameric, and hexameric species (with improved root-mean-square deviations compared to the original $c(s)$ distributions). Numbers above these peaks describe the relative (%) area of the colored region, and best-fit frictional ratios (f/f_0) are noted for each dataset. All experiments were performed with 150 μM protein in 25 mM sodium phosphate, pH 6.2, at 25 °C. In addition to the samples shown here, a further three S33C-fragment adducts were analyzed by SV-AUC (data not shown) but like S33C-S**54** and S33C-S**68**, produced broad and polydisperse $c(s)$ distributions.
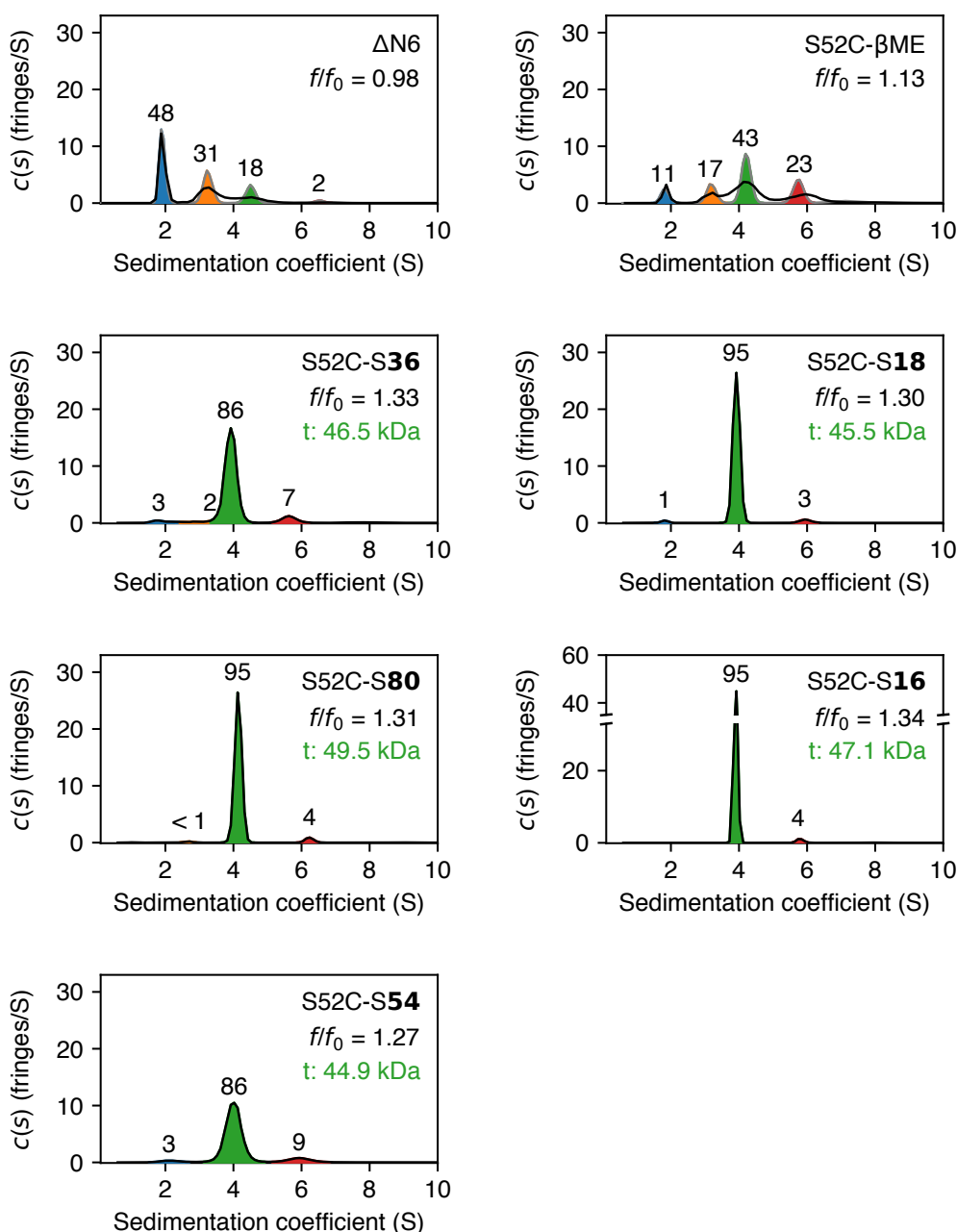
Figure S12. SV-AUC $c(s)$ distributions for various S52C-fragment adducts, compared with ΔN6. The first four peaks in each sample were assigned to monomer (blue), dimer (orange), tetramer (green), and hexamer (red). The molecular masses estimated by SEDFIT[3] for the green peaks (t) were consistent with the mass of a tetramer – based on molecular mass of the monomeric S52C-fragment adducts (Figure S9), actual molecular masses of the tetramer range between 44.9-45.9 kDa. To gain more accurate estimates of oligomer populations from $c(s)$ distributions with peak overlap (i.e., for S52C-βME, as well as for ΔN6), additional processing was performed with Bayesian prior expectations[7] to generate distributions (gray) with baseline-resolved peaks (and with improved root-mean-square deviations compared to the original $c(s)$ distributions). The numbers above each peak describe the relative (%) area of the colored region, and best-fit frictional ratios (f/f_0) are noted for each dataset. All experiments were performed with 150 μM protein in 25 mM sodium phosphate, pH 6.2, at 25 °C.
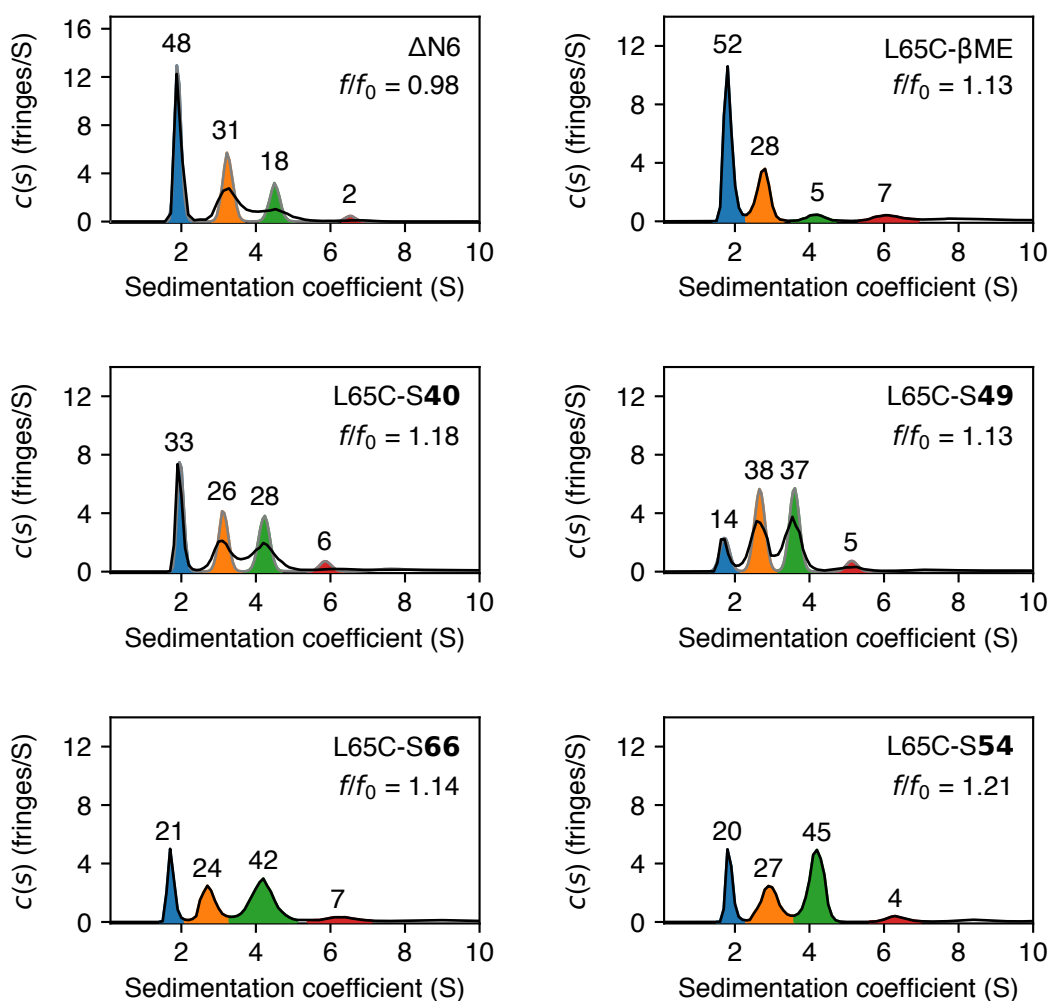
Figure S13. SV-AUC $c(s)$ distributions for various L65C-fragment adducts, compared with ΔN6. The first four peaks in each sample were assigned to monomer (blue), dimer (orange), tetramer (green), and hexamer (red). To gain more accurate estimates of oligomer populations from $c(s)$ distributions with peak overlap (i.e., for L65C-S**40** and L65C-S**49**, as well as for ΔN6), additional processing was performed with Bayesian prior expectations[7] to generate distributions (gray) with baseline-resolved peaks (and with improved or equally good root-mean-square deviations compared to the original $c(s)$ distributions). Numbers above these peaks describe the relative (%) area of the colored region, and best-fit frictional ratios (f/f_0) are noted for each dataset. All experiments were performed with 150 μM protein in 25 mM sodium phosphate, pH 6.2, at 25 °C.
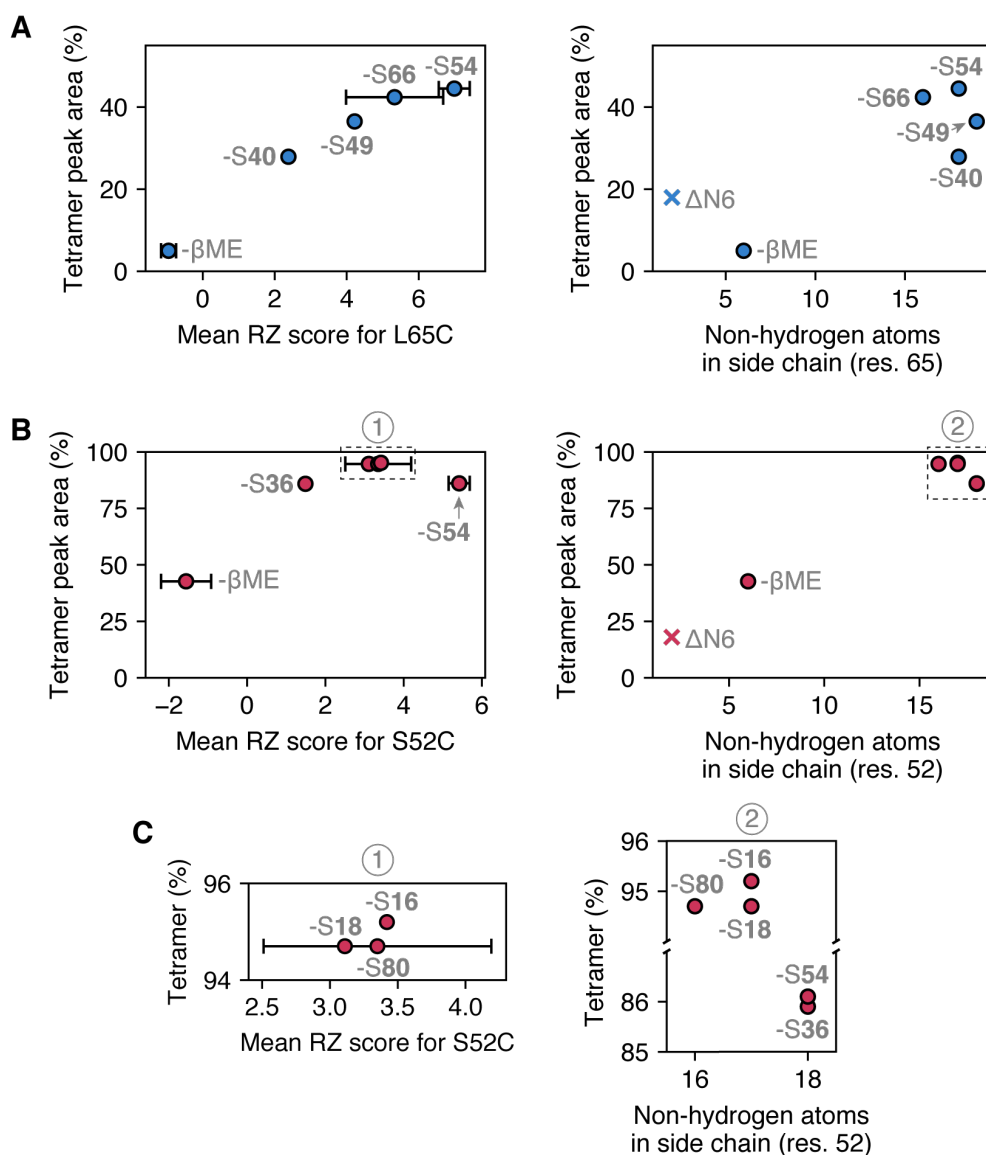
Figure S14. Comparison of *c*(*s*) tetramer peak areas for a range of L65C-fragment adducts (**A**) and S52C-fragment adducts (**B**) against various properties of the associated fragment. **A:** For L65C, samples showed a positive correlation between fragment RZ score and tetramer peak area (left panel). Increasing fragment size was also generally associated with a larger tetramer peak area (right panel), but this relationship is less clear (partly due to the limited variance in fragment size). **B:** Most fragments used to generate S52C-fragment adducts produced high tetramer populations (> 85% peak area), regardless of RZ score (left panel). However, the tetramer peak area of S52C-fragment adducts showed a positive relationship with the size of the attached fragment (and therefore the size of the sidechain at residue 52), although note again that fragments are clustered in a narrow size range. In both **A** and **B**, the apparent relationship between fragment RZ score/size (respectively) and tetramer peak area does not necessarily mean that these variables are directly responsible for dictating tetramer populations when tethering fragments to residues 65/52, or that variables other than the two considered here cannot play a role. **C:** Magnified views of regions 1-2 (labelled in **A** and **B**). For fragments which were screened in more than one tethering cocktail, RZ scores are shown as the mean ± one standard deviation. The mean and standard deviation of the βME RZ scores were calculated in Figure S7.

A

B

r = -0.78
m = -5.3

× ΔN6
■ S33C-βME
■ S33C-S**79**
▲ S52C-βME
▲ S52C-S**54**
● L65C-βME
● L65C-S**40**
● L65C-S**49**
● L65C-S**54**
● L65C-S**66**

— ΔN6
— L65C-βME
— L65C-S**40**
— L65C-S**49**
— L65C-S**54**
— L65C-S**66**
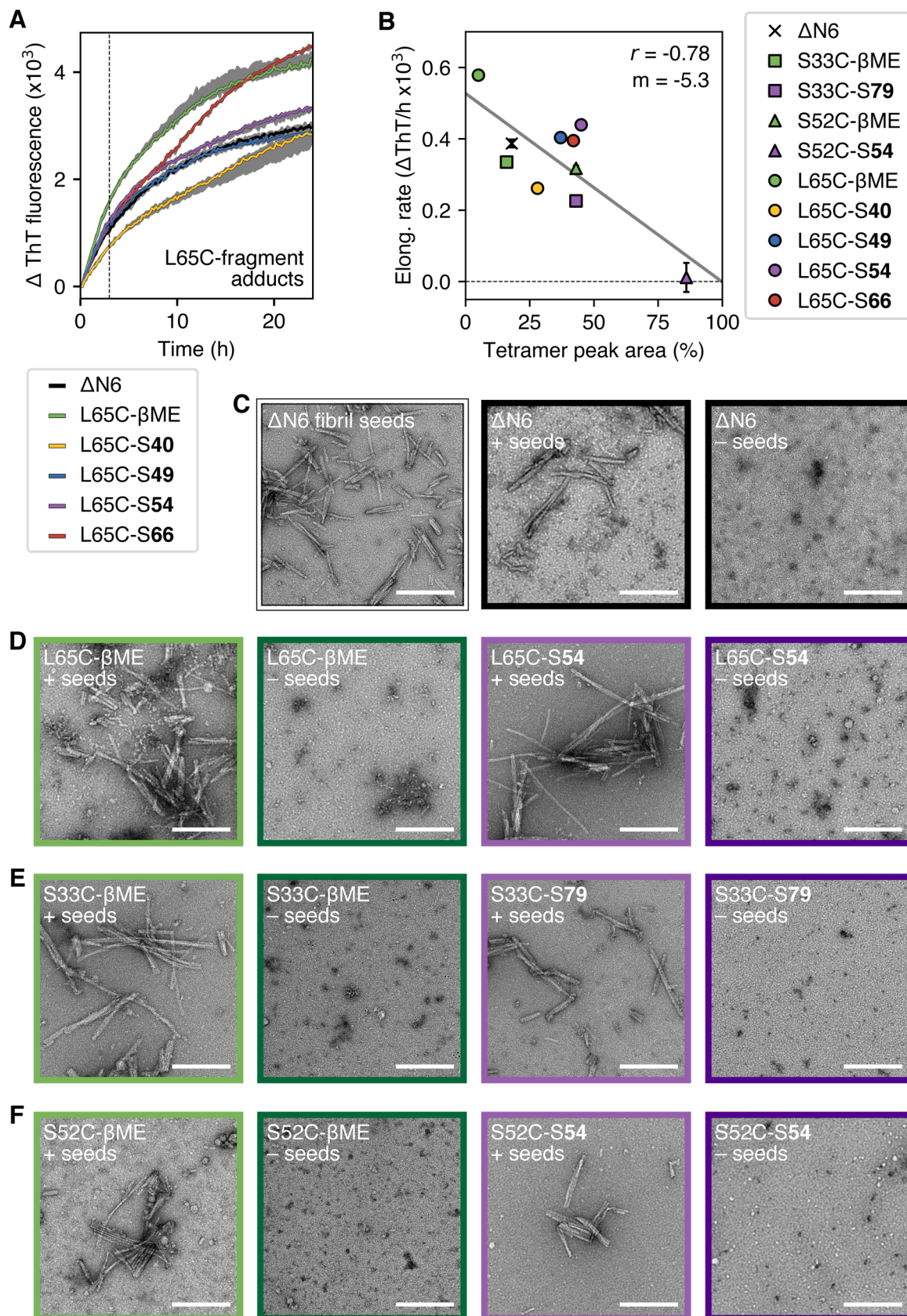
C

D

E

F

Figure S15. A: Thioflavin T (ThT) fluorescence data showing the growth of amyloid fibril mass over time as a consequence of the elongation of ΔN6 fibril seeds (15 μM) by various L65C-fragment adducts (150 μM). The median ThT fluorescence curve is shown for each sample, with the highest and lowest values observed shaded in gray (n = 3). Elongation rates were calculated by determining the mean rate at which ThT fluorescence increased over the first 3 hours of the experiment (i.e., up until the dotted line). Experiments were performed under quiescent conditions in 25 mM sodium phosphate, pH 6.2, 25 °C. **B:** The initial rate at which various ΔN6-fragment adducts (150 μM) elongate pre-formed ΔN6 amyloid fibrils (15 μM) shows a negative correlation with the tetramer population of these adducts. Error bars (standard deviation) are shown around the mean elongation rates (n = 3) but in most cases are smaller than the displayed data point. The global linear regression line (Pearson's correlation coefficient, *r* = -0.78; slope, m = -5.3 ΔThT fluorescence/h/% tetramer peak area) is shown in solid gray. A dotted gray line has been used to highlight the *x* intercept (which occurs at a tetramer peak area of 100%). **C-F:** Representative negative-stain transmission electron micrographs of the insoluble material taken after incubating ΔN6 (black panels in **C**), L65C-fragment adducts (**D**), S33C-fragment adducts (**E**), and S52C-fragment adducts (**F**) in the presence or absence of ΔN6 fibril seeds (white panel in **C**). The lack of fibrillar material in the unseeded samples confirmed that *de novo* fibril formation does not occur over 24 h under these conditions for any of the protein-fragment adducts tested, and therefore that the observed changes in ThT fluorescence intensity for the seeded samples were due to elongation of the pre-formed ΔN6 fibrils. As the elongation efficiency of ΔN6 is known to be poor under similar conditions to those used in this experiment[8], elongated fibril seeds will not differ dramatically in length compared to the starting material when judged by electron microscopy. Consequently, samples which were unable to effectively elongate the seeds (e.g., S52C-S**54**) were expected to appear similar to other samples which did show a significant increase in ThT fluorescence over 24 h (e.g., S52C-βME), as was observed. Scale bar: 200 nm.
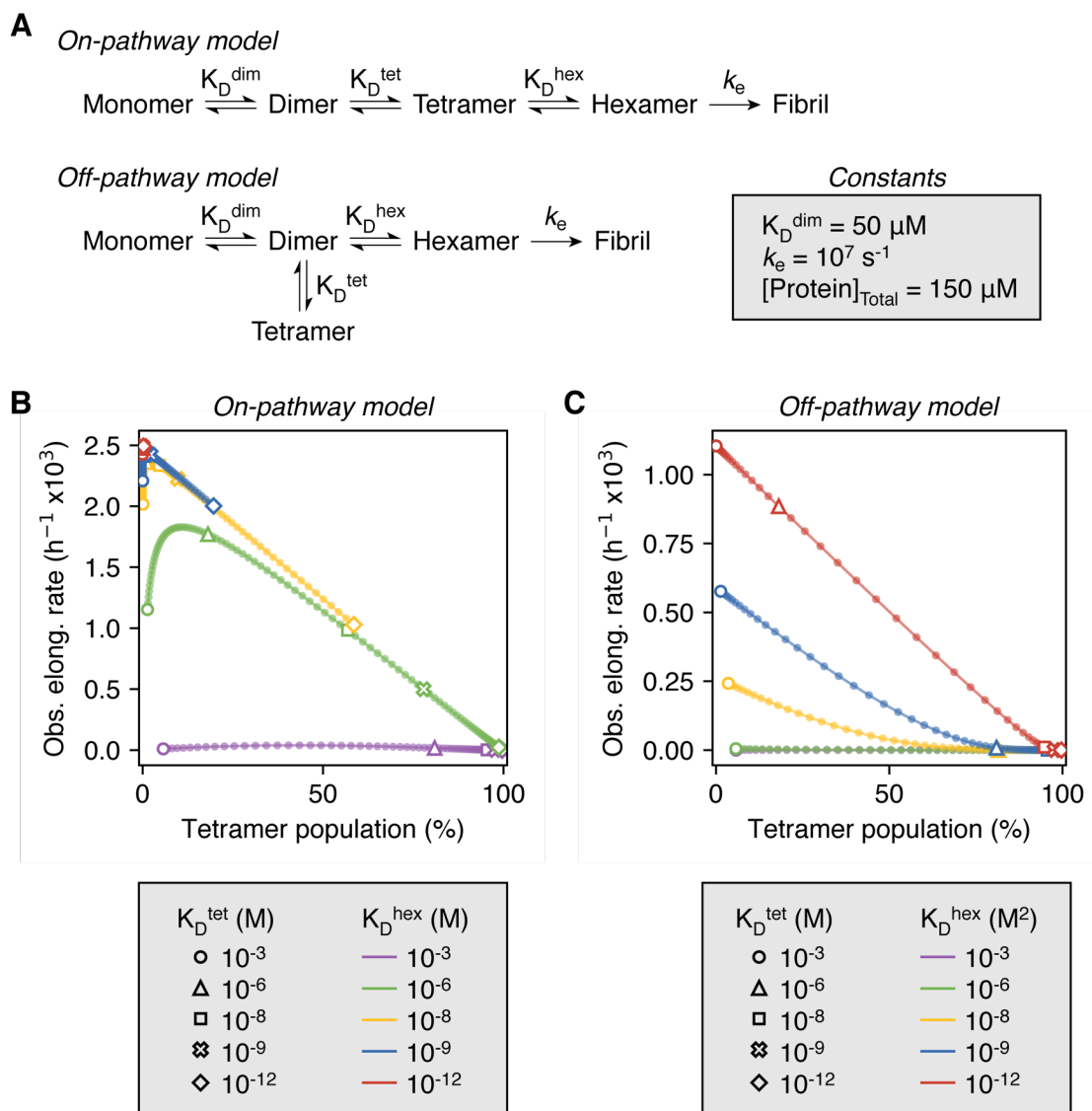
A *On-pathway model*

$$\text{Monomer} \xrightleftharpoons{K_D^{dim}} \text{Dimer} \xrightleftharpoons{K_D^{tet}} \text{Tetramer} \xrightleftharpoons{K_D^{hex}} \text{Hexamer} \xrightarrow{k_e} \text{Fibril}$$

Off-pathway model

$$\text{Monomer} \xrightleftharpoons{K_D^{dim}} \text{Dimer} \xrightleftharpoons{K_D^{hex}} \text{Hexamer} \xrightarrow{k_e} \text{Fibril}$$
$$\big\updownarrow K_D^{tet}$$
$$\text{Tetramer}$$

Constants

K_D^{dim} = 50 µM
k_e = 10^7 s^{-1}
[Protein]$_{Total}$ = 150 µM

B *On-pathway model*

C *Off-pathway model*

K_D^{tet} (M)		K_D^{hex} (M)
○	10^{-3}	— 10^{-3}
△	10^{-6}	— 10^{-6}
□	10^{-8}	— 10^{-8}
✪	10^{-9}	— 10^{-9}
◇	10^{-12}	— 10^{-12}

K_D^{tet} (M)		K_D^{hex} (M^2)
○	10^{-3}	— 10^{-3}
△	10^{-6}	— 10^{-6}
□	10^{-8}	— 10^{-8}
✪	10^{-9}	— 10^{-9}
◇	10^{-12}	— 10^{-12}

Figure S16. Simulated fibril elongation rates for two ΔN6 amyloid assembly models. In both models (**A**) dimers and hexamers were assumed to be on-pathway to fibrils, with hexamers as the species responsible for fibril elongation, based on previous studies[8]. Tetramers were treated as either on- (**B**) or off-pathway (**C**) to fibrils. The dissociation constants for tetramerization and hexamerization (K_D^{tet} and K_D^{hex}) were varied: K_D^{tet} from 10^{-3}-10^{-12} M in both models (100 data points, five of which are specifically highlighted in the legend and the rest shown as small, filled circles); K_D^{hex} from 10^{-3}-10^{-12} M or 10^{-3}-10^{-12} M^2 in the on- and off-pathway models, respectively (note the differences in the units). Equilibrium tetramer concentrations, [Tetramer]$_{eq}$, were calculated after integration of each model at time infinity for each pair of K_D^{tet} and K_D^{hex} values, and then were converted to a fractional population, p_{tet} = 4 x [Tetramer]$_{eq}$ / [Protein]$_{Total}$. Observed elongation rates ('Obs. elong. rate'), estimated as [Hexamer]$_{eq}$ x k_e (where k_e is the microscopic elongation rate), were similarly calculated. Previous studies[8] have determined K_D^{hex} to be on the order of 10^{-9} M^2, and the trend between elongation rate and tetramer population observed at this value of K_D^{hex} in the off-pathway model (blue line in **C**) is consistent with the observed experimental data (Figure S15B). By contrast, the relationships between tetramer population and observed elongation rate in the on-pathway model (**B**) are not consistent with the trend in Figure S15B at any of the values of K_D^{hex}: when the affinity for hexamer formation is high

(i.e., $K_D^{hex} \leq 10^{-8}$ M), tetramers cannot be populated to a large extent, whereas for those K_D^{hex} values where tetramers can be populated up to ~100% (e.g., $K_D^{hex} = 10^{-6}$ M), then the observed elongation rate shows a biphasic scaling, with the maximal elongation rate no longer occurring at the lowest tetramer populations. The dimerization dissociation constant (K_D^{dim}) used for both models was selected based on prior studies[8] and k_e was assumed to be 10^8 s^{-1}.
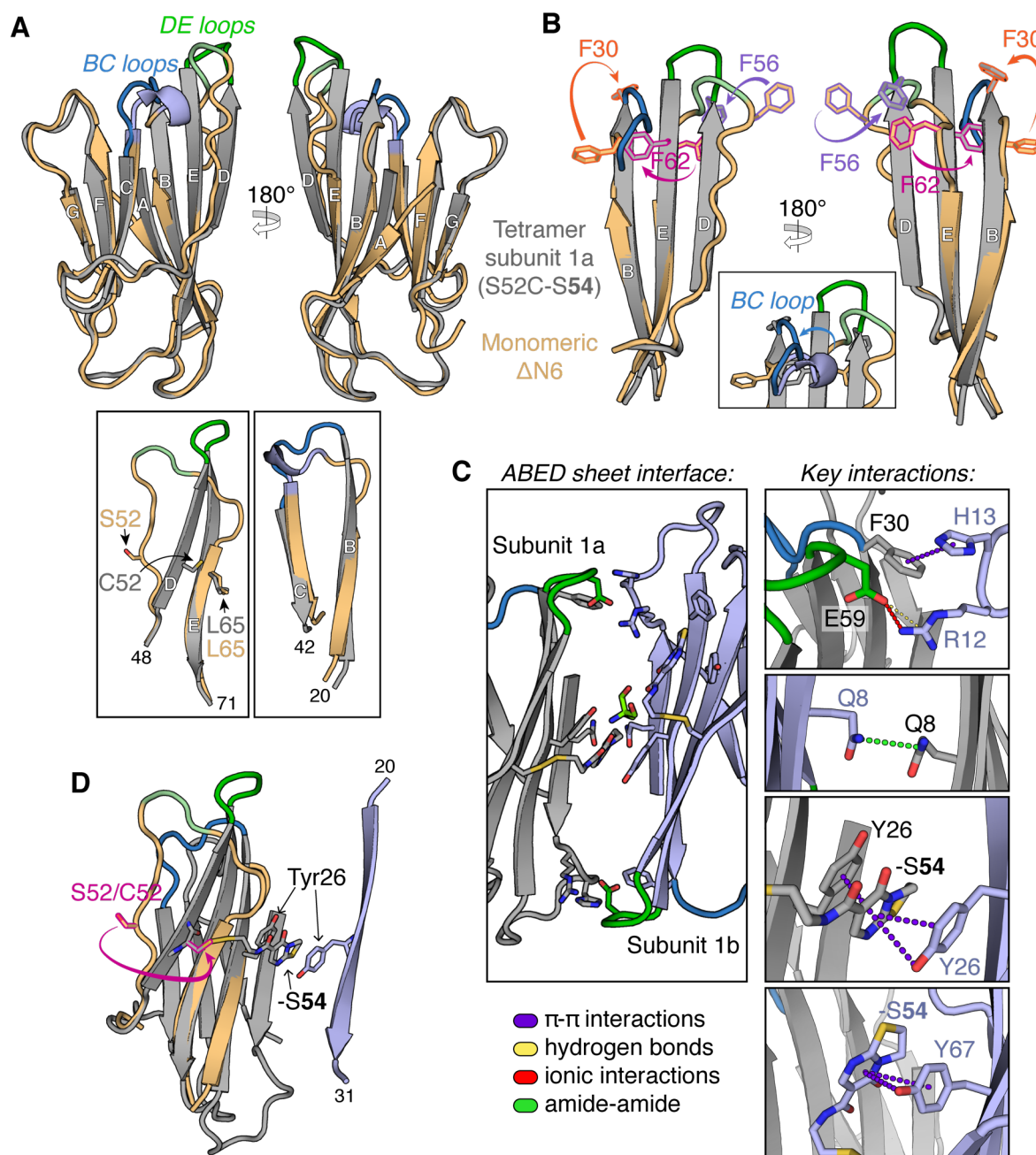
Figure S17. Comparison of monomeric ΔN6 PDB 2XKU[2] and subunit 1a of the tetramer formed by S52C-S**54** ΔN6 provides insight into key structural changes associated with tetramerization and the protein-ligand interactions which drive this oligomerization event. **A:** The subunits of the S52C-S**54** tetramer are native-like (subunit 1a shown in gray), but with perturbations to the D strand and the DE/BC loops (insets; showing residues 48-71 and 20-42). The left inset additionally highlights the proximity of residues 52 and 65 in the S52C-S**54** structure, rationalizing why covalent functionalization of these positions has similar effects on the oligomeric distribution of ΔN6. Monomeric ΔN6 is shown in pale orange. In both structures, the DE and BC loops are colored in green and blue, respectively. **B:** The straightening of the D strand which has occurred in the tetrameric S52C-S**54** ΔN6 structure is accompanied by rearrangement of a network of phenylalanine residues which run across the D, E, and B β-strands, ultimately resulting in the flipping of Phe30 to the solvent-accessible face of the ABED β-

sheet and rearrangement of the BC loop (inset). For clarity, only the D, E, and B β-strands and associated loops are shown. **C:** Non-covalent protein-protein and protein-ligand interactions which occur within the ABED sheet interface of the S52C-S**54** tetramer. Four of these interactions are formed between Glu59-Arg12 and Phe30-His13 (each interaction occurring twice, at the top and bottom of the interface). Both Glu59 (DE loop) and Phe30 (part of the phenylalanine network in **B**) have shifted significantly from their position in monomeric ΔN6, indicating that the structural changes that have occurred in S52C-S**54** (**A**, **B**) are necessary for formation of the ABED sheet interface. Non-covalent interactions were inferred from the S52C-S**54** crystal structure using Arpeggio[9]. A Tris molecule is shown in green. **D:** Binding of a -S**54** fragment adduct between two Tyr26 residues within the ABED sheet interface may be the driving force between D strand straightening, as residue 52 is too far from Tyr26 in monomeric ΔN6 (where the D strand is present as a β-bulge) for this interaction to occur. Subunits 1a and 1b from the S52C-S**54** crystal structure are shown in gray (full structure) and pale blue (B strand only; residues 20-31), respectively. Only the D, E, and B β-strands of monomeric ΔN6 (pale orange) are shown for clarity.
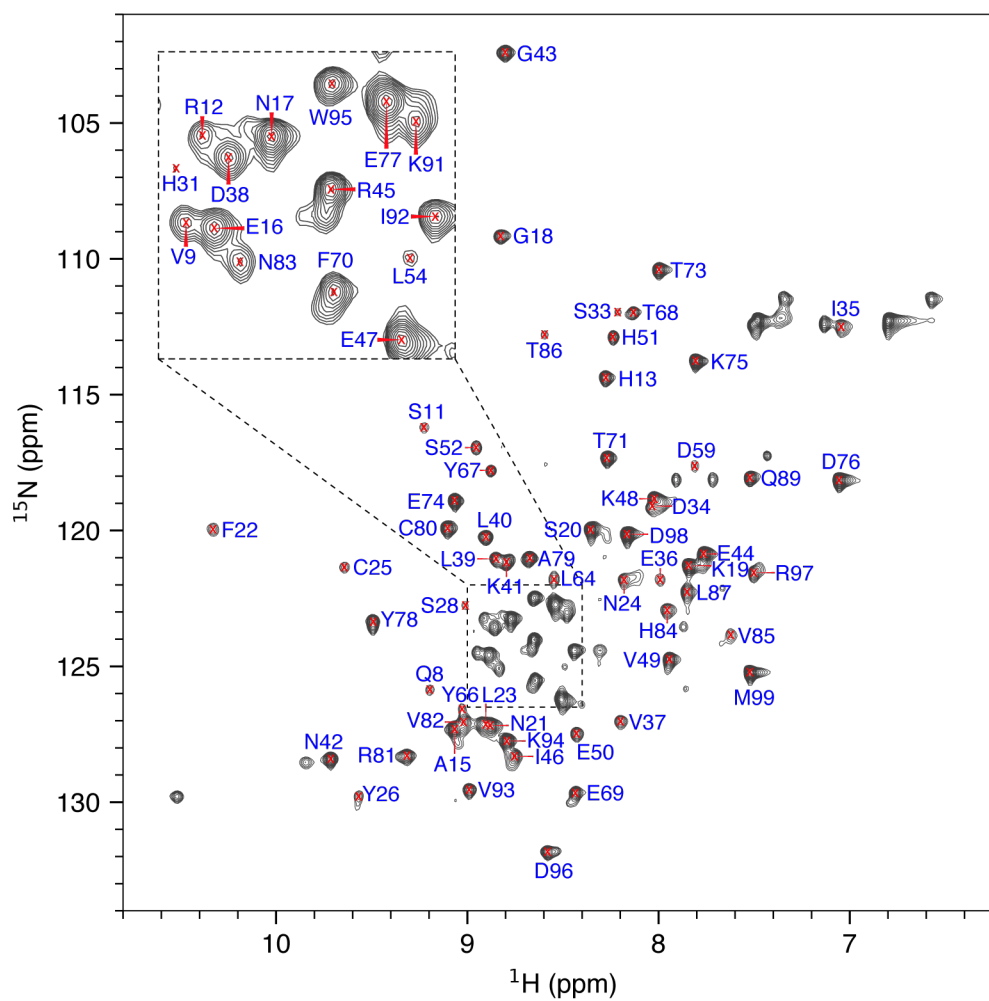
Figure S18. ^{1}H-^{15}N SOFAST HMQC spectrum of ^{15}N-ΔN6, acquired at 750 MHz, 25 °C, using 150 µM protein in 25 mM sodium phosphate, pH 6.2. Peaks which could be confidently assigned to the backbone amide of a specific residue (based on comparison to ΔN6 ^{1}H-^{15}N data acquired at pH 7.5[2]) are labelled.
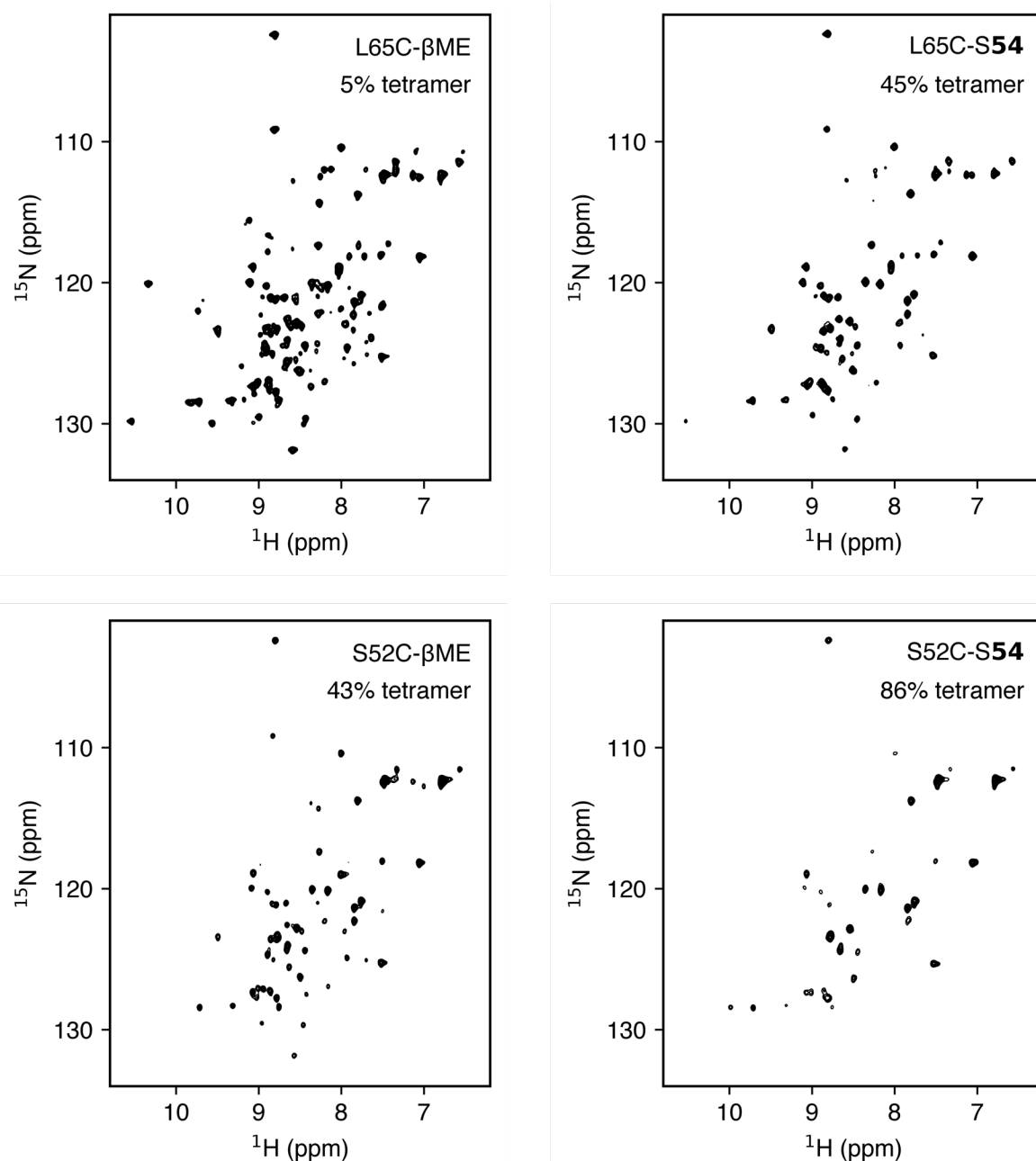
Figure S19. ^{1}H-^{15}N SOFAST HMQC spectra for ^{15}N-labelled L65C- and S52C-fragment adducts, acquired at 750 MHz, 25 °C, using 150 μM protein in 25 mM sodium phosphate, pH 6.2. The percentages listed in the top right of each spectrum correspond to the tetramer peak area in the $c(s)$ distribution for that sample. Contour levels for each spectrum were normalized to the L65C-βME spectrum according to the number of scans. All spectra showed well-dispersed resonances with similar ^{1}H-^{15}N chemical shifts to those of unliganded ΔN6^2 (Figures S18), implying that the protein populations which contribute towards the observable resonances have a native-like structure.
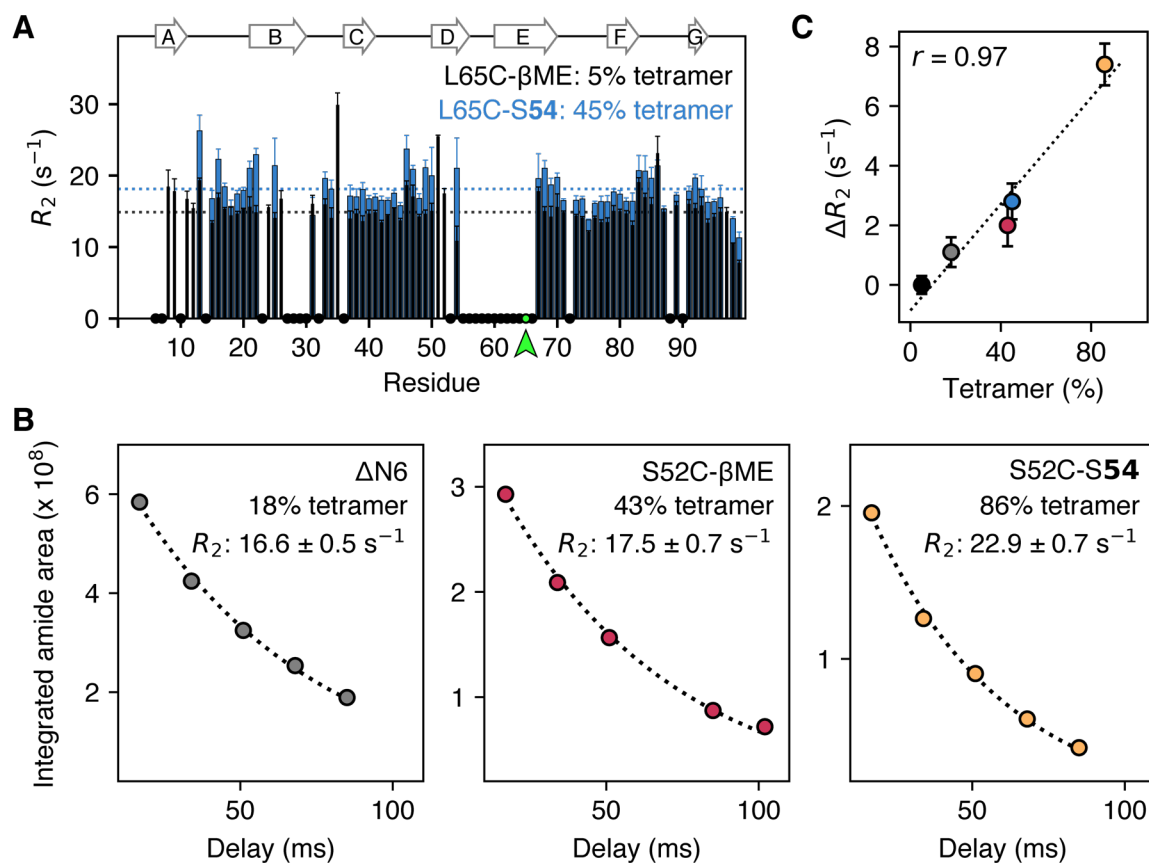
Figure S20. Backbone ^{15}N transverse relaxation (R_2) rates for the -βME and -S**54** adducts of L65C and S52C indicate that monomer-tetramer exchange lies in the fast-intermediate exchange regime. **A:** Per-residue ^{15}N R_2 rates (± the error of the exponential fit) for L65C-β$_2$m (black) and L65C-S**54** (blue). The universal increase in ^{15}N R_2 rates for all observed ^{1}H-^{15}N resonances for L65C-S**54** (relative to L65C-βME) indicates that this sample is in exchange with larger oligomers, which, based on the SV-AUC $c(s)$ distributions, are predominantly tetramers (as the populations of dimers and hexamers are similar for both the -βME and -S**54** adducts). Dotted lines show the mean ^{15}N R_2 rate for each sample (only taking into account residues for which R_2 rates could be measured in both samples). Residues where blue bars are not shown are those which were broadened beyond detection for L65C-S**54**. Residues which could not be observed in either sample are indicated by black circles (or a green circle, for residue 65, which is also highlighted by an arrow). The locations of the β-strands in the S52C-S**54** tetramer crystal structure are shown above the plot. **B:** Due to low sensitivity, per-residue ^{15}N R_2 measurements for S52C-βME and S52C-S**54** were not possible, and thus mean ^{15}N R_2 rates across the whole amide region (7.6-9.2 ppm) were obtained for these samples. Such datasets were also acquired for ΔN6 (shown) and both L65C adducts from **A** (not shown; L65C-βME: 15.5 ± 0.3 s^{-1}; L65C-S**54**: 18.3 ± 0.6 s^{-1}). Dotted lines represent the exponential decay function which was fitted to the data (circles), to obtain the ^{15}N R_2 rate (± the error of the exponential fit). Percentages listed in **A** and **B** represent tetramer peak areas from the corresponding $c(s)$ distributions. **C:** Mean ^{15}N R_2 rates across the whole amide region (shown relative to the R_2 rate measured for L65C-βME) increase linearly (Pearson's correlation coefficient, $r = 0.97$) as a function of $c(s)$ tetramer peak area. This suggests that tetramerization is fast on the relaxation timescale and thus, $\Delta R_2 \approx p_{tet}*R_{2,tet}$). Color scheme follows parts **A** and **B** (i.e., ΔN6, gray; L65C-βME, black; L65C-S**54**, blue; S52C-βME, pink; S52C-S**54**, pale orange).
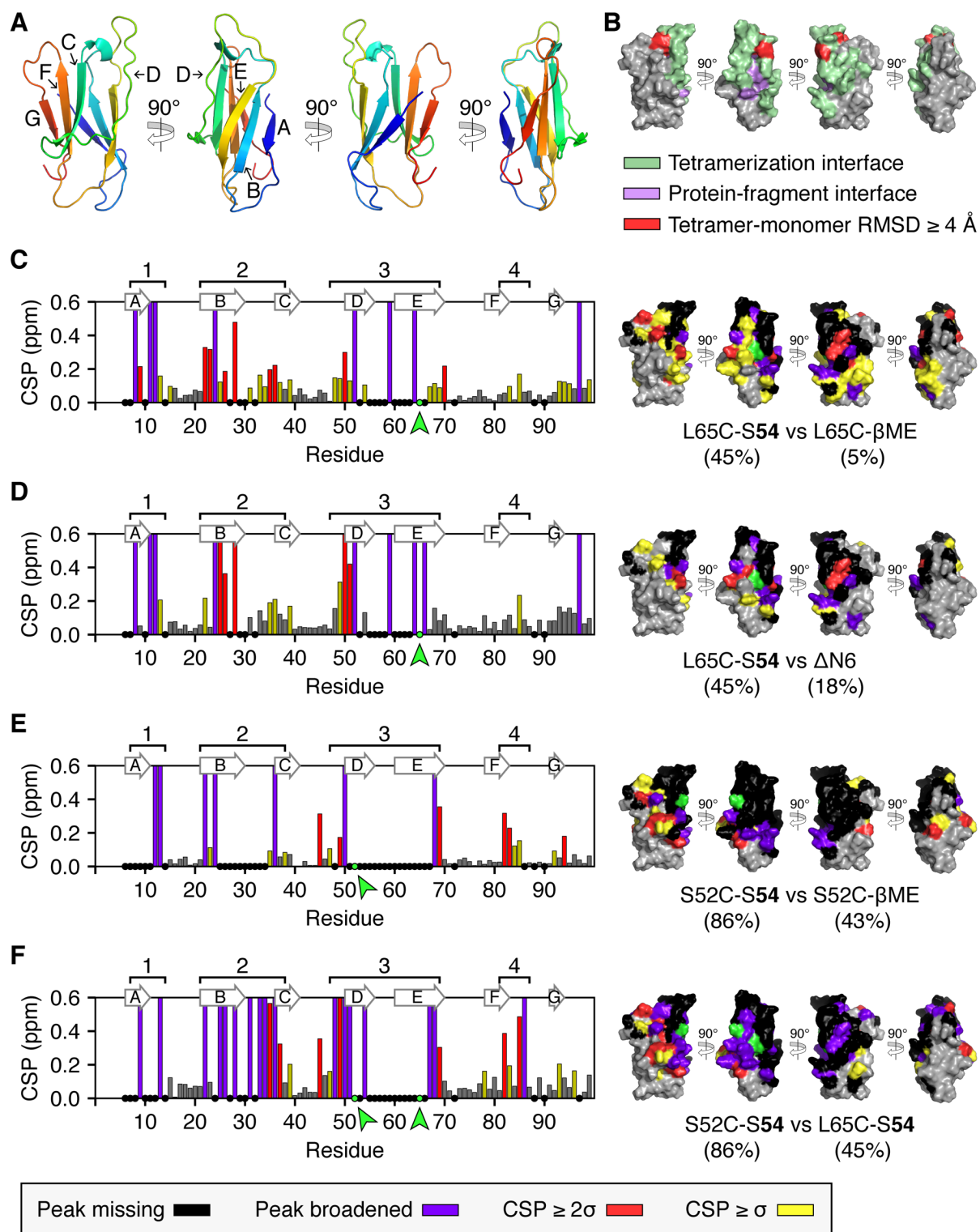
Figure S21. Solution-phase NMR data indicates that the tetramers formed by S52C- and L65C-fragment adducts are structurally similar and also consistent with the high-resolution structure observed for the S52C-S**54** tetramer by X-ray crystallography. A cartoon representation of ΔN6 (PDB 2XKU[2]) is shown in **A** with the β-strands labelled and in the same orientation as in the four views of ΔN6 shown in **B-F**. **B:** Regions of ΔN6 which are expected to experience a change in chemical environment upon

tetramerization, based on the S52C-S**54** crystal structure, are highlighted: residues within the S52C-S**54** tetramerization interface (defined as any residue within 6 Å of another subunit within the tetramer) are shown in green and residues outside this interface but which are either in proximity (≤ 6 Å) to the -S**54** fragment or which have a mean RMSD ≥ 4 Å relative to the monomeric ΔN6 NMR ensemble (PDB 2XKU[2]) are shown in purple and red, respectively. **C-F:** The changes in peak positions and intensities in ^{1}H-^{15}N SOFAST HMQC spectra which are observed when comparing different L65C- or S52C-fragment adducts. The absence of a second set of ^{1}H-^{15}N peaks in liganded ΔN6 spectra (see Figure S19) suggests that the exchange between monomer and tetramer lies in the fast-intermediate regime on the chemical shift timescale. Therefore, the observed chemical shift/intensity changes should report both on the covalent attachment of ligands and on tetramer formation (since tetramers are the oligomers whose population changes most significantly relative to their corresponding -βME adduct). All the proteins experience chemical shift perturbations (CSPs) and loss of peak intensity in up to four main regions (labelled 1-4) in samples with higher tetramer populations – although region 4 only shows perturbations in samples which are almost exclusively tetrameric (e.g., S52C-S**54**; 86% tetramer peak area in the $c(s)$ distribution). All four perturbed regions involve residues which are within or adjacent to the surfaces highlighted in **B**, indicating that the tetramers formed by both the S52C- and L65C-fragment adducts in solution are consistent with the S52C-S**54** crystal structure. Percentages under the sample names correspond to the tetramer peak areas in the $c(s)$ distributions. Residues which were not visible (or could not be confidently assigned based on comparison to previous ΔN6 assignments[2]) for either of the samples being compared are shown as black circles. Residues which were visible for the sample with the lower tetramer population but were broadened beyond detection for the sample with the higher tetramer population are shown by purple bars. Other residues are colored by the magnitude of the CSP relative to the standard deviation (σ) of the dataset. The covalent tethering site(s) are shown in green (and highlighted by an arrow). The locations of the β-strands in the S52C-S**54** tetramer crystal structure are shown above each plot.
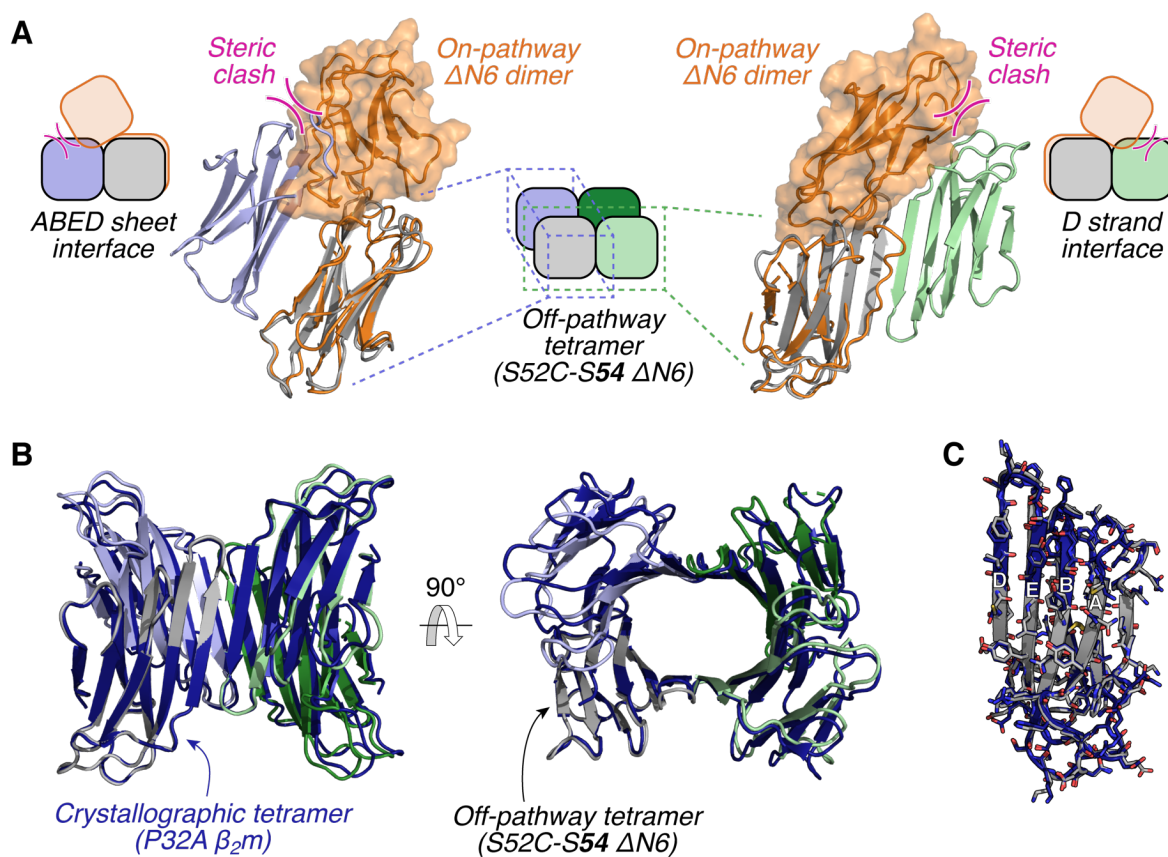
Figure S22. Comparison of the S52C-S**54** ΔN6 tetramer (subunits colored gray, pale blue, pale green, and dark green) with other ΔN6 and full-length β_2m oligomers. The covalent fragments in the S52C-S**54** structure are not shown, for clarity. **A:** Comparison with a structural model of an on-pathway ΔN6 dimer (orange; which self-associates to form an on-pathway hexamer)[8] shows that the S52C-S**54** tetramer would need to completely dissociate in order to form these on-pathway species, thereby rationalizing why stabilization of this tetramer inhibits the elongation of ΔN6 amyloid fibrils. **B-C:** The S52C-S**54** crystal structure bears strong resemblance to a crystallographic tetramer formed by the P32A variant of full-length β_2m (dark blue, PDB 2F8O[10]; aligned on the gray subunit of the S52C-S**54** tetramer). The RMSD between the two structures for all non-hydrogen atoms in chain A (**C**; residues 7-99) is 1.1 Å. However, while the solution-state relevance of the P32A tetramer is unknown, the solution NMR data obtained for S52C-S**54** suggests that the tetramer structure observed in the crystal lattice reflects the structure of the tetrameric species which is present in solution.

Supplementary Tables

Table S1. Data collection and refinement statistics for the S52C-S**54** crystal structure.

	S52C-S**54**
Data collection	
Space group	P 4_3 2_1 2
Cell dimensions	
a, b, c (Å)	87.57 87.57 56.46
α, β, γ (°)	90.00 90.00 90.00
Resolution (Å)	61.92 - 2.40 (2.53 - 2.40)
R_{pim} (%)	0.033 (0.399)
I / σ(I)	9.8 (1.6)
Completeness (%)	100.0 (100.0)
Redundancy	23.1 (23.6)
CC(1/2)	0.999 (0.789)
Refinement	
Resolution (Å)	61.92 - 2.40
No. of reflections	208,526
No. of unique reflections	9,026
R_{work} / R_{free} (%)	23.33 / 28.83
No. of atoms	
Protein	1520
Non-covalent ligands	8
Water	33
RSMD	
Bond lengths (Å)	0.0071
Bond angles (°)	1.5544
B-factor (Å^2)	13.997

Values for the highest-resolution shell are shown in parentheses.

Supplementary Materials and Methods

Protein expression and purification

ΔN6 was expressed and purified as described previously[8]. Expression constructs for the S33C, S52C, and L65C ΔN6 variants were generated by mutagenesis of a pET23a ΔN6 expression plasmid (pINK)[11] using a Q5 Site-Directed Mutagenesis Kit (New England Biolabs). These variants were expressed in BL21(DE3)pLysS *E. coli* cells in lysogeny broth (for ^{14}N-labelled protein) or minimal media supplemented with ^{15}N-NH$_4$Cl (for ^{15}N-labelled protein) (media recipe: 10 g/L K$_2$HPO$_4$, 10 g/L KH$_2$PO$_4$, 7.5 g/L Na$_2$HPO$_4$, 9 g/L K$_2$SO$_4$, 1 g/L ^{15}N-NH$_4$Cl, 2 mM MgCl$_2$, 0.1 mM CaCl$_2$, 0.04% w/v D-glucose). Cultures were grown at 37 °C (shaking at 200 rpm) to an optical density at 600 nm of 0.6, before inducing protein expression with 1 mM isopropyl β-D-1-thiogalactopyranoside (IPTG).

After ~16 h, the cells were harvested by centrifugation (3000 rpm, 15 min, 4 °C, Beckman Coulter JLA 8.1000 rotor), resuspended in lysis buffer (~16 mL lysis buffer per g of cells; 25 mM Tris-HCl, pH 8.0, 100 μg/mL lysozyme, 50 μg/mL phenylmethane sulfonyl fluoride, 20 μg/mL DNase, 1 mM ethylenediaminetetraacetic acid), homogenized, and lysed (2x20 kpsi; Constant Systems Cell Disruptor). The insoluble fraction was isolated by centrifugation (15,000 rpm, 30 min, 4 °C, Beckman Coulter JLA 12.250 rotor) and was washed three times with 25 mM Tris-HCl, pH 8.0 to remove cellular membranes. The inclusion bodies which remained were resolubilized by stirring in 25 mM Tris-HCl, pH 8.0, 8 M urea (~10 mL resolubilization buffer per g of cell pellet used to prepare the inclusion bodies) for 2 h. The resolubilized sample was centrifuged to remove any remaining insoluble debris.

Anion exchange chromatography was performed in 25 mM Tris-HCl, pH 8.0, 8 M urea with a NaCl gradient (0-1 M over 420 mL), using a column packed with Q Sepharose Fast Flow resin (GE Healthcare; 37 mL column volume). Dithiothreitol (DTT; 10 mM) was added to samples for 20 min (at ~20 °C) prior to loading onto the anion exchange column. The appropriate fractions from anion exchange were pooled and refolded by rapidly diluting (10-fold) into refolding buffer (25 mM Tris-HCl, pH 8.0, 0.64 M L-arginine, 2 mM reduced glutathione, 0.2 mM oxidized glutathione). The refolded protein was dialyzed first into 25 mM Tris-HCl, pH 8.0, and then into 25 mM NH$_4$HCO$_3$, all at 4 °C (SnakeSkin dialysis tubing, molecular weight cut-off 3500 Da; Thermo Scientific). The samples were lyophilized, and then resuspended at

500-600 μM for size exclusion chromatography, in 5 mL aliquots (15 mM NH_4HCO_4, pH 8.0). Prior to size exclusion chromatography, covalently bound glutathione was removed from the surface-exposed cysteine by incubation with DTT (20 equivalents, 30 min at 20 °C for S33C and S52C; 40 equivalents, 2 h at 20 °C for L65C). Samples were loaded onto a HiLoad 26/60 Superdex 75 prep grade column (GE Healthcare), pre-equilibrated with 15 mM NH_4HCO_3, pH 8.0, and the peak corresponding to monomeric protein was pooled and lyophilized. The purified product was positively identified by mass spectrometry. The oligomeric purity of the final product (after lyophilization) was confirmed by analytical size exclusion chromatography, performed on a Superdex 75 10/300 GL column which had been calibrated with dextran blue (~2000 kDa), bovine serum albumin (66 kDa), ovalbumin (43 kDa), chymotrypsinogen A (25 kDa), cytochrome *c* (12.4 kDa), aprotinin (6.5 kDa), and vitamin B12 (1.3 kDa).

Typical yields of ^{14}N-labelled protein were 15-30 mg per L expression culture, while typical yields of ^{15}N-labelled protein were 10-14 mg per L expression culture.

Computational solvent mapping (FTMap)

Computational solvent mapping was performed against all 30 members of the ΔN6 NMR ensemble (PDB 2XKU[2]) using the FTMap server (http://ftmap.bu.edu)[1]. The PDB files generated by this server show the predicted binding preferences for 16 different solvent ('probe') molecules. The generated binding poses for each probe are grouped into 'probe clusters' (based on their location on the protein's surface), which are in turn grouped into 'consensus clusters'. The quality of consensus clusters provides information about the ligandability of pockets on the surface of a protein. The criteria used to classify consensus clusters generated against ΔN6 are shown in Table S2 – these differ slightly from criteria recommended by Kozakov *et al.*[12], as the inherent specificity of non-covalent interactions between a protein and a covalently tethered ligand (as a consequence of restricting the ability of the ligand to diffuse through solution) allows certain criteria to be relaxed.

Table S2. Criteria for assessing the quality of consensus clusters generated by the FTMap server for each ΔN6 structure. Pockets containing low, medium, and high quality consensus clusters all represent regions which should be feasible to target with small molecules, but for pockets with only low quality clusters, it is unlikely to be possible to develop sub-micromolar binders[1,12].

Consensus cluster quality	Number of probe clusters	Distance to next nearest consensus cluster
High	≥ 16	≤ 8 Å
Medium	≥ 16	> 8 Å
Low	13-15	–
Poor	< 13	–

Design of the disulfide fragment library

Structure-data (SD) files for ~12,000 mercaptoethyl amide-functionalized small molecules (general structure of which is shown in Figure S23) were prepared. These molecules represented all the mercaptoethyl amide compounds which: (1) could be prepared from commercially available carboxylic acids (available from Alfa Aesar, Sigma Aldrich, or Fluorochem, according to the ZINC15 database[13]: zinc15.docking.org) that were anticipated to be compatible with the reaction conditions shown in Figure S3A and described on p. 34; (2) contained variable R groups which were "fragment-like" (i.e., 8-17 non-hydrogen atoms, ≥ 1 ring, ≤ 2 rotatable bonds, logP between 0-3.5, and ≤ 2 stereogenic centers); and (3) aside from the thiol in the mercaptoethyl chain, did not contain any functional groups capable of forming covalent bonds with amino acid side chains at near-neutral pH. Using Canvas (Schrödinger, version 2.1.013), hashed fingerprints were generated (MOLPRINT2D[14], with Mol2 atom/bond-typing, 64-bit) and used with a diversity-selection algorithm (sphere exclusion with a sphere size of 0.5 and Tanimoto similarity metrics[15]) to select a subset of 1000 diverse molecules for molecular docking experiments. An equivalent collection of 1000 methyl amides (Figure S23) was also generated by modification of the SD files of the 1000 selected mercaptoethyl amides.
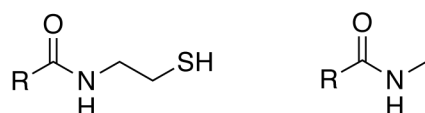
Figure S23. General structure of the mercaptoethyl amide-functionalized compounds (left) and methyl amide-functionalized (right) compounds used in molecular docking experiments.

All 1000 mercaptoethyl amide-functionalized compounds were docked against the S33C, S52C, and L65C variants of ΔN6 using CovDock (virtual screening mode[16]; Schrödinger), while the methyl amide-functionalized (i.e., non-covalent) analogues were docked against the whole surface of ΔN6 using Glide[17,18] (standard precision mode; Schrödinger). Compounds were prioritized for synthesis and experimental testing in the tethering screen by selecting those for which there was significant overlap between the top binding pose generated by CovDock, and any of the top three binding poses generated by Glide for the analogous non-covalent compound. Based on the molecular docking data and synthetic accessibility, a library of 76 compounds was ultimately generated (see Figure S3 for library structures and below for the synthetic method).

Synthesis of the disulfide fragment library

General materials and methods

Reagents and solvents were purchased from commercial suppliers and were used without further purification. In situations where combinations of solvents have been used, the relative quantities are given as a ratio of volumes. All reactions were performed at room temperature. Thin layer chromatography was performed on 0.25 mm Merck aluminium plates coated with silica gel and fluorescent indicator F254. Product spots were visualized with UV light (λ_{max} = 254 nm) and/or by staining with basic potassium permanganate.

Synthesis of disulfide-linked fragments

Cysteamine 2-chlorotrityl resin (150 mg, 0.24-0.27 mmol; Novabiochem) was swelled in DMF for 20-30 min prior to reaction. The carboxylic acid starting material (5 equivalents) was resuspended in DMF (2-3 mL) and added to the resin along with Oxyma (5 equivalents) and DIC (5 equivalents). Reactions were left to proceed until free amines were not detected on the solid-phase resin by the Kaiser test[19]. All reactions were complete within two days.

Fluorenylmethyloxycarbonyl (Fmoc)-protected compounds were deprotected prior to resin cleavage using piperidine (20% v/v in DMF, 5 x 2 mL, each time agitated for 2 min). Compounds protected with *tert*-butoxycarbonyl (Boc) and *tert*-butyl groups were deprotected by the TFA used during resin cleavage.

After the reaction reached completion, the resin was isolated and washed with DMF (3 x 2 mL), DCM (3 x 2 mL), and diethyl ether (3 x 2 mL), and then dried under reduced pressure. The thiol intermediate was cleaved from the dried resin in either 7:3 TFA:DCM (for compounds which lacked protecting groups containing an acid-labile *tert*-butyl moiety), 7:2:1 TFA:DCM:water (for Boc-protected compounds), or 9:1 TFA:water (for *tert*-butyl-protected compounds), all with agitation over a period of 2 h and in a 2 mL volume. The resin was removed by filtration, and the cleavage solution was evaporated under nitrogen gas to afford the thiol intermediate. Thiols were oxidized to symmetrical disulfides using iodine (0.5 equivalents) in a mixture of methanol:DCM (2-5 mL; the specific ratio was selected for each compound to maximize solubility, in the minimum volume possible), and the solution was stirred for 2 h. Remaining iodine was quenched by the addition of a saturated aqueous sodium thiosulfate solution, adding dropwise until the solution stopped changing color. The solvent was evaporated under nitrogen gas, and the product was re-suspended in DCM:butanol (3-5 mL; the precise ratio again being selected based on fragment solubility) and washed with water (3 x 2 mL). The vast majority of disulfide-linked fragments remained largely in the organic phase, which was concentrated under reduced pressure to obtain the final product. However, fragments which contained free amine groups after deprotection remained in the aqueous phase. For these samples the aqueous phase was lyophilized, resuspended in a minimal volume of methanol, filtered, and concentrated under reduced pressure.

In total, 84 amide coupling and thiol oxidation reactions were performed. Although mass spectrometry was consistent with the formation of the desired products for all 84 reactions, for eight of these compounds, ^{1}H NMR spectra suggested that the purity of the products was poor, and thus these compounds were excluded from the screening library. For the remaining 76 compounds, the desired disulfide-linked fragments were obtained with a mean crude yield of 57% (ranging from 11% to 80%; for compound characterization).

Preparation of individual protein-fragment adducts

Individual protein-fragment adducts were prepared in two steps: (1) pre-incubation of the ΔN6 cysteine variant of interest (300 μM) with DTT (80 μM, 75 μM, or 150 μM, for L65C, S33C, S52C, respectively) for 20 min; and then (2) incubation with an excess of the desired fragment, as a symmetrical disulfide (Table S3). Reactions were performed at ambient temperature in 25

mM sodium phosphate, pH 8.0, with 20% v/v DMSO, over 40-72 h. In some cases, a +32 Da adduct was observed to form in addition to the desired protein-fragment adduct, but incubation of the sample with additional DTT was found to be successful in reversing formation of this adduct and driving formation of a single species. To obtain fully labelled βME adducts, βME was oxidized to a symmetrical disulfide (2,2'-disulfanediylbis(ethan-1-ol)) prior to labelling (synthesis of this compound described on p. 65).

Table S3. Molar equivalents of different disulfide fragments which were added to S33C, S52C, and L65C in order to prepare individual samples of the various protein-fragment adducts used in SV-AUC experiments, ThT aggregation assays, and NMR experiments.

Disulfide fragment	Molar equivalents added to:		
	S33C	S52C	L65C
Oxidized βME	5	5	7.5
Di-S**16**	–	5	–
Di-S**18**	–	5	–
Di-S**36**	–	1.5	–
Di-S**40**	–	–	4
Di-S**49**	–	–	2.5
Di-S**54**	1.5	1	1.5
Di-S**66**	–	–	5
Di-S**68**	2.5	–	–
Di-S**79**	2.5	–	–
Di-S**80**	–	5	–

After complete protein labelling had been achieved (monitored by mass spectrometry), samples were dialyzed in 25 mM sodium phosphate, pH 6.2 (500-fold volume of buffer relative to the total sample volume) for 20-26 h at 4 °C, using dialysis tubes with a 3.5 kDa molecular weight cut-off (Generon). The final dialysis step was always performed for at least 12 h. The dialysate was used to dilute samples for all subsequent experiments and as the reference in the AUC sample cells. Dialyzed samples were spun in a benchtop microcentrifuge at 13,500 rpm for 15 min prior to use, and the identity of all samples was reconfirmed by mass spectrometry, to ensure that any oligomers which had formed by the protein had not led to reshuffling of disulfide bonds.

As many of the fragments absorbed at 280 nm, bicinchoninic acid (BCA) assays[20] were used to determine the concentration of protein-fragment adducts after dialysis (Thermo Scientific Pierce BCA Protein Assay Kit).

Preparation of ΔN6 fibril seeds for thioflavin T aggregation assays

Lyophilized ΔN6 was resuspended at 30 μM in 25 mM sodium phosphate, pH 6.2, 137 mM sodium chloride, 0.02% w/v sodium azide, with 10 μM thioflavin T (ThT). Samples (100 μL) were incubated at 37 °C in sealed 96-well clear-bottomed non-treated polystyrene plates (Corning), shaking at 600 rpm for 100 h. Fibrils which formed were isolated by centrifugation (14,000 rpm in a benchtop microcentrifuge, 20 min), resuspended in 25 mM sodium phosphate, pH 6.2 at a concentration of 800 μM (monomer equivalent), and then sonicated (15 s at 20% amplitude using a Sonics & Materials VCX 130 PB sonicator with a 3 mm stepped microtip). The presence of fibrillar seeds was confirmed by negative stain electron microscopy (EM) (Figure S15C).

Negative-stain transmission electron microscopy

Replicate samples from the ThT assay were pooled. Insoluble material was separated by centrifugation (14,000 rpm in a benchtop microcentrifuge, 15 min), and the pellet resuspended in the same volume of 25 mM sodium phosphate, pH 6.2. The resuspended insoluble material was diluted 2-fold with acidified water (pH 2, adjusted with hydrochloric acid) and 10 μL was immediately added to a glow-discharged carbon-coated copper grid for 1 min. Excess liquid was blotted away and the grid was briefly washed with 10 μL 1% w/v uranyl acetate before being stained with another 10 μL 1% w/v uranyl acetate for 1 min. Micrographs were recorded on a Tecnai F20 transmission electron microscope operating at 200 keV or a Tecnai T12 transmission electron microscope operating at 120 kEv, at ~30,000x magnification.

Characterization of Synthesized Compounds

General notes on compound characterization

All ^{1}H NMR spectra were acquired on Bruker AVANCE spectrometers, operating at 400 MHz or 500 MHz for ^{1}H, and at 125 MHz for ^{13}C. Spectra were collected at 298 K, and referenced using residual solvent signals as internal standards unless otherwise noted. Chemical shifts (δ) are expressed in parts per million (ppm) and the following abbreviations are used: s (singlet), d (doublet), t (triplet), q (quartet), m (multiplet), br (broad), and app (apparent). Where a diastereoisomeric mixture of products was present, peaks associated specifically with the major ('maj') and minor ('min') diastereoisomers have been labelled accordingly. High-resolution mass spectrometry (HRMS) was performed using a Bruker maXis Impact QTOF mass spectrometer, with an electrospray ionization (ESI) source.

All symmetrical disulfides have been numbered based on the identity of the variable R group (Figure S3), and have been given the prefix Di-S.

N,N'-(disulfanediylbis(ethane-2,1-diyl))bis(4-hydroxybenzamide) (Di-S1)
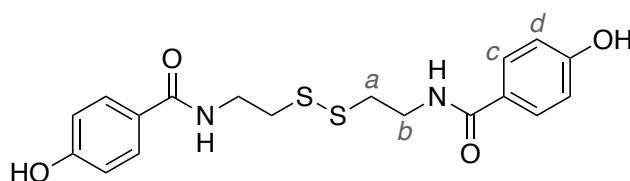
Yellow solid, crude yield: 44%; ^{1}H NMR (MeOD, 400 MHz): δ 3.28 (t, 4H, J = 6.7 Hz, H$_a$), 3.73 (t, 4H, J = 6.7 Hz, H$_b$), 6.82 (d, 4H, J = 8.8 Hz, H$_d$), 7.73 (d, 4H, J = 8.8 Hz, H$_c$); HRMS (ESI/Q-TOF) m/z: [M+Na]$^+$ calculated for C$_{18}$H$_{20}$N$_2$O$_4$S$_2$Na 415.0757; found 415.0757.

N,N'-(disulfanediylbis(ethane-2,1-diyl))bis(4-cyanobenzamide) (Di-S2)
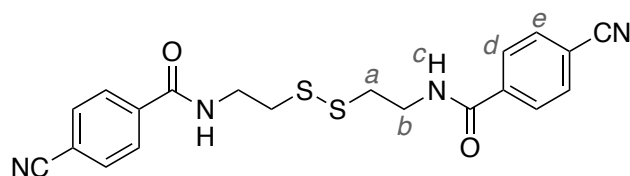
White solid, crude yield: 67%; ^{1}H NMR (DMSO-d$_6$, 400 MHz): δ 2.94 (t, 4H, J = 6.8 Hz, H$_a$), 3.57 (app q, 4H, J = 6.4 Hz, H$_b$), 7.93-8.01 (m, 8H, H$_d$, H$_e$), 8.91 (t, 2H, J = 5.4 Hz, H$_c$); HRMS (ESI/Q-TOF) m/z: [M+Na]$^+$ calculated for C$_{20}$H$_{18}$N$_4$O$_2$S$_2$Na 433.0763; found 433.0765.

N,N'-(disulfanediylbis(ethane-2,1-diyl))bis(2-(4-hydroxyphenyl)acetamide)
(Di-S3)
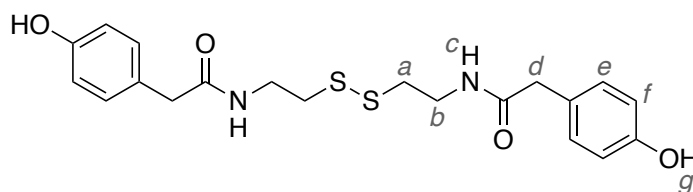
White solid, crude yield: 36%; ^{1}H NMR (DMSO-d_6, 400 MHz): δ 2.75 (t, 4H, J = 6.8 Hz, H$_a$), 3.27 (s, 4H, H$_d$), 3.27-3.34 (m, 4H, H$_b$), 6.66 (d, 4H, J = 8.4 Hz, H$_f$), 7.02 (d, 4H, J = 8.4 Hz, H$_e$), 8.10 (t, 2H, J = 5.5 Hz, H$_c$), 9.20 (s, 2H, H$_g$); HRMS (ESI/Q-TOF) m/z: [M+Na]$^+$ calculated for $C_{20}H_{24}N_2O_4S_2Na$ 443.1070; found 443.1067.

N,N'-(disulfanediylbis(ethane-2,1-diyl))bis(3-hydroxy-4-methylbenzamide)
(Di-S4)
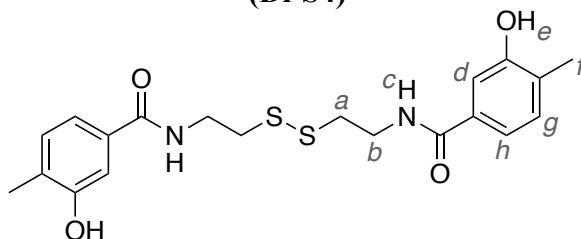
Yellow solid, crude yield: 41%; ^{1}H NMR (DMSO-d_6, 400 MHz): δ 2.14 (s, 6H, H$_f$), 2.90 (t, 4H, J = 6.9 Hz, H$_a$), 3.52 (app q, 4H, J = 6.3 Hz, H$_b$), 7.11 (d, 2H, J = 7.8 Hz, H$_g$), 7.18 (br d, 2H, J = 7.8 Hz, H$_h$), 7.26 (br s, 2H, H$_d$), 8.46 (t, 2H, J = 5.5 Hz, H$_c$), 9.51 (s, 2H, H$_e$); HRMS (ESI/Q-TOF) m/z: [M+Na]$^+$ calculated for $C_{20}H_{24}N_2O_4S_2Na$ 443.1070; found 443.1070.

N,N'-(disulfanediylbis(ethane-2,1-diyl))bis(1-methyl-2-oxo-1,2-dihydropyridine-4-carboxamide)
(Di-S5)
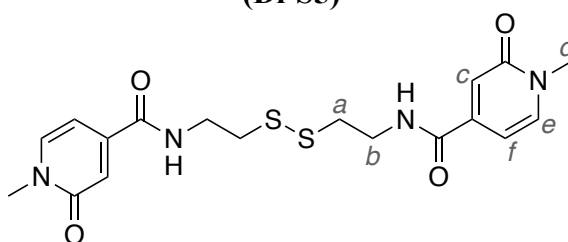
Cream solid, crude yield: 50%; ^{1}H NMR (MeOD, 400 MHz): δ 2.95 (t, 4H, J = 6.7 Hz, H$_a$), 3.58 (s, 6H, H$_d$), 3.66 (t, 4H, J = 6.7 Hz, H$_b$), 6.66 (dd, 2H, J = 7.0 Hz, 1.8 Hz, H$_f$), 6.89 (d, 2H, J = 1.8 Hz, H$_c$), 7.73 (d, 2H, J = 7.0 Hz, H$_e$); HRMS (ESI/Q-TOF) m/z: [M+Na]$^+$ calculated for $C_{18}H_{22}N_4O_4S_2Na$ 445.0975; found 445.0974.

_N,N'_-(disulfanediylbis(ethane-2,1-diyl))bis(6-methyl-3-oxo-2,3-dihydropyridazine-4-carboxamide)
(Di-S6)
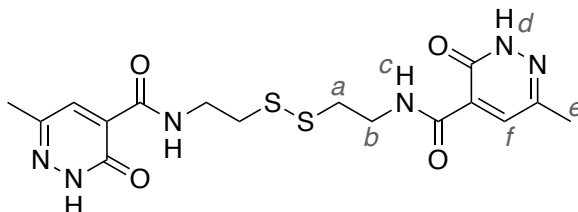
White solid, crude yield: 77%; ^{1}H NMR (DMSO-d_6, 400 MHz): δ 2.34 (s, 6H, H$_e$), 2.92 (t, 4H, J = 6.6 Hz, H$_a$), 3.59-3.67 (m, 4H, H$_b$), 7.98 (s, 2H, H$_f$), 9.79 (t, 2H, J = 5.7 Hz, H$_c$), 13.53 (s, 2H, H$_d$); HRMS (ESI/Q-TOF) m/z: [M+Na]$^+$ calculated for C$_{16}$H$_{20}$N$_6$O$_4$S$_2$Na 447.0880; found 447.0877.

_N,N'_-(disulfanediylbis(ethane-2,1-diyl))bis(3-(1-methyl-1_H_-pyrazol-4-yl)propanamide)
(Di-S7)
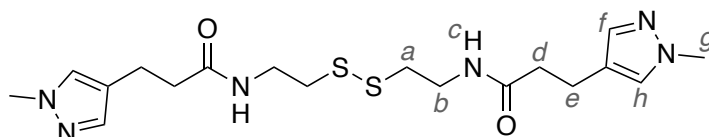
Cream solid, crude yield: 55%; ^{1}H NMR (MeOD, 400 MHz): δ 2.42 (t, 4H, J = 7.3 Hz, H$_d$), 2.72-2.79 (m, 8H, H$_a$, H$_e$), 3.45 (t, 4H, J = 6.6 Hz, H$_b$), 3.81 (s, 6H, H$_g$), 7.29 (s, 2H, H$_f$/H$_h$), 7.37 (s, 2H, H$_f$/H$_h$), 8.04-8.15 (br m, 2H, H$_c$); HRMS (ESI/Q-TOF) m/z: [M+H]$^+$ calculated for C$_{18}$H$_{29}$N$_6$O$_2$S$_2$ 425.1788; found 425.1798.

_N,N'_-(disulfanediylbis(ethane-2,1-diyl))bis(3-isopropylisoxazole-5-carboxamide)
(Di-S8)
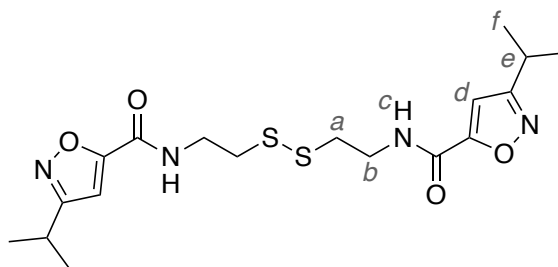
White solid, crude yield: 54%; ^{1}H NMR (CDCl$_3$, 400 MHz): δ 1.30 (d, 12H, J = 6.9 Hz, H$_f$), 2.95 (t, 4H, J = 6.4 Hz, H$_a$), 3.05-3.16 (m, 2H, H$_e$), 3.79 (app q, 4H, J = 6.3 Hz, H$_b$), 6.82 (s, 2H, H$_d$), 7.03-7.11 (br m, 2H, H$_c$); HRMS (ESI/Q-TOF) m/z: [M+H]$^+$ calculated for C$_{18}$H$_{27}$N$_4$O$_4$S$_2$ 427.1468; found 427.1480.

N,N'-(disulfanediylbis(ethane-2,1-diyl))bis(1-amino-4-methylcyclohex-3-ene-1-carboxamide)
(Di-S9)
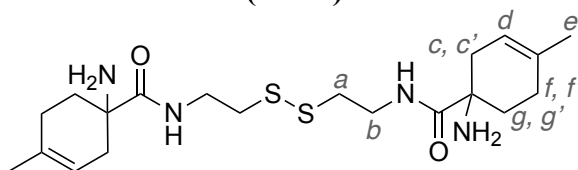
The amine group of the carboxylic acid starting material was Boc-protected. Obtained a pale yellow oil, crude yield: 12%; ^{1}H NMR (MeOD, 400 MHz): δ 1.75 (s, 6H, H$_e$), 1.97-2.06 (m, 2H, H$_g$), 2.09-2.37 (m, 8H, H$_c$^{maj}, H$_c$^{min}, H$_f$, H$_f$', H$_g$'), 2.67-2.80 (m, 2H, H$_c$'^{maj}, H$_c$'^{min}), 2.90 (t, 1.6H, J = 6.7 Hz, H$_a$^{maj}), 3.04-3.25 (m, 2.4H, H$_a$^{min}), 3.51-3.73 (m, 4H, H$_b$^{maj}, H$_b$^{min}), 5.45 (s, 2H, H$_d$); HRMS (ESI/Q-TOF) m/z: [M+H]$^+$ calculated for C$_{20}$H$_{35}$N$_4$O$_2$S$_2$ 427.2196; found 427.2194.

N,N'-(disulfanediylbis(ethane-2,1-diyl))bis(3-isopropyl-4,5-dihydroisoxazole-5-carboxamide)
(Di-S10)
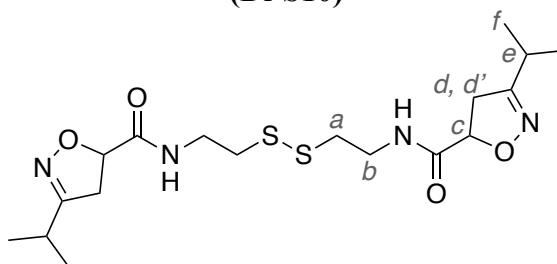
Orange solid, crude yield: 56%; ^{1}H NMR (MeOD, 400 MHz): δ 1.17 (d, 12H, J = 6.9 Hz, H$_f$), 2.65-2.74 (m, 2H, H$_e$), 2.82-2.91 (m, 4H, H$_a$), 3.19 (dd, 2H, J = 17.5 Hz, 5.8 Hz, H$_d$), 3.36 (dd, 2H, J = 17.5 Hz, 11.5 Hz, H$_d$'), 3.50-3.57 (m, 4H, H$_b$), 4.93 (dd, 2H, J = 11.5 Hz, 5.8 Hz, H$_c$); HRMS (ESI/Q-TOF) m/z: [M+H]$^+$ calculated for C$_{18}$H$_{31}$N$_4$O$_4$S$_2$ 431.1781; found 431.1767.

N,N'-(disulfanediylbis(ethane-2,1-diyl))bis(3-(2-oxotetrahydrofuran-3-yl)propanamide)
(Di-S11)
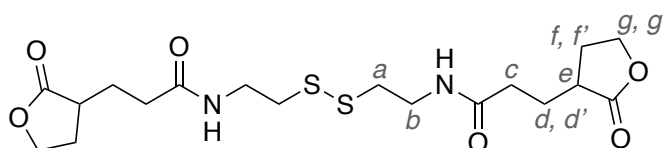
Cream solid, crude yield: 47%; ^{1}H NMR (MeOD, 400 MHz): δ 1.69-1.81 (m, 2H, H$_d$), 1.91-2.04 (m, 2H, H$_f$), 2.05-2.16 (m, 2H, H$_d$'), 2.36 (t, 4H, J = 7.6 Hz, H$_c$), 2.39-2.49 (m, 2H, H$_f$'), 2.60-2.70 (m, 2H, H$_e$), 2.84 (t, 4H, J = 6.7 Hz, H$_a$), 3.49 (t, 4H, J = 6.7 Hz, H$_b$), 4.17-4.26 (m,

2H, H$_g$), 4.36 (t, 2H, J = 8.7 Hz, 2.6 Hz, H$_g$'); HRMS (ESI/Q-TOF) m/z: [M+H]$^+$ calculated for C$_{18}$H$_{29}$N$_2$O$_6$S$_2$ 433.1462; found 433.1372.

(2*R*,2'*R*)-*N*,*N*'-(disulfanediylbis(ethane-2,1-diyl))bis(2-cyclohexyl-2-hydroxyacetamide) (Di-S12)
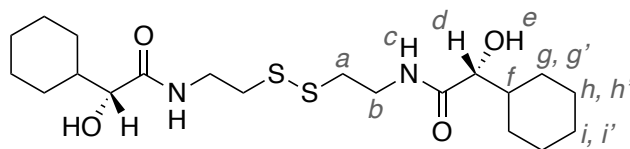
Cream solid, crude yield: 65%; ^{1}H NMR (DMSO-d$_6$, 400 MHz): δ 0.98-1.75 (m, 22H, H$_f$, H$_g$, H$_g$', H$_h$, H$_h$', H$_i$, H$_i$'), 2.80 (t, 4H, J = 6.9 Hz, H$_a$), 3.30-3.44 (m, 4H, H$_b$), 3.62-3.68 (m, 2H, H$_d$), 5.30 (d, 2H, J = 5.4 Hz, H$_e$), 7.86 (t, 2H, J = 5.8 Hz, H$_c$); HRMS (ESI/Q-TOF) m/z: [M+H]$^+$ calculated for C$_{20}$H$_{37}$N$_2$O$_4$S$_2$ 433.2189; found 433.2193.

N,*N*'-(disulfanediylbis(ethane-2,1-diyl))bis(1*H*-pyrrolo[2,3-*b*]pyridine-4-carboxamide) (Di-S13)
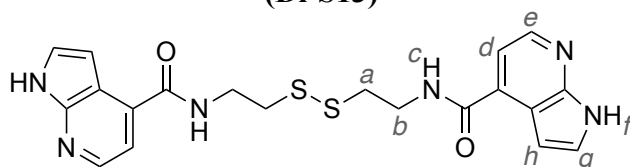
Cream solid, crude yield: 67%; ^{1}H NMR (DMSO-d$_6$, 400 MHz): δ 3.00 (t, 4H, J = 6.8 Hz, H$_a$), 3.63 (app q, 4H, J = 6.4 Hz, H$_b$), 6.80 (dd, 2H, J = 3.4 Hz, 1.9 Hz, H$_h$), 7.35 (d, 2H, J = 4.9 Hz, H$_d$), 7.55-7.60 (m, 2H, H$_g$), 8.29 (d, 2H, J = 4.9 Hz, H$_e$), 8.69 (t, 2H, J = 5.5 Hz, H$_c$), 11.85 (br s, 2H, H$_f$); HRMS (ESI/Q-TOF) m/z: [M+H]$^+$ calculated for C$_{20}$H$_{21}$N$_6$O$_2$S$_2$ 441.1162; found 441.1163.

N,*N*'-(disulfanediylbis(ethane-2,1-diyl))bis(benzo[*c*]isoxazole-3-carboxamide) (Di-S14)
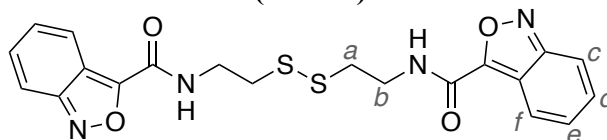
Brown solid, crude yield: 61%; ^{1}H NMR (MeOD, 400 MHz): δ 3.05 (t, 4H, J = 6.9 Hz, H$_a$), 3.79 (t, 4H, J = 6.9 Hz, H$_b$), 7.20 (dd, 2H, J = 8.8 Hz, 6.4 Hz, H$_d$/H$_e$), 7.42 (ddd, 2H, J = 9.2 Hz, 6.4 Hz, 0.9 Hz, H$_d$/H$_e$), 7.63 (d, 2H, J = 9.2 Hz, H$_c$/H$_f$), 7.95 (d, 2H, J = 8.8 Hz, H$_c$/H$_f$); HRMS (ESI/Q-TOF) m/z: [M+H]$^+$ calculated for C$_{20}$H$_{19}$N$_4$O$_4$S$_2$ 443.0842; found 443.0844.

N,N'-(disulfanediylbis(ethane-2,1-diyl))bis(isoindoline-1-carboxamide) (Di-S15)
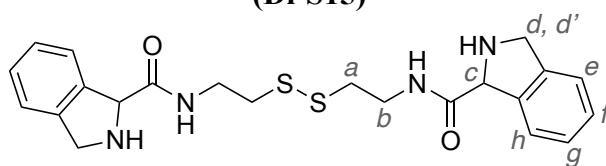
The amine group of the carboxylic acid starting material was Boc-protected. Obtained a dark purple solid, crude yield: 36%; ^{1}H NMR (MeOD, 400 MHz): δ 2.74 (t, 2.2H, $J = 6.9$ Hz, H_a^{maj}), 2.89 (t, 1.8H, $J = 6.5$ Hz, H_a^{min}), 3.35-3.72 (m, 4H, H_b^{maj}, H_b^{min}), 4.63-4.71 (m, 2H, H_d^{maj}, H_d^{min}), 4.75-4.85 (m, 2H, $H_{d'}^{maj}$, $H_{d'}^{min}$), 5.51 (s, 0.9H, H_c^{min}), 5.56 (s, 1.1H, H_c^{maj}), 7.39-7.49 (m, 6H, H_e, H_f, H_g), 7.55-7.65 (m, 2H, H_h); HRMS (ESI/Q-TOF) m/z: [M+H]$^+$ calculated for $C_{22}H_{27}N_4O_2S_2$ 443.1570; found 443.1520.

N,N'-(disulfanediylbis(ethane-2,1-diyl))bis(2,3-dihydrobenzofuran-5-carboxamide) (Di-S16)
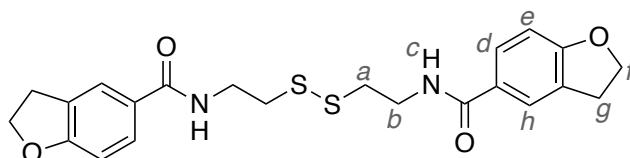
Orange solid, crude yield: 55%; ^{1}H NMR (CDCl$_3$, 400 MHz): δ 2.97 (t, 4H, $J = 6.4$ Hz, H_a), 3.20 (t, 4H, $J = 8.8$ Hz, H_g), 3.76 (app q, 4H, $J = 6.2$ Hz, H_b), 4.61 (t, 4H, $J = 8.8$ Hz, H_f), 6.75 (d, 2H, $J = 8.3$ Hz, H_e), 6.94 (t, 2H, $J = 5.7$ Hz, H_c), 7.62 (dd, 2H, $J = 8.3$ Hz, 1.6 Hz, H_d), 7.71 (br s, 2H, H_h); HRMS (ESI/Q-TOF) m/z: [M+H]$^+$ calculated for $C_{22}H_{25}N_2O_4S_2$ 445.1250; found 445.1250.

N,N'-(disulfanediylbis(ethane-2,1-diyl))bis(2-phenylbutanamide) (Di-S17)
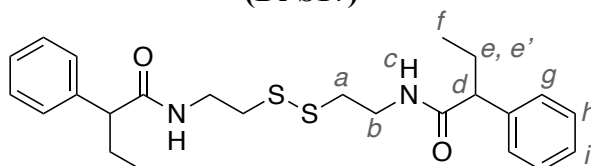
Yellow oil, crude yield: 52%; ^{1}H NMR (CDCl$_3$, 400 MHz): δ 0.90 (t, 6H, $J = 6.5$ Hz, H_f), 1.74-1.88 (m, 2H, H_e), 2.13-2.26 (m, 2H, $H_{e'}$), 2.64-2.76 (m, 4H, H_a), 3.32 (t, 2H, $J = 7.4$ Hz, H_d), 3.41-3.53 (m, 4H, H_b), 6.30-6.42 (m, 2H, H_c), 7.22-7.37 (m, 10H, H_g, H_h, H_i); HRMS (ESI/Q-TOF) m/z: [M+H]$^+$ calculated for $C_{24}H_{33}N_2O_2S_2$ 445.1978; found 445.1977. NMR spectrum referenced to DCM which was added as an internal standard (5.30 ppm).

N,N'-(disulfanediylbis(ethane-2,1-diyl))bis(4-(dimethylamino)benzamide) (Di-S18)
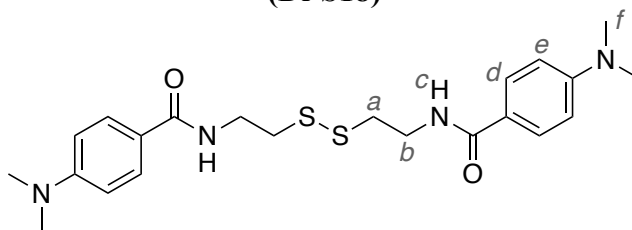
Yellow solid, crude yield: 57%; ^{1}H NMR (CDCl$_3$, 400 MHz): δ 2.93 (t, 4H, J = 6.4 Hz, H$_a$), 2.99 (s, 12H, H$_f$), 3.74 (app q, 4H, J = 6.1 Hz, H$_b$), 6.63 (d, 4H, J = 8.7 Hz, H$_e$), 6.93-7.00 (br m, 2H, H$_c$), 7.75 (d, 4H, J = 8.7 Hz, H$_d$); HRMS (ESI/Q-TOF) m/z: [M+Na]$^+$ calculated for C$_{22}$H$_{30}$N$_4$O$_2$S$_2$Na 469.1702; found 469.1708.

N,N'-(disulfanediylbis(ethane-2,1-diyl))bis(4-nitrobenzamide) (Di-S19)
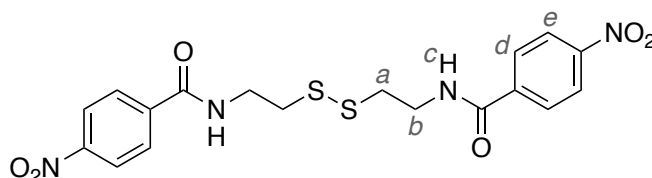
White solid, crude yield: 69%; ^{1}H NMR (DMSO-d$_6$, 400 MHz): δ 2.96 (t, 4H, J = 6.8 Hz, H$_a$), 3.59 (app q, 4H, J = 6.4 Hz, H$_b$), 8.06 (d, 4H, J = 8.8 Hz, H$_d$/H$_e$), 8.31 (d, 4H, J = 8.8 Hz, H$_d$/H$_e$), 8.99 (t, 2H, J = 5.4 Hz, H$_c$); HRMS (ESI/Q-TOF) m/z: [M+Na]$^+$ calculated for C$_{18}$H$_{18}$N$_4$O$_6$S$_2$Na 473.0560; found 473.0558.

N,N'-(disulfanediylbis(ethane-2,1-diyl))bis(4,5,6,7-tetrahydrobenzo[d]isoxazole-3-carboxamide) (Di-S20)
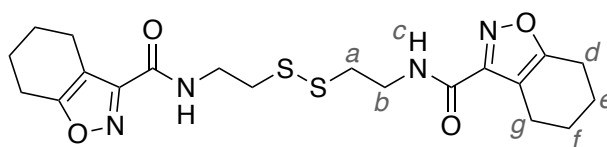
Orange solid, crude yield: 59%; ^{1}H NMR (CDCl$_3$, 400 MHz): δ 1.69-1.89 (m, 8H, H$_e$, H$_f$), 2.70 (app q, 8H, J = 5.9 Hz, H$_d$, H$_g$), 2.92 (t, 4H, J = 6.5 Hz, H$_a$), 3.74 (app q, 4H, J = 6.3 Hz, H$_b$), 7.20-7.28 (br m, 2H, H$_c$); HRMS (ESI/Q-TOF) m/z: [M+Na]$^+$ calculated for C$_{20}$H$_{26}$N$_4$O$_4$S$_2$Na 473.1288; found 473.1291.

N,N'-(disulfanediylbis(ethane-2,1-diyl))bis(4-propionyl-1H-pyrrole-2-carboxamide)
(Di-S21)
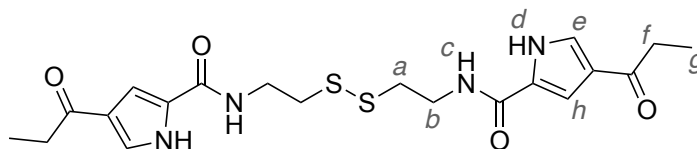
Cream solid, crude yield: 46%; ^{1}H NMR (DMSO-d$_6$, 400 MHz): δ 1.03 (t, 6H, J = 7.3 Hz, H$_g$), 2.75 (q, 4H, J = 7.3 Hz, H$_f$), 2.89 (t, 4H, J = 6.8 Hz, H$_a$), 3.51 (app q, 4H, J = 6.3 Hz, H$_b$), 7.19 (br s, 2H, H$_h$), 7.57-7.62 (m, 2H, H$_e$), 8.42 (t, 2H, J = 5.5 Hz, H$_c$), 12.08 (s, 2H, H$_d$); HRMS (ESI/Q-TOF) m/z: [M+Na]$^+$ calculated for C$_{20}$H$_{26}$N$_4$O$_4$S$_2$Na 473.1288; found 473.1285.

N,N'-(disulfanediylbis(ethane-2,1-diyl))bis(2-nitronicotinamide)
(Di-S22)
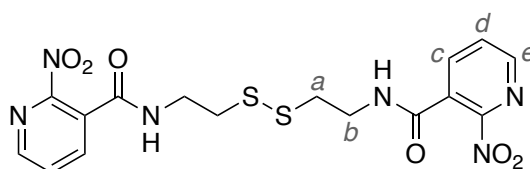
Yellow solid, crude yield: 46%; ^{1}H NMR (MeOD, 400 MHz): δ 2.98 (t, 4H, J = 6.7 Hz, H$_a$), 3.70 (t, 4H, J = 6.7 Hz, H$_b$), 7.81 (dd, 2H, J = 7.7 Hz, 4.8 Hz, H$_d$), 8.18 (dd, 2H, J = 7.7 Hz, 1.7 Hz, H$_c$), 8.61 (dd, 2H, J = 4.8 Hz, 1.7 Hz, H$_e$); HRMS (ESI/Q-TOF) m/z: [M+H]$^+$ calculated for C$_{16}$H$_{17}$N$_6$O$_6$S$_2$ 453.0646; found 453.0654.

N,N'-(disulfanediylbis(ethane-2,1-diyl))bis(2-(methylthio)benzamide)
(Di-S23)
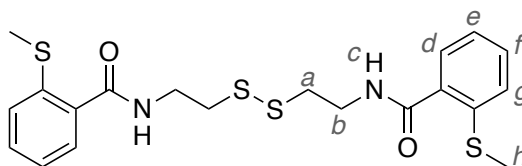
Cream solid, crude yield: 54%; ^{1}H NMR (CDCl$_3$, 400 MHz): δ 2.45 (s, 6H, H$_h$), 2.99 (t, 4H, J = 6.3 Hz, H$_a$), 3.80 (app q, 4H, J = 6.2 Hz, H$_b$), 6.92-7.01 (br m, 2H, H$_c$), 7.17 (td, 2H, J = 7.5 Hz, 1.1 Hz, H$_e$), 7.30 (dd, 2H, J = 7.9 Hz, 1.1 Hz, H$_g$), 7.37 (td, 2H, J = 7.9 Hz, 1.5 Hz, H$_f$), 7.56 (dd, 2H, J = 7.5 Hz, 1.5 Hz, H$_d$); HRMS (ESI/Q-TOF) m/z: [M+H]$^+$ calculated for C$_{20}$H$_{25}$N$_2$O$_2$S$_4$ 453.0793; found 453.0801.

N,N'-(disulfanediylbis(ethane-2,1-diyl))bis(4-isopropyl-1,2,3-thiadiazole-5-carboxamide)
(Di-S25)
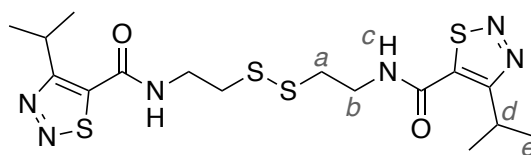
Orange solid, crude yield: 76%; ^{1}H NMR (CDCl$_3$, 400 MHz): δ 1.46 (d, 12H, J = 6.9 Hz, H$_e$), 2.97 (t, 4H, J = 6.4 Hz, H$_a$), 3.59-3.72 (m, 2H, H$_d$), 3.78 (app q, 4H, J = 6.3 Hz, H$_b$), 6.71-6.83 (br m, 2H, H$_c$); HRMS (ESI/Q-TOF) m/z: [M+H]$^+$ calculated for C$_{16}$H$_{25}$N$_6$O$_2$S$_4$ 461.0916; found 461.0914.

N,N'-(disulfanediylbis(ethane-2,1-diyl))bis(5-chloro-2-methylpyrimidine-4-carboxamide)
(Di-S26)
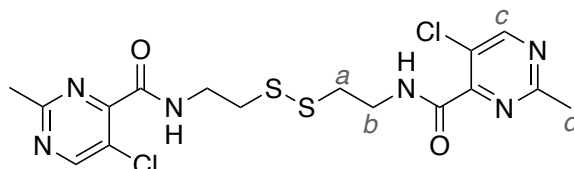
Dark orange solid, crude yield: 46%; ^{1}H NMR (MeOD, 400 MHz): δ 2.70 (s, 6H, H$_d$), 3.00 (t, 4H, J = 6.8 Hz, H$_a$), 3.73 (t, 4H, J = 6.8 Hz, H$_b$), 8.80 (s, 2H, H$_c$); HRMS (ESI/Q-TOF) m/z: [M+H]$^+$ calculated for C$_{16}$H$_{19}$N$_6$OS$_2$ 461.0382; found 461.0383.

N,N'-(disulfanediylbis(ethane-2,1-diyl))bis(1,8-naphthyridine-2-carboxamide)
(Di-S28)
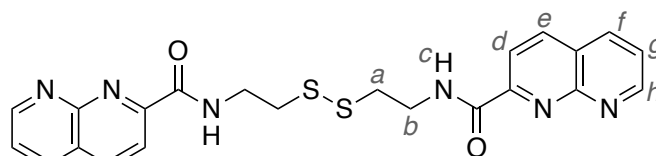
Dark orange oil, crude yield: 38%; ^{1}H NMR (DMSO-d$_6$, 400 MHz): δ 3.06 (t, 4H, J = 6.9 Hz, H$_a$), 3.71 (app q, 4H, J = 6.6 Hz, H$_b$), 7.73 (dd, 2H, J = 8.1 Hz, 4.2 Hz, H$_g$), 8.27 (d, 2H, J = 8.5 Hz, H$_d$), 8.58 (dd, 2H, J = 8.1 Hz, 2.0 Hz, H$_f$), 8.68 (d, 2H, J = 8.5 Hz, H$_e$), 9.20 (dd, 2H, J = 4.2 Hz, 2.0 Hz, H$_h$), 9.25 (t, 2H, J = 6.1 Hz, H$_c$); HRMS (ESI/Q-TOF) m/z: [M+H]$^+$ calculated for C$_{22}$H$_{21}$N$_6$O$_2$S$_2$ 465.1162; found 465.1174.

N,N'-(disulfanediylbis(ethane-2,1-diyl))bis(3-(3-chloroisoxazol-5-yl)propanamide) (Di-S30)
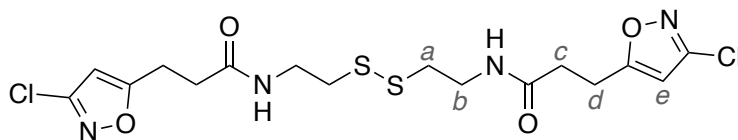
Cream solid, crude yield: 58%; ^{1}H NMR (MeOD, 400 MHz): δ 2.61 (t, 4H, J = 7.3 Hz, H_c), 2.80 (t, 4H, J = 6.7 Hz, H_a), 3.08 (t, 4H, J = 7.3 Hz, H_d), 3.48 (t, 4H, J = 6.7 Hz, H_b), 6.31 (s, 2H, H_e); HRMS (ESI/Q-TOF) m/z: $[M+H]^+$ calculated for $C_{16}H_{21}N_4OS_2$ 467.0376; found 467.0374.

N,N'-(disulfanediylbis(ethane-2,1-diyl))bis(3-(3-hydroxyprop-1-yn-1-yl)benzamide) (Di-S31)
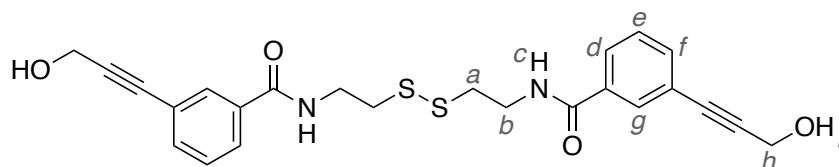
Yellow oil, crude yield: 80%; ^{1}H NMR (DMSO-d_6, 400 MHz): δ 2.87-2.97 (m, 4H, H_a), 3.49-3.60 (m, 4H, H_b), 4.32 (d, 4H, J = 5.9 Hz, H_h), 5.36 (t, 2H, J = 5.9 Hz, H_i), 7.36-8.01 (m, 8H, H_d, H_e, H_f, H_g), 8.70-8.79 (m, 2H, H_c); HRMS (ESI/Q-TOF) m/z: $[M+H]^+$ calculated for $C_{24}H_{25}N_2O_4S_2$ 469.1250; found 469.1248.

N,N'-(disulfanediylbis(ethane-2,1-diyl))bis(chromane-3-carboxamide) (Di-S33)
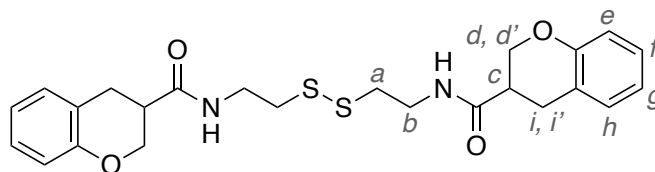
Cream solid, crude yield: 51%; ^{1}H NMR (MeOD, 400 MHz): δ 2.79-2.95 (m, 8H, H_a, H_c, H_i), 2.98-3.10 (m, 2H, H_i'), 3.53 (t, 4H, J = 6.7 Hz, H_b), 3.92-4.02 (m, 2H, H_d), 4.29-4.40 (m, 2H, H_d'), 6.74 (d, 2H, J = 8.0 Hz, H_h), 6.78-6.85 (m, 2H, H_f), 7.00-7.10 (m, 4H, H_e, H_g); HRMS (ESI/Q-TOF) m/z: $[M+H]^+$ calculated for $C_{24}H_{29}N_2O_4S_2$ 473.1563; found 473.1568.

N,N'-(disulfanediylbis(ethane-2,1-diyl))bis(benzo[*b*]thiophene-2-carboxamide)
(Di-S34)
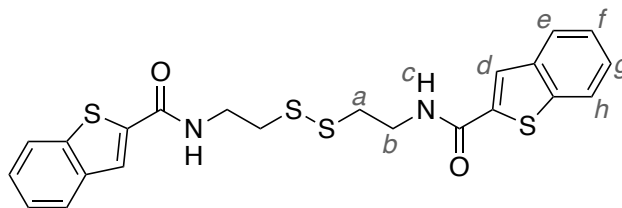
White solid, crude yield: 51%; ^{1}H NMR (CDCl$_3$, 400 MHz): δ 3.03 (t, 4H, J = 6.4 Hz, H$_a$), 3.83 (app q, 4H, J = 6.3 Hz, H$_b$), 7.16 (t, 2H, J = 5.5 Hz, H$_c$), 7.34-7.46 (m, 4H, H$_f$, H$_g$), 7.77-7.89 (m, 4H, H$_e$, H$_h$), 7.94 (s, 2H, H$_d$); HRMS (ESI/Q-TOF) m/z: [M+H]$^+$ calculated for C$_{22}$H$_{21}$N$_2$O$_2$S$_4$ 473.0480; found 473.0480.

N,N'-(disulfanediylbis(ethane-2,1-diyl))bis(benzo[*d*]thiazole-6-carboxamide)
(Di-S35)
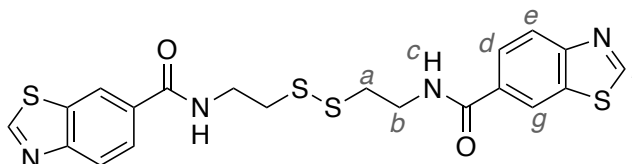
Cream solid, crude yield: 52%; ^{1}H NMR (CDCl$_3$, 400 MHz): δ 3.04 (t, 4H, J = 6.4 Hz, H$_a$), 3.86 (app q, 4H, J = 6.2 Hz, H$_b$), 7.24-7.30 (br m, 2H, H$_c$), 7.95 (dd, 2H, J = 8.5 Hz, 1.7 Hz, H$_d$), 8.14 (d, 2H, J = 8.5 Hz, H$_e$), 8.53 (d, 2H, J = 1.7 Hz, H$_g$), 9.09 (s, 2H, H$_f$); HRMS (ESI/Q-TOF) m/z: [M+H]$^+$ calculated for C$_{20}$H$_{19}$N$_4$O$_2$S$_4$ 475.0385; found 475.0379.

N,N'-(disulfanediylbis(ethane-2,1-diyl))bis(3-acetyl-4,5-dimethyl-1*H*-pyrrole-2-carboxamide)
(Di-S36)
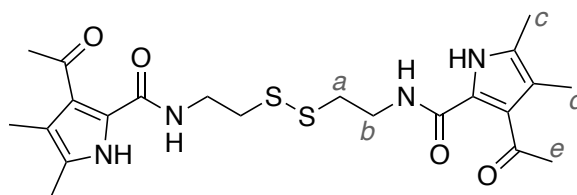
Cream solid, crude yield: 36%; ^{1}H NMR (MeOD, 400 MHz): δ 2.43 (s, 6H, H$_c$/H$_d$/H$_e$), 2.47 (s, 6H, H$_c$/H$_d$/H$_e$), 2.50 (s, 6H, H$_c$/H$_d$/H$_e$), 2.96 (t, 4H, J = 6.7 Hz, H$_a$), 3.68 (t, 4H, J = 6.7 Hz, H$_b$); HRMS (ESI/Q-TOF) m/z: [M+H]$^+$ calculated for C$_{22}$H$_{31}$N$_4$O$_4$S$_2$ 479.1781; found 479.1784.

***N,N'*-(disulfanediylbis(ethane-2,1-diyl))bis(5-acetyl-2,4-dimethyl-1*H*-pyrrole-3-carboxamide)**
(Di-S37)
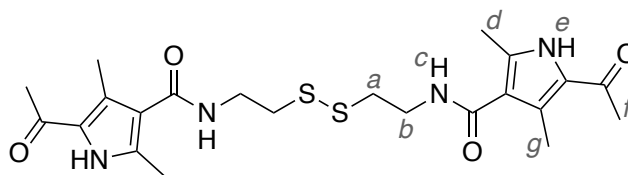
Dark blue solid, crude yield: 52%; ^{1}H NMR (DMSO-d_6, 400 MHz): δ 2.29 (s, 6H, H$_d$/H$_f$/H$_g$), 2.33 (s, 6H, H$_d$/H$_f$/H$_g$), 2.34 (s, 6H, H$_d$/H$_f$/H$_g$), 2.90 (t, 4H, J = 6.7 Hz, H$_a$), 3.49 (app q, 4H, J = 6.3 Hz, H$_b$), 7.72 (t, 2H, J = 5.6 Hz, H$_c$), 11.45 (s, 2H, H$_e$); HRMS (ESI/Q-TOF) m/z: [M+H]$^+$ calculated for C$_{22}$H$_{31}$N$_4$O$_4$S$_2$ 479.1781; found 479.1775.

(2*S*,2'*S*)-*N,N'*-(disulfanediylbis(ethane-2,1-diyl))bis(2-amino-3-(4-hydroxyphenyl)propanamide)
(Di-S39)
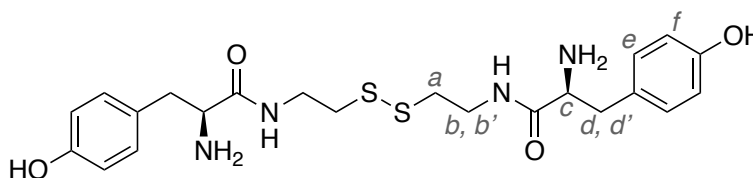
Carboxylic acid starting material was *tert*-butyl- and Fmoc- protected on the phenolic hydroxyl and amine groups, respectively. Obtained a white solid, crude yield: 33%; ^{1}H NMR (MeOD, 400 MHz): δ 2.65-2.80 (m, 4H, H$_a$), 2.93-3.19 (m, 4H, H$_d$, H$_d$'), 3.37-3.63 (m, 4H, H$_b$, H$_b$'), 4.08 (t, 2H, J = 7.3 Hz, H$_c$), 6.75-6.80 (m, 4H, H$_f$), 7.08-7.15 (m, 4H, H$_e$); HRMS (ESI/Q-TOF) m/z: [M+H]$^+$ calculated for C$_{22}$H$_{31}$N$_4$O$_4$S$_2$ 479.1781; found 479.1777.

***N,N'*-(disulfanediylbis(ethane-2,1-diyl))bis(2-(dimethylamino)-4-methylpyrimidine-5-carboxamide)**
(Di-S40)
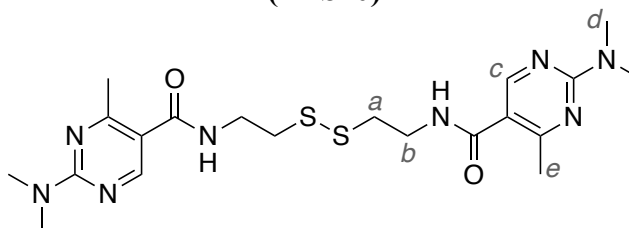
Orange solid, crude yield: 63%; ^{1}H NMR (MeOD, 400 MHz): δ 2.48 (s, 6H, H$_e$), 2.97 (t, 4H, J = 6.7 Hz, H$_a$), 3.20 (s, 12H, H$_d$), 3.66 (t, 4H, J = 6.7 Hz, H$_b$), 8.33 (s, 2H, H$_c$); HRMS (ESI/Q-TOF) m/z: [M+H]$^+$ calculated for C$_{20}$H$_{31}$N$_8$O$_2$S$_2$ 479.2006; found 479.2010.

N,N'-(disulfanediylbis(ethane-2,1-diyl))bis(1-(*tert*-butyl)-5-methyl-1*H*-pyrazole-3-carboxamide)
(Di-S41)
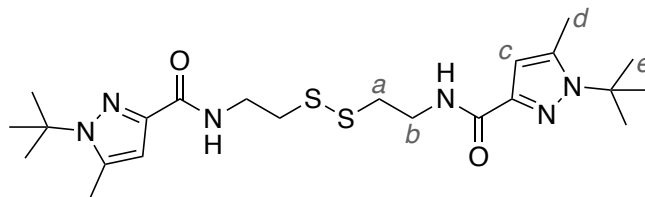
Pale yellow solid, crude yield: 56%; ^{1}H NMR (MeOD, 400 MHz): δ 1.64 (s, 18H, H$_e$), 2.47 (s, 6H, H$_d$), 2.95 (t, 4H, J = 6.9 Hz, H$_a$), 3.66 (t, 4H, J = 6.9 Hz, H$_b$), 6.48 (s, 2H, H$_c$); HRMS (ESI/Q-TOF) m/z: [M+H]$^+$ calculated for C$_{22}$H$_{37}$N$_6$O$_2$S$_2$ 481.2414; found 481.2422.

N,N'-(disulfanediylbis(ethane-2,1-diyl))bis(4,5,6,7-tetrahydrobenzo[*c*]thiophene-1-carboxamide)
(Di-S42)
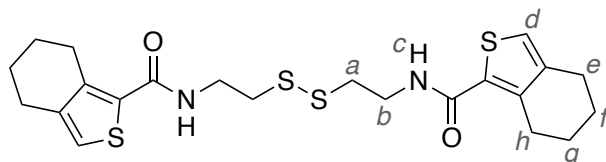
Orange solid, crude yield: 70%; ^{1}H NMR (CDCl$_3$, 400 MHz): δ 1.66-1.81 (m, 8H, H$_f$, H$_g$), 2.69 (t, 4H, J = 5.8 Hz, H$_e$), 2.88-3.01 (m, 8H, H$_a$, H$_h$), 3.73 (app q, 4H, J = 6.1 Hz, H$_b$), 6.36 (t, 2H, J = 5.3 Hz, H$_c$), 6.94 (s, 2H, H$_d$); HRMS (ESI/Q-TOF) m/z: [M+H]$^+$ calculated for C$_{22}$H$_{28}$N$_2$O$_2$S$_4$Na 503.0926; found 503.0923.

N,N'-(disulfanediylbis(ethane-2,1-diyl))bis(4,5,6,7-tetrahydrobenzo[*d*]thiazole-2-carboxamide)
(Di-S43)
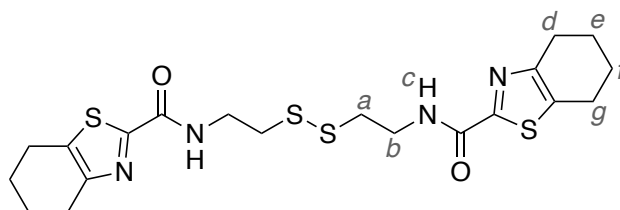
Orange solid, crude yield: 63%; ^{1}H NMR (CDCl$_3$, 400 MHz): δ 1.80-1.91 (m, 8H, H$_e$, H$_f$), 2.71-2.85 (m, 8H, H$_d$, H$_g$), 2.91 (t, 4H, J = 6.4 Hz, H$_a$), 3.75 (app q, 4H, J = 6.4 Hz, H$_b$), 7.54 (t, 2H, J = 5.7 Hz, H$_c$); HRMS (ESI/Q-TOF) m/z: [M+H]$^+$ calculated for C$_{20}$H$_{27}$N$_4$O$_2$S$_4$ 483.1011; found 483.1011.

N,N'-(disulfanediylbis(ethane-2,1-diyl))bis(2-(5-methyl-2,4-dioxo-3,4-dihydropyrimidin-1(2H)-yl)acetamide)
(Di-S44)
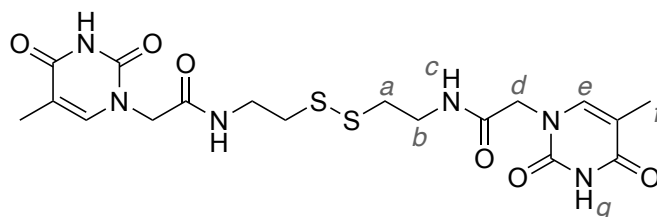
White solid, crude yield: 45%; ^{1}H NMR (DMSO-d$_6$, 400 MHz): δ 1.74 (s, 6H, H$_f$), 2.78 (t, 4H, J = 6.8 Hz, H$_a$), 3.37 (app q, 4H, J = 6.4 Hz, H$_b$), 4.27 (s, 4H, H$_d$), 7.42 (s, 2H, H$_e$), 8.33 (t, 2H, J = 5.5 Hz, H$_c$), 11.26 (s, 2H, H$_g$); HRMS (ESI/Q-TOF) m/z: [M+H]$^+$ calculated for C$_{18}$H$_{25}$N$_6$O$_6$S$_2$ 485.1272; found 485.1273.

N,N'-(disulfanediylbis(ethane-2,1-diyl))bis(thieno[3,2-b]thiophene-2-carboxamide)
(Di-S45)
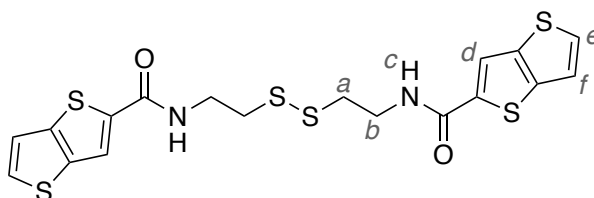
Cream solid, crude yield: 50%; ^{1}H NMR (CDCl$_3$, 400 MHz): δ 3.02 (t, 4H, J = 6.4 Hz, H$_a$), 3.82 (app q, 4H, J = 6.2 Hz, H$_b$), 7.00-7.08 (br m, 2H, H$_c$), 7.28 (d, 2H, J = 5.2 Hz, H$_f$), 7.53 (d, 2H, J = 5.2 Hz, H$_e$), 7.92 (s, 2H, H$_d$); HRMS (ESI/Q-TOF) m/z: [M+Na]$^+$ calculated for C$_{18}$H$_{16}$N$_2$O$_2$S$_6$Na 506.9428; found 506.9425.

N,N'-(disulfanediylbis(ethane-2,1-diyl))bis(2-chloro-6-methoxyisonicotinamide)
(Di-S46)
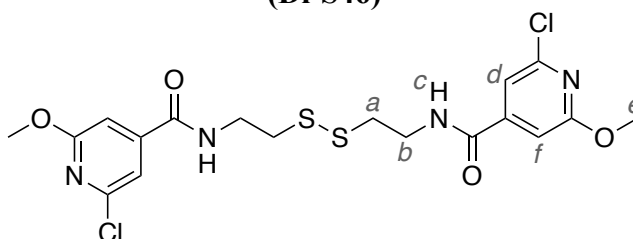
White solid, crude yield: 73%; ^{1}H NMR (CDCl$_3$, 400 MHz): δ 2.99 (t, 4H, J = 6.4 Hz, H$_a$), 3.78 (app q, 4H, J = 6.3 Hz, H$_b$), 3.98 (s, 6H, H$_e$), 7.07-7.12 (m, 4H, H$_c$, H$_d$/H$_f$), 7.31 (d, 2H, J = 1.1 Hz, H$_d$/H$_f$); HRMS (ESI/Q-TOF) m/z: [M+H]$^+$ calculated for C$_{18}$H$_{21}$N$_4$OS$_2$ 491.0376; found 491.0375.

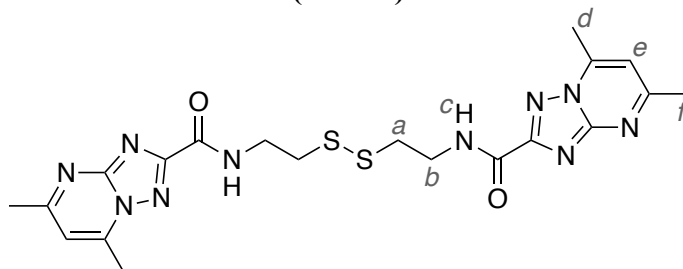**N,N'-(disulfanediylbis(ethane-2,1-diyl))bis(6,6-dimethyl-5-oxothiomorpholine-3-carboxamide)**
(Di-S47)
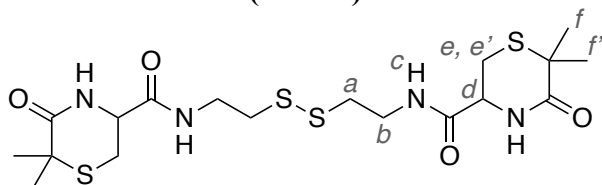
Yellow solid, crude yield: 66%; ^{1}H NMR (MeOD, 400 MHz): δ 1.51 (s, 6H, H$_f$), 1.55 (s, 6H, H$_f$'), 2.88 (t, 4H, J = 6.7 Hz, H$_a$), 3.07 (dd, 2H, J = 14.3 Hz, 5.6 Hz, H$_e$), 3.18 (dd, 2H, J = 14.3 Hz, 4.4 Hz, H$_e$'), 3.53-3.60 (m, 4H, H$_b$), 4.28-4.32 (m, 2H, H$_d$), 8.32 (t, 2H, J = 5.6 Hz, H$_c$); HRMS (ESI/Q-TOF) m/z: [M+H]$^+$ calculated for C$_{18}$H$_{31}$N$_4$O$_4$S$_4$ 495.1223; found 495.1217.

N,N'-(disulfanediylbis(ethane-2,1-diyl))bis(2-(2-methylimidazo[1,2-a]pyridin-3-yl)acetamide)
(Di-S48)
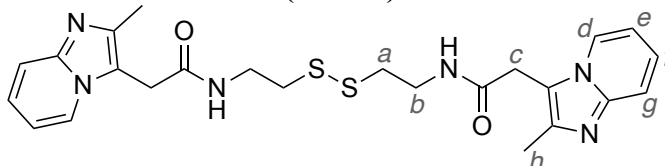
Orange solid, crude yield: 11%; ^{1}H NMR (MeOD, 400 MHz): δ 2.55 (d, 6H, J = 3.0 Hz, H$_h$), 2.84-2.90 (m, 4H, H$_a$), 3.51-3.59 (m, 4H, H$_b$), 4.10 (d, 4H, J = 2.2 Hz, H$_c$), 7.44-7.52 (m, 2H, H$_e$), 7.80-7.88 (m, 2H, H$_g$), 7.89-7.98 (m, 2H, H$_f$), 8.64-8.70 (m, 2H, H$_d$); HRMS (ESI/Q-TOF) m/z: [M+H]$^+$ calculated for C$_{24}$H$_{29}$N$_6$O$_2$S$_2$ 497.1788; found 497.1786.

N,N'-(disulfanediylbis(ethane-2,1-diyl))bis(5,7-dimethyl-[1,2,4]triazolo[1,5-a]pyrimidine-2-carboxamide)
(Di-S49)

Yellow solid, crude yield: 72%; ^{1}H NMR (CDCl$_3$, 400 MHz): δ 2.65 (s, 6H, H$_d$/H$_f$), 2.83 (s, 6H, H$_d$/H$_f$), 2.96 (t, 4H, J = 6.4 Hz, H$_a$), 3.84 (app q, 4H, J = 6.3 Hz, H$_b$), 6.89 (s, 2H, H$_e$), 7.98 (t, 2H, J = 6.0 Hz, H$_c$); HRMS (ESI/Q-TOF) m/z: [M+H]$^+$ calculated for C$_{20}$H$_{25}$N$_{10}$O$_2$S$_2$ 501.1598; found 501.1604.

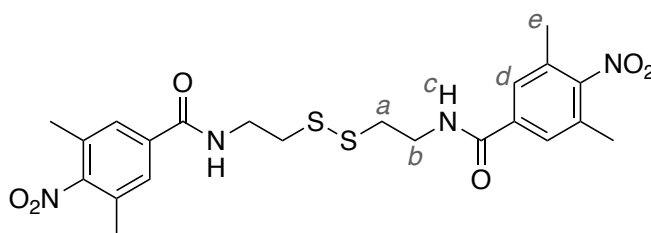**N,N'-(disulfanediylbis(ethane-2,1-diyl))bis(5-chloro-4-methoxythiophene-3-carboxamide)**
(Di-S50)
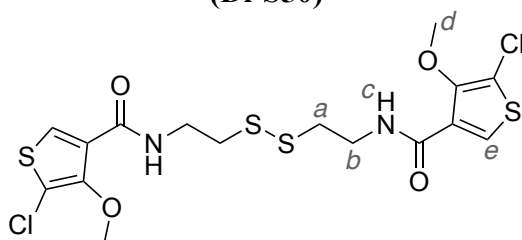
Orange oil, crude yield: 57%; ^{1}H NMR (CDCl$_3$, 400 MHz): δ 2.91 (t, 4H, J = 6.2 Hz, H$_a$), 3.75 (app q, 4H, J = 6.1 Hz, H$_b$), 4.05 (s, 6H, H$_d$), 7.66-7.76 (br m, 2H, H$_c$), 7.85 (s, 2H, H$_e$); HRMS (ESI/Q-TOF) m/z: [M+Na]$^+$ calculated for C$_{16}$H$_{18}$N$_2$OS$_4$Na 522.9419; found 522.9416.

N,N'-(disulfanediylbis(ethane-2,1-diyl))bis(5-methyl-2-(trifluoromethyl)furan-3-carboxamide)
(Di-S51)
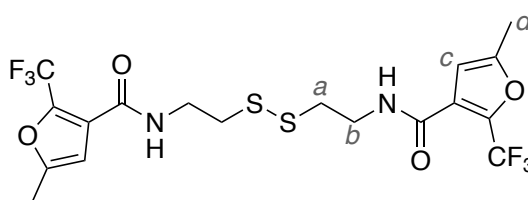
Blue oil, crude yield: 55%; ^{1}H NMR (MeOD, 400 MHz): δ 2.35 (s, 6H, H$_d$), 2.92 (t, 4H, J = 6.7 Hz, H$_a$), 3.62 (t, 4H, J = 6.7 Hz, H$_b$), 6.44 (s, 2H, H$_c$); HRMS (ESI/Q-TOF) m/z: [M+H]$^+$ calculated for C$_{18}$H$_{19}$F$_6$N$_2$O$_4$S$_2$ 505.0685; found 505.0687.

**N,N'-(disulfanediylbis(ethane-2,1-diyl))bis(3,5-dimethyl-4-nitrobenzamide)**
(Di-S53)

White solid, crude yield: 73%; ^{1}H NMR (CDCl$_3$, 400 MHz): δ 2.33 (s, 12H, H$_e$), 3.00 (t, 4H, J = 6.4 Hz, H$_a$), 3.81 (app q, 4H, J = 6.2 Hz, H$_b$), 6.92-7.00 (br m, 2H, H$_c$), 7.59 (s, 4H, H$_d$); HRMS (ESI/Q-TOF) m/z: [M+H]$^+$ calculated for C$_{22}$H$_{27}$N$_4$O$_6$S$_2$ 507.1367; found 507.1362.

N,N'-(disulfanediylbis(ethane-2,1-diyl))bis(5-oxo-2,3-dihydro-5*H*-thiazolo[3,2-*a*]pyrimidine-6-carboxamide)
**(Di-S54)**
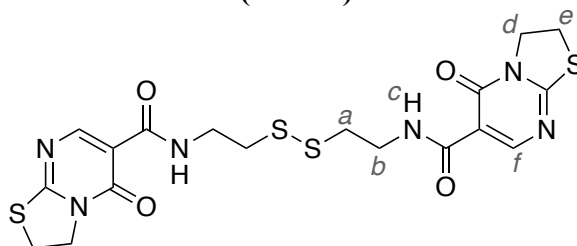
White solid, crude yield: 65%; ^{1}H NMR (DMSO-d$_6$, 400 MHz): δ 2.89 (t, 4H, J = 6.5 Hz, H$_a$), 3.55-3.65 (m, 8H, H$_b$, H$_e$), 4.47 (t, 4H, J = 7.9 Hz, H$_d$), 8.48 (s, 2H, H$_f$), 9.06 (t, 2H, J = 5.6 Hz, H$_c$); HRMS (ESI/Q-TOF) m/z: [M+H]$^+$ calculated for C$_{18}$H$_{21}$N$_6$O$_4$S$_4$ 513.0502; found 513.0503.

N,N'-(disulfanediylbis(ethane-2,1-diyl))bis(2-(methylsulfonyl)benzamide)
(Di-S55)
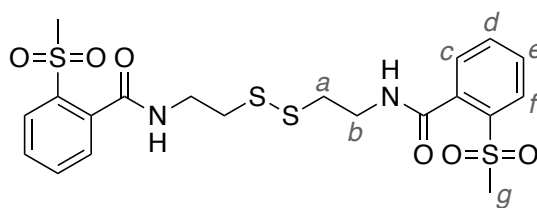
White solid, crude yield: 59%; ^{1}H NMR (MeOD, 400 MHz): δ 3.00 (t, 4H, J = 6.8 Hz, H$_a$), 3.30 (s, 6H, H$_g$), 3.70 (t, 4H, J = 6.8 Hz, H$_b$), 7.58 (dd, 2H, J = 7.5 Hz, 1.3 Hz, H$_c$/H$_f$), 7.67 (td, 2H, J = 7.7 Hz, 1.3 Hz, H$_d$/H$_e$), 7.74 (td, 2H, J = 7.5 Hz, 1.2 Hz, H$_d$/H$_e$), 8.03 (dd, 2H, J = 7.7 Hz, 1.2 Hz, H$_c$/H$_f$); HRMS (ESI/Q-TOF) m/z: [M+H]$^+$ calculated for C$_{20}$H$_{25}$N$_2$O$_6$S$_4$ 517.0590; found 517.0596. NMR spectrum referenced to DCM which was added as an internal standard (5.49 ppm).

N,N'-(disulfanediylbis(ethane-2,1-diyl))bis(7a-methyl-5-oxohexahydropyrrolo[2,1-*b*]thiazole-3-carboxamide)
(Di-S56)
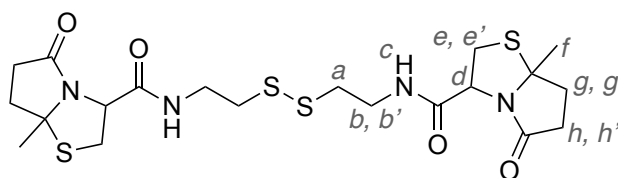
Orange solid, crude yield: 68%; ^{1}H NMR (CDCl$_3$, 400 MHz): δ 1.65 (s, 6H, H$_f$), 2.20-2.31 (m, 2H, H$_g$), 2.41-2.52 (m, 2H, H$_g$'), 2.56-2.68 (m, 2H, H$_h$), 2.73-2.85 (m, 6H, H$_a$, H$_h$'), 3.40-3.55

(m, 4H, H_b, H_e), 3.55-3.67 (m, 2H, H_b'), 3.91 (dd, 2H, J = 12.2 Hz, 7.1 Hz, H_e'), 4.76 (dd, 2H, J = 8.7 Hz, 7.1 Hz, H_d), 7.04-7.12 (br m, 2H, H_c); HRMS (ESI/Q-TOF) m/z: [M+Na]$^+$ calculated for $C_{20}H_{30}N_4O_4S_4Na$ 541.1042; found 541.1048.

N,*N'*-(disulfanediylbis(ethane-2,1-diyl))bis(5-methoxy-3-methyl-1*H*-indole-2-carboxamide)
### (Di-S57)
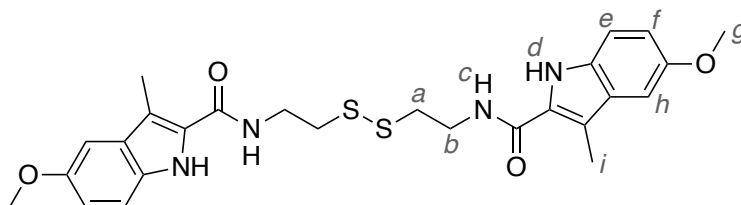
Cream solid, crude yield: 65%; ^{1}H NMR (DMSO-d_6, 400 MHz): δ 2.47 (s, 6H, H_i), 2.98 (t, 4H, J = 6.8 Hz, H_a), 3.62 (app q, 4H, J = 6.4 Hz, H_b), 3.77 (s, 6H, H_g), 6.83 (dd, 2H, J = 8.8 Hz, 2.3 Hz, H_f), 7.02 (d, 2H, J = 2.2 Hz, H_h), 7.26 (d, 2H, J = 8.8 Hz, H_e), 7.97 (t, 2H, J = 5.5 Hz, H_c), 10.99 (s, 2H, H_d); HRMS (ESI/Q-TOF) m/z: [M+H]$^+$ calculated for $C_{26}H_{31}N_4O_4S_2$ 527.1781; found 527.1784.

N,*N'*-(disulfanediylbis(ethane-2,1-diyl))bis(6-methoxy-3-methylbenzofuran-2-carboxamide)
### (Di-S58)
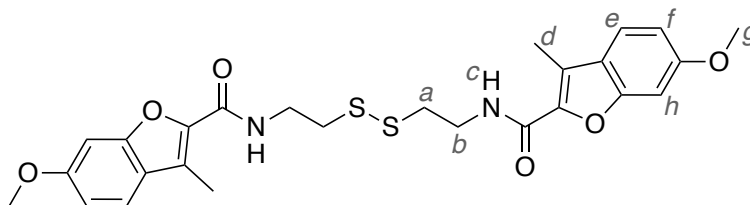
White solid, crude yield: 61%; ^{1}H NMR (CDCl$_3$, 400 MHz): δ 2.58 (s, 6H, H_d), 2.99 (t, 4H, J = 6.4 Hz, H_a), 3.79-3.88 (m, 10H, H_b, H_g), 6.88-6.94 (m, 4H, H_f, H_h), 6.95-7.03 (br m, 2H, H_c), 7.45 (d, 2H, J = 8.4 Hz, H_e); HRMS (ESI/Q-TOF) m/z: [M+H]$^+$ calculated for $C_{26}H_{29}N_2O_6S_2$ 529.1462; found 529.1465.

N,N'-(disulfanediylbis(ethane-2,1-diyl))bis(1-(methylsulfonyl)piperidine-2-carboxamide)
(Di-S60)
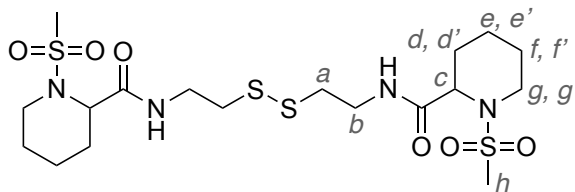
Yellow oil, crude yield: 66%; ^{1}H NMR (MeOD, 400 MHz): δ 1.40-1.63 (m, 4H, H_f, $H_{f'}$), 1.63-1.85 (m, 6H, H_d, H_e, $H_{e'}$), 2.15-2.24 (m, 2H, $H_{d'}$), 2.87 (t, 4H, J = 6.6 Hz, H_a), 2.96 (s, 6H, H_h), 3.36-3.46 (m, 2H, H_g), 3.54 (t, 4H, J = 6.6 Hz, H_b), 3.67-3.76 (m, 2H, $H_{g'}$), 4.49-4.54 (m, 2H, H_c); HRMS (ESI/Q-TOF) m/z: [M+H]$^+$ calculated for $C_{18}H_{35}N_4O_6S_4$ 531.1434; found 531.1379.

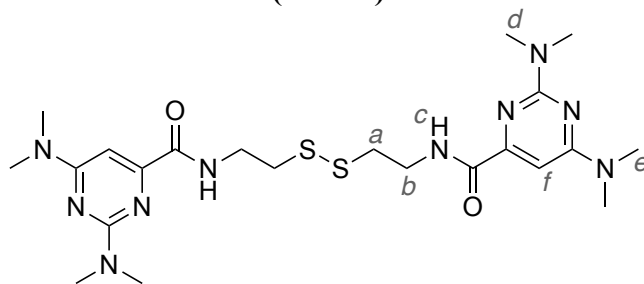**N,N'-(disulfanediylbis(ethane-2,1-diyl))bis(2,4-dichloro-5-fluorobenzamide)**
(Di-S61)
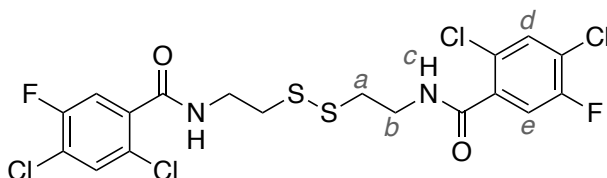
Cream solid, crude yield: 58%; ^{1}H NMR (CDCl$_3$, 400 MHz): δ 2.97 (t, 4H, J = 6.4 Hz, H_a), 3.80 (app q, 4H, J = 6.2 Hz, H_b), 6.95-7.02 (br m, 2H, H_c), 7.46 (d, 2H, J_{H-F} = 6.3 Hz, H_d), 7.47 (d, 2H, J_{H-F} = 8.9 Hz, H_e); HRMS (ESI/Q-TOF) m/z: [M+H]$^+$ calculated for $C_{18}H_{15}F_2N_2OS_2$ 532.9292; found 532.9287.

**N,N'-(disulfanediylbis(ethane-2,1-diyl))bis(2,6-dichloro-5-fluoronicotinamide)**
(Di-S62)
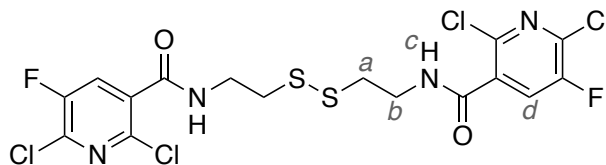
Cream solid, crude yield: 62%; ^{1}H NMR (CDCl$_3$, 400 MHz): δ 2.97 (t, 4H, J = 6.4 Hz, H_a), 3.82 (app q, 4H, J = 6.3 Hz, H_b), 7.21-7.33 (br m, 2H, H_c), 7.89 (d, 2H, J_{H-F} = 7.4 Hz, H_d); HRMS (ESI/Q-TOF) m/z: [M+H]$^+$ calculated for $C_{16}H_{13}F_2N_4OS_2$ 534.9202; found 534.9192.

_N,N'_-(disulfanediylbis(ethane-2,1-diyl))bis(2,6-bis(dimethylamino)pyrimidine-4-carboxamide)
**(Di-S63)**

Pale yellow solid, crude yield: 76%; ^{1}H NMR (CDCl$_3$, 400 MHz): δ 2.96 (t, 4H, J = 6.5 Hz, H$_a$), 3.14 (s, 24H, H$_d$, H$_e$), 3.74 (app q, 4H, J = 6.4 Hz, H$_b$), 6.72-7.02 (br s, 2H, H$_f$), 8.41-8.82 (br s, 2H, H$_c$); HRMS (ESI/Q-TOF) m/z: [M+H]$^+$ calculated for C$_{22}$H$_{37}$N$_{10}$O$_2$S$_2$ 537.2537; found 537.2553.

_N,N'_-(disulfanediylbis(ethane-2,1-diyl))bis(3_H_-benzo[_e_]indole-2-carboxamide)
(Di-S64)
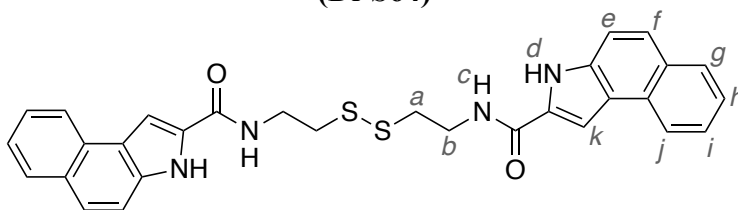
Pale brown solid, crude yield: 58%; ^{1}H NMR (DMSO-d$_6$, 400 MHz): δ 3.02 (t, 4H, J = 6.8 Hz, H$_a$), 3.65 (app q, 4H, J = 6.4 Hz, H$_b$), 7.27 (d, 2H, J = 1.7 Hz, H$_k$), 7.42-7.55 (m, 6H, H$_h$, H$_i$, H$_e$/H$_f$), 7.67 (d, 2H, J = 8.7 Hz, H$_e$/H$_f$), 7.91 (d, 2H, J = 7.9 Hz, H$_g$/H$_j$), 8.67 (t, 2H, J = 5.7 Hz, H$_c$), 8.73 (d, 2H, J = 8.1 Hz, H$_g$/H$_j$), 12.48 (s, 2H, H$_d$); HRMS (ESI/Q-TOF) m/z: [M+Na]$^+$ calculated for C$_{30}$H$_{26}$N$_4$O$_2$S$_2$Na 561.1389; found 561.1382.
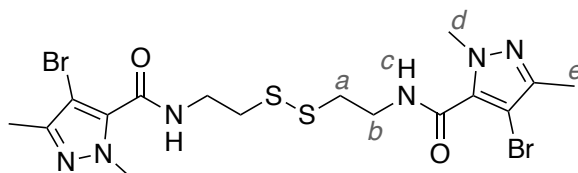
_N,N'_-(disulfanediylbis(ethane-2,1-diyl))bis(2-(pyrrolidin-1-ylmethyl)thiazole-5-carboxamide)
(Di-S65)
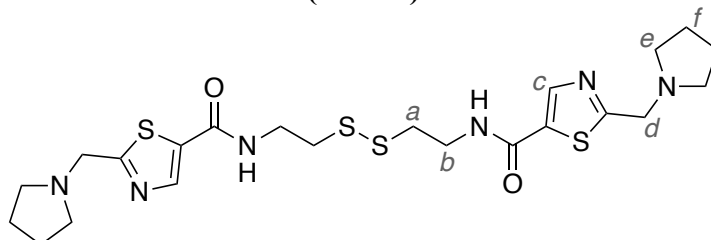
Orange solid, crude yield: 46%; ^{1}H NMR (MeOD, 400 MHz): δ 2.08-2.20 (br m, 8H, H$_f$), 2.98 (t, 4H, J = 6.8 Hz, H$_a$), 3.42-3.69 (br m, 8H, H$_e$), 2.69 (t, 4H, J = 6.8 Hz, H$_b$), 4.89 (s, 4H, H$_d$),
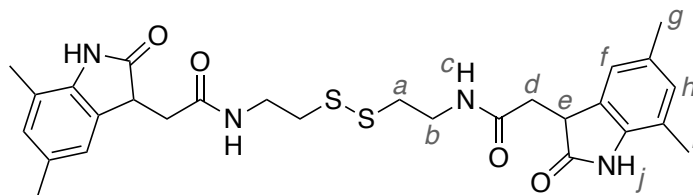
8.41 (s, 2H, H_c); HRMS (ESI/Q-TOF) m/z: $[M+H]^+$ calculated for $C_{22}H_{33}N_6O_2S_4$ 541.1542; found 541.1540.

N,N'-(disulfanediylbis(ethane-2,1-diyl))bis(4-bromo-1,3-dimethyl-1*H*-pyrazole-5-carboxamide)
### (Di-S66)

White solid, crude yield: 55%; ^{1}H NMR (CDCl$_3$, 400 MHz): δ 2.22 (s, 6H, H_e), 2.93 (t, 4H, J = 6.3 Hz, H_a), 3.79 (app q, 4H, J = 6.2 Hz, H_b), 4.08 (s, 6H, H_d), 7.05-7.15 (br m, 2H, H_c); HRMS (ESI/Q-TOF) m/z: $[M+H]^+$ calculated for $C_{16}H_{23}N_6O_2S_2$ 552.9685; found 552.9679.

N,N'-(disulfanediylbis(ethane-2,1-diyl))bis(2-(5,7-dimethyl-2-oxoindolin-3-yl)acetamide)
### (Di-S67)

Yellow solid, crude yield: 78%; ^{1}H NMR (DMSO-d$_6$, 400 MHz): δ 2.15 (s, 6H, H_g/H_i), 2.17 (d, 6H, J = 2.8 Hz, H_g/H_i), 2.51-2.56 (m, 4H, H_d), 2.77 (t, 4H, J = 6.7 Hz, H_a), 3.28-3.36 (m, 4H, H_b), 3.69 (t, 2H, J = 5.8 Hz, H_e), 6.83 (s, 2H, H_f/H_h), 6.89-6.93 (m, 2H, H_f/H_h), 8.21-8.27 (br m, 2H, H_c), 9.22 (s, 2H, H_j); HRMS (ESI/Q-TOF) m/z: $[M+H]^+$ calculated for $C_{28}H_{35}N_4O_4S_2$ 555.2094; found 555.2092.

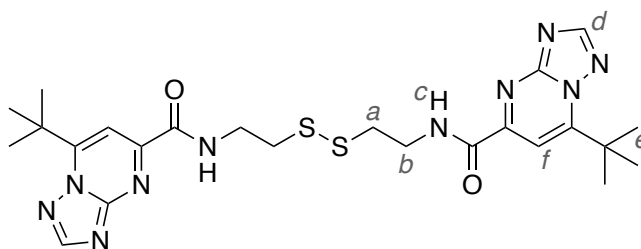### *N,N'*-(disulfanediylbis(ethane-2,1-diyl))bis(1-benzylpiperidine-2-carboxamide)
(Di-S68)
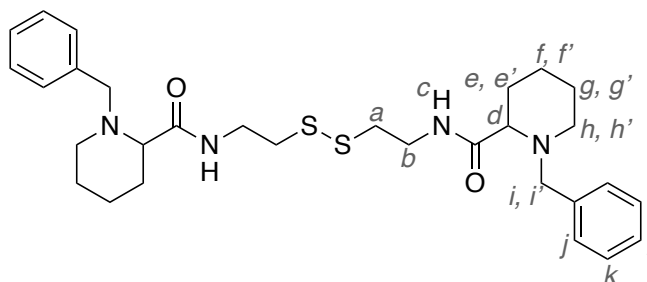
Orange oil, crude yield: 56%; ^{1}H NMR (DMSO-d$_6$, 400 MHz): δ 1.28-2.13 (m, 12H, H$_e$, H$_e$',
H$_f$, H$_f$', H$_g$, H$_g$'), 2.83-3.00 (m, 6H, H$_a$, H$_h$), 3.18-3.30 (m, 2H, H$_h$'), 3.43-3.63 (m, 4H, H$_b$),
3.66-3.81 (m, 2H, H$_d$), 4.00-4.17 (m, 2H, H$_i$), 4.24-4.38 (m, 2H, H$_i$'), 7.39-7.52 (m, 10H, H$_j$,
H$_k$, H$_l$), 8.89 (br m, 2H, H$_c$); HRMS (ESI/Q-TOF) m/z: [M+H]$^+$ calculated for C$_{30}$H$_{43}$N$_4$O$_2$S$_2$
555.2822; found 555.2767.

N,N'-(disulfanediylbis(ethane-2,1-diyl))bis(2-(3-methyl-2-oxo-3,4-dihydroquinazolin-1(2*H*)-yl)acetamide)
### (Di-S69)
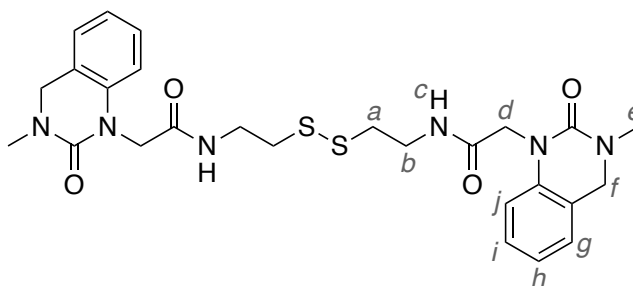
Cream solid, crude yield: 75%; ^{1}H NMR (DMSO-d$_6$, 400 MHz): δ 2.75 (t, 4H, J = 6.7 Hz, H$_a$),
2.90 (s, 6H, H$_e$), 3.31-3.40 (m, 4H, H$_b$), 4.38 (s, 4H, H$_d$), 4.41 (s, 4H, H$_f$), 6.66 (d, 2H, J = 8.4
Hz, H$_j$), 6.95 (t, 2H, J = 7.4 Hz, H$_h$), 7.10-7.22 (m, 4H, H$_g$, H$_i$), 8.20 (t, 2H, J = 5.5 Hz, H$_c$);
HRMS (ESI/Q-TOF) m/z: [M+Na]$^+$ calculated for C$_{26}$H$_{32}$N$_6$O$_4$S$_2$Na 579.1819; found
579.1815.

N,N'-(disulfanediylbis(ethane-2,1-diyl))bis(7-(tert-butyl)-[1,2,4]triazolo[1,5-*a*]pyrimidine-5-carboxamide)
### (Di-S71)

Cream solid, crude yield: 78%; ^{1}H NMR (CDCl$_3$, 400 MHz): δ 1.62 (s, 18H, H$_e$), 2.98 (t, 4H,
J = 6.5 Hz, H$_a$), 3.84 (app q, 4H, J = 6.4 Hz, H$_b$), 7.86 (s, 2H, H$_f$), 8.51 (t, 2H, J = 6.0 Hz, H$_c$),
8.59 (s, 2H, H$_d$); HRMS (ESI/Q-TOF) m/z: [M+H]$^+$ calculated for C$_{24}$H$_{33}$N$_{10}$O$_2$S$_2$ 557.2224;
found 557.2223.

N,N'-(disulfanediylbis(ethane-2,1-diyl))bis(2-(6-methyl-3-oxo-2,3-dihydro-4H-benzo[b][1,4]oxazin-4-yl)acetamide)
**(Di-S72)**
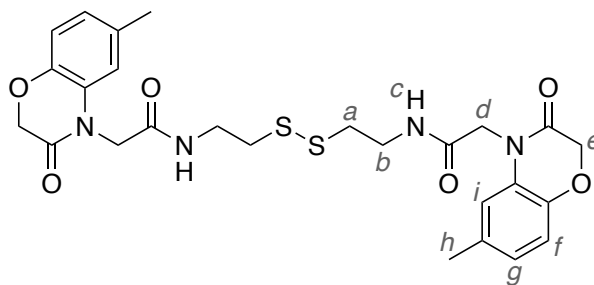
White solid, crude yield: 73%; ^{1}H NMR (DMSO-d$_6$, 400 MHz): δ 2.23 (s, 6H, H$_h$), 2.79 (t, 4H, J = 6.6 Hz, H$_a$), 3.38 (app q, 4H, J = 6.3 Hz, H$_b$), 4.46 (s, 4H, H$_d$), 4.63 (s, 4H, H$_e$), 6.73 (s, 2H, H$_i$), 6.79 (d, 2H, J = 8.1 Hz, H$_g$), 6.88 (d, 2H, J = 8.1 Hz, H$_f$), 8.36 (t, 2H, J = 5.6 Hz, H$_c$); HRMS (ESI/Q-TOF) m/z: [M+H]$^+$ calculated for C$_{26}$H$_{31}$N$_4$O$_6$S$_2$ 559.1680; found 559.1673.

N,N'-(disulfanediylbis(ethane-2,1-diyl))bis(9-hydroxy-9H-fluorene-9-carboxamide)
(Di-S73)
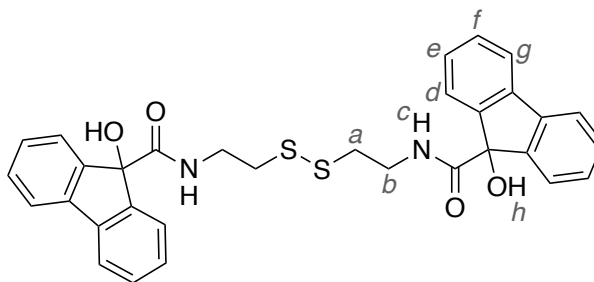
Cream solid, crude yield: 56%; ^{1}H NMR (CDCl$_3$, 400 MHz): δ 2.51 (t, 4H, J = 6.4 Hz, H$_a$), 3.34 (app q, 4H, J = 6.3 Hz, H$_b$), 4.67 (br s, 2H, H$_h$), 5.76-5.85 (br m, 2H, H$_c$), 7.30 (t, 4H, J = 7.5 Hz, H$_e$/H$_f$), 7.37-7.46 (m, 8H, H$_d$/H$_e$/H$_f$/H$_g$), 7.66 (d, 4H, J = 7.3 Hz, H$_d$/H$_g$); HRMS (ESI/Q-TOF) m/z: [M+H]$^+$ calculated for C$_{32}$H$_{29}$N$_2$O$_4$S$_2$ 569.1563; found 569.1568.
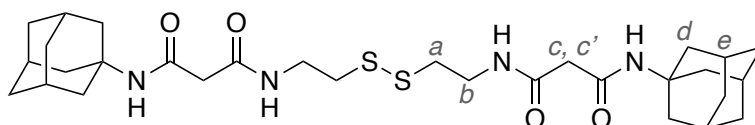
N,N'-(disulfanediylbis(ethane-2,1-diyl))bis(3-((4-chloro-1H-pyrazol-1-yl)methyl)benzamide)
(Di-S74)
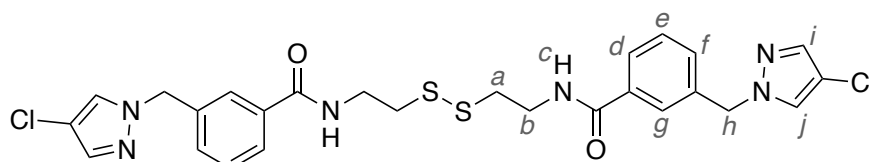
Cream solid, crude yield: 74%; ^{1}H NMR (CDCl$_3$, 400 MHz): δ 2.96 (t, 4H, J = 6.4 Hz, H$_a$), 3.77 (app q, 4H, J = 6.2 Hz, H$_b$), 5.23 (s, 4H, H$_h$), 7.12 (t, 2H, J = 5.5 Hz, H$_c$), 7.32 (d, 2H, J =

7.7 Hz, H_f), 7.25 (s, 2H, H_i/H_j), 7.38 (t, 2H, J = 7.7 Hz, H_e), 7.42 (s, 2H, H_i/H_j), 7.72 (s, 2H, H_g), 7.75 (d, 2H, J = 7.7 Hz, H_d); HRMS (ESI/Q-TOF) m/z: $[M+H]^+$ calculated for $C_{26}H_{27}N_6OS_2$ 589.1005; found 589.1008.

$N^1,N^{1'}$-(disulfanediylbis(ethane-2,1-diyl))bis(N^3-((3s,5s,7s)-adamantan-1-yl)malonamide)
### (Di-S75)

Cream solid, crude yield: 56%; ¹H NMR (MeOD, 400 MHz): δ 1.67-1.75 (m, 12H, H_f), 1.97-2.11 (m, 18H, H_d, H_e), 2.84 (t, 4H, J = 6.7 Hz, H_a), 3.10 (s, 2H, H_c), 3.12 (s, 2H, $H_{c'}$), 3.52 (t, 4H, J = 6.7 Hz, H_b); HRMS (ESI/Q-TOF) m/z: $[M+H]^+$ calculated for $C_{30}H_{47}N_4O_4S_2$ 591.3033; found 591.3020.

N,N'-(disulfanediylbis(ethane-2,1-diyl))bis(2-(3-hydroxy-2,5-dioxo-1-phenylpyrrolidin-3-yl)acetamide)
(Di-S76)
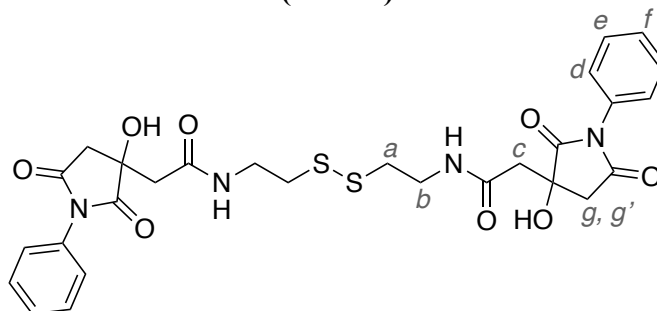
Orange solid, crude yield: 61%; ¹H NMR (MeOD, 400 MHz): δ 2.70-3.21 (m, 12H, H_a, H_c, H_g, $H_{g'}$), 3.40-3.58 (m, 4H, H_b), 7.30 (d, 4H, J = 7.4 Hz, H_d), 7.38-7.44 (m, 2H, H_f), 7.44-7.51 (m, 4H, H_e); HRMS (ESI/Q-TOF) m/z: $[M+H]^+$ calculated for $C_{28}H_{31}N_4O_8S_2$ 615.1578; found 615.1508.

N,N'-(((((disulfanediylbis(ethane-2,1-diyl))bis(azanediyl))bis(carbonyl))bis(6-methyl-3,1-phenylene))bis(tetrahydrofuran-2-carboxamide)
(Di-S77)
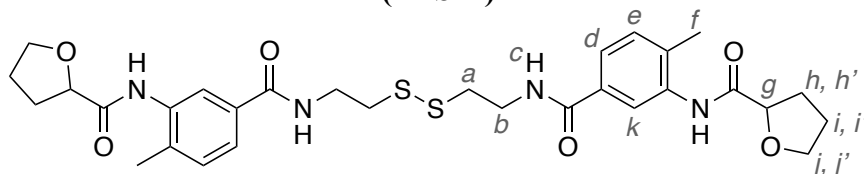
Orange oil, crude yield: 58%; ^{1}H NMR (MeOD, 400 MHz): δ 1.92-2.03 (m, 4H, H_i, H_i'), 2.05-2.17 (m, 2H, H_h), 2.24-2.40 (m, 8H, H_f, H_h'), 2.96 (t, 4H, J = 6.8 Hz, H_a), 3.63-3.71 (m, 4H, H_b), 3.90-3.98 (m, 2H, H_j), 4.07-4.15 (m, 2H, H_j'), 4.47 (dd, 2H, J = 8.2 Hz, 5.8 Hz, H_g), 7.32 (d, 2H, J = 8.0 Hz, H_e), 7.60 (dd, 2H, J = 8.0 Hz, 1.7 Hz, H_d), 7.92 (d, 2H, J = 1.7 Hz, H_k), 8.61 (t, 2H, J = 5.4 Hz, H_c); HRMS (ESI/Q-TOF) m/z: [M+H]$^+$ calculated for $C_{30}H_{39}N_4O_6S_2$ 615.2306; found 615.2237.

N,N'-(disulfanediylbis(ethane-2,1-diyl))bis(3-(2,6,6-trimethyl-4-oxo-4,5,6,7-tetrahydro-1*H*-indol-1-yl)propanamide)
(Di-S78)
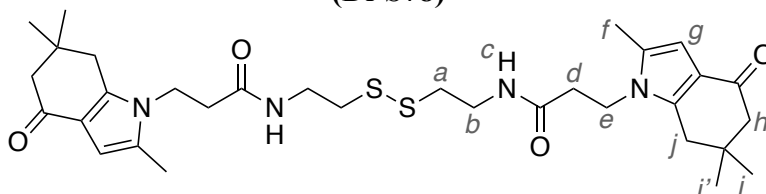
Orange solid, crude yield: 67%; ^{1}H NMR (CDCl$_3$, 400 MHz): δ 1.06 (s, 12H, H_i, H_i'), 2.19 (s, 6H, H_f), 2.22 (s, 4H, H_h/H_j), 2.56 (t, 4H, J = 7.0 Hz, H_d), 2.60 (s, 4H, H_h/H_j), 2.67 (t, 4H, J = 6.5 Hz, H_a), 3.43 (app q, 4H, J = 6.3 Hz, H_b), 4.09 (t, 4H, J = 7.0 Hz, H_e), 6.09 (s, 2H, H_g), 7.15 (t, 2H, J = 5.9 Hz, H_c); HRMS (ESI/Q-TOF) m/z: [M+H]$^+$ calculated for $C_{32}H_{47}N_4O_4S_2$ 615.3033; found 615.3047.

(2*S*,2'*S*)-*N,N*'-(disulfanediylbis(ethane-2,1-diyl))bis(2-amino-3-(5-bromothiophen-2-yl)propanamide)
(Di-S79)

The amine group of the carboxylic acid starting material was Boc-protected. Obtained an orange oil, crude yield: 44%; ^{1}H NMR (MeOD, 400 MHz): δ 2.81 (t, 4H, J = 6.7 Hz, H_a), 3.25-3.65 (m, 8H, H_b, H_b', H_d, H_d'), 4.13 (t, 2H, J = 6.8 Hz, H_c), 6.83 (d, 2H, J = 3.7 Hz, H_e), 7.00 (d, 2H, J = 3.7 Hz, H_f); HRMS (ESI/Q-TOF) m/z: [M+H]$^+$ calculated for $C_{18}H_{25}N_4O_2S_4$ 614.9222; found 614.9151.

N,N'-(disulfanediylbis(ethane-2,1-diyl))bis(2-fluoro-4-iodonicotinamide)
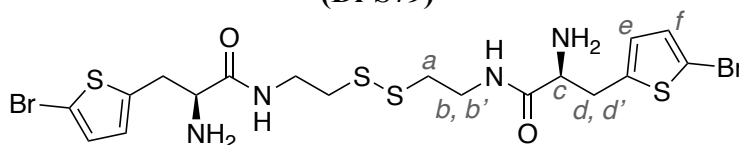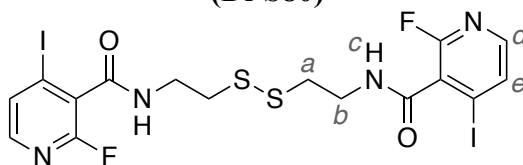**(Di-S80)**

Yellow solid, crude yield: 58%; ^{1}H NMR (MeOD, 400 MHz): δ 3.02 (t, 4H, J = 6.7 Hz, H$_a$), 3.70-3.77 (m, 4H, H$_b$), 7.82 (d, 2H, J = 5.3 Hz, H$_d$/H$_e$), 7.90 (d, 2H, J = 5.3 Hz, H$_d$/H$_e$), 8.99-9.09 (br m, 2H, H$_c$); HRMS (ESI/Q-TOF) m/z: [M+H]$^+$ calculated for C$_{16}$H$_{15}$F$_2$I$_2$N$_4$O$_2$S$_2$ 650.8688; found 650.8689.

N,N'-(disulfanediylbis(ethane-2,1-diyl))bis(1-(4-(trifluoromethyl)phenyl)piperidine-4-carboxamide)
**(Di-S81)**
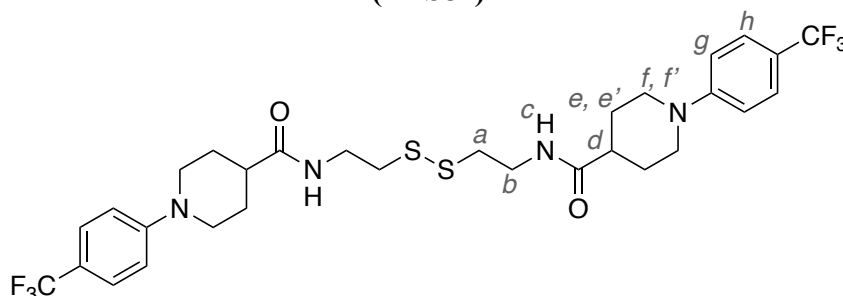
Cream solid, crude yield: 65%; ^{1}H NMR (CDCl$_3$, 400 MHz): δ 1.87-2.13 (m, 8H, H$_e$, H$_e$'), 2.41-2.56 (m, 2H, H$_d$), 2.86 (t, 4H, J = 6.4 Hz, H$_a$), 2.89-3.94 (m, 4H, H$_f$), 3.60 (app q, 4H, J = 6.3 Hz, H$_b$), 3.76-3.90 (m, 4H, H$_f$'), 6.45-6.72 (br m, 2H, H$_c$), 6.91-7.20 (br m, 4H, H$_g$), 7.50 (d, 4H, J = 8.5 Hz, H$_h$); HRMS (ESI/Q-TOF) m/z: [M+H]$^+$ calculated for C$_{30}$H$_{37}$F$_6$N$_4$O$_2$S$_2$ 663.2257; found 663.2259.

N,N'-(disulfanediylbis(ethane-2,1-diyl))bis(5-(1-methyl-3-(trifluoromethyl)-1H-pyrazol-5-yl)thiophene-2-carboxamide)
(Di-S82)
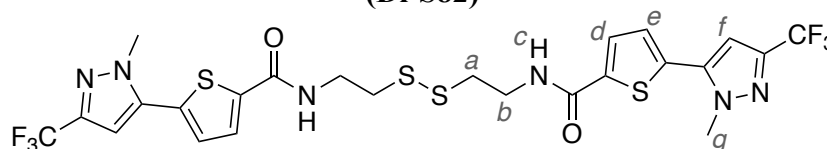
Cream solid, crude yield: 72%; ^{1}H NMR (CDCl$_3$, 400 MHz): δ 3.01 (t, 4H, J = 6.4 Hz, H$_a$), 3.81 (app q, 4H, J = 6.3 Hz, H$_b$), 4.03 (s, 6H, H$_g$), 6.67 (s, 2H, H$_f$), 7.00 (t, 2H, J = 5.8 Hz, H$_c$), 7.18 (d, 2H, J = 3.9 Hz, H$_d$/H$_e$), 7.66 (d, 2H, J = 3.9 Hz, H$_d$/H$_e$); HRMS (ESI/Q-TOF) m/z: [M+H]$^+$ calculated for C$_{24}$H$_{23}$F$_6$N$_6$O$_2$S$_4$ 669.0664; found 669.0660.

***N,N'*-(disulfanediylbis(ethane-2,1-diyl))bis(2-(3-methyl-5-(trifluoromethyl)-1*H*-pyrazol-1-yl)thiazole-4-carboxamide)**
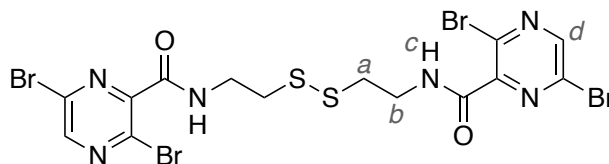**(Di-S83)**
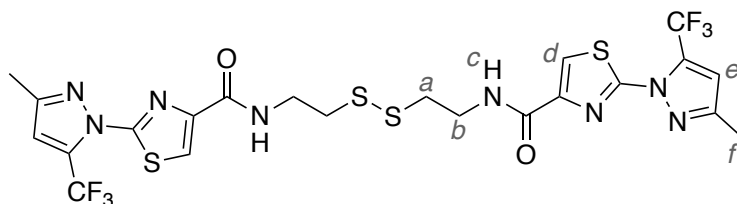
Cream solid, crude yield: 73%; ^{1}H NMR (CDCl$_3$, 400 MHz): δ 2.35 (s, 6H, H$_f$), 2.93 (t, 4H, J = 6.4 Hz, H$_a$), 3.79 (app q, 4H, J = 6.3 Hz, H$_b$), 6.68 (s, 2H, H$_e$), 7.50 (t, 2H, J = 5.8 Hz, H$_c$), 7.90 (s, 2H, H$_d$); HRMS (ESI/Q-TOF) m/z: [M+H]$^+$ calculated for C$_{22}$H$_{21}$F$_6$N$_8$O$_2$S$_4$ 671.0569; found 671.0565.

***N,N'*-(disulfanediylbis(ethane-2,1-diyl))bis(3,6-dibromopyrazine-2-carboxamide)**
(Di-S84)

White solid, crude yield: 55%; ^{1}H NMR (CDCl$_3$, 400 MHz): δ 3.00 (t, 4H, J = 6.5 Hz, H$_a$), 3.82 (app q, 4H, J = 6.3 Hz, H$_b$), 7.84-7.92 (br m, 2H, H$_c$), 8.57 (s, 2H, H$_d$); HRMS (ESI/Q-TOF) m/z: [M+H]$^+$ calculated for C$_{14}$H$_{13}$N$_6$O$_2$S$_2$ 676.7269; found 676.7262.

Oxidation of βME for obtaining covalent protein-βME adducts

<div align="center">

2,2'-disulfanediylbis(ethan-1-ol)

(Oxidized βME)

</div>

HO⌒⌒S-S⌒⌒OH
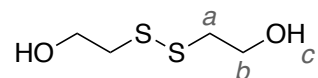
β-mercaptoethanol (684 mg, 8.75 mmol) and hydrogen peroxide (827 μL of a 30% w/w stock, 8.75 mmol) were added sequentially to sodium iodide (13.5 mg, 0.09 mmol, 1 mol%) in EtOAc (10 mL). The reaction mixture was stirred for 10 min before quenching with 1:1 saturated aqueous sodium thiosulfate:water (10 mL). The product was extracted with EtOAc (3 x 50 mL) and the combined organic layers were washed with 1:1 brine:saturated aqueous sodium thiosulfate (15 mL), dried over $MgSO_4$, and concentrated under reduced pressure to afford a colorless oil (542 mg, 3.5 mmol, 80%). R_f: 0.14 (7:3 EtOAc:hexane); ^{1}H NMR ($CDCl_3$, 500 MHz): δ 2.60 (br s, 2H, H_c,), 2.87 (t, 4H, $J = 5.8$ Hz, H_a,), 3.86-3.93 (m, 4H, H_b,); ^{13}C NMR ($CDCl_3$, 125 MHz): δ 41.4, 60.5.

References

(1)   Kozakov, D.; Grove, L. E.; Hall, D. R.; Bohnuud, T.; Mottarella, S. E.; Luo, L.; Xia, B.; Beglov, D.; Vajda, S. The FTMap family of web servers for determining and characterizing ligand-binding hot spots of proteins. *Nat. Protoc.* **2015**, *10*, 733–755.

(2)   Eichner, T.; Kalverda, A. P.; Thompson, G. S.; Homans, S. W.; Radford, S. E. Conformational conversion during amyloid formation at atomic resolution. *Mol. Cell* **2011**, *41*, 161–172.

(3)   Schuck, P. Size-distribution analysis of macromolecules by sedimentation velocity ultracentrifugation and Lamm equation modeling. *Biophys. J.* **2000**, *78*, 1606–1619.

(4)   Schuck, P.; Zhao, H. *Sedimentation Velocity Analytical Ultracentrifugation: Interacting Systems*; CRC Press: Boca Raton, 2018.

(5)   Rezaei Araghi, R.; Bird, G. H.; Ryan, J. A.; Jenson, J. M.; Godes, M.; Pritz, J. R.; Grant, R. A.; Letai, A.; Walensky, L. D.; Keating, A. E. Iterative optimization yields Mcl-1–targeting stapled peptides with selective cytotoxicity to Mcl-1–dependent cancer cells. *Proc. Natl. Acad. Sci. U. S. A.* **2018**, *115*, E886–E895.

(6)   Jurrus, E.; Engel, D.; Star, K.; Monson, K.; Brandi, J.; Felberg, L. E.; Brookes, D. H.; Wilson, L.; Chen, J.; Liles, K.; Chun, M.; Li, P.; Gohara, D. W.; Dolinsky, T.; Konecny, R.; Koes, D. R.; Nielsen, J. E.; Head-Gordon, T.; Geng, W.; Krasny, R.; Wei, G.-W.; Holst, M. J.; McCammon, J. A.; Baker, N. A. Improvements to the APBS biomolecular solvation software suite. *Protein Sci.* **2018**, *27*, 112–128.

(7)   Brown, P. H.; Balbo, A.; Schuck, P. Using prior knowledge in the determination of macromolecular size-distributions by analytical ultracentrifugation. *Biomacromolecules* **2007**, *8*, 2011–2024.

(8)   Karamanos, T. K.; Jackson, M. P.; Calabrese, A. N.; Goodchild, S. C.; Cawood, E. E.; Thompson, G. S.; Kalverda, A. P.; Hewitt, E. W.; Radford, S. E. Structural mapping of oligomeric intermediates in an amyloid assembly pathway. *Elife* **2019**, *8*, e46574.

(9)   Jubb, H. C.; Higueruelo, A. P.; Ochoa-Montaño, B.; Pitt, W. R.; Ascher, D. B.; Blundell, T. L. Arpeggio: a web server for calculating and visualising interatomic interactions in protein structures. *J. Mol. Biol.* **2017**, *429*, 365–371.

(10)   Eakin, C. M.; Berman, A. J.; Miranker, A. D. A native to amyloidogenic transition regulated by a backbone trigger. *Nat. Struct. Mol. Biol.* **2006**, *13*, 202–208.

(11)   Smith, D. P.; Radford, S. E. Role of the single disulphide bond of β2-microglobulin in amyloidosis in vitro. *Protein Sci.* **2001**, *10*, 1775–1784.

(12)   Kozakov, D.; Hall, D. R.; Napoleon, R. L.; Yueh, C.; Whitty, A.; Vajda, S. New frontiers in druggability. *J. Med. Chem.* **2015**, *58*, 9063–9088.

(13)   Sterling, T.; Irwin, J. J. ZINC 15 – ligand discovery for everyone. *J. Chem. Inf. Model.* **2015**, *55*, 2324–2337.

(14) Duan, J.; Dixon, S. L.; Lowrie, J. F.; Sherman, W. Analysis and comparison of 2D fingerprints: insights into database screening performance using eight fingerprint methods. *J. Mol. Graph. Model.* **2010**, *29*, 157–170.

(15) Bajusz, D.; Rácz, A.; Héberger, K. Why is Tanimoto index an appropriate choice for fingerprint-based similarity calculations? *J. Cheminform.* **2015**, *7*, 20.

(16) Toledo Warshaviak, D.; Golan, G.; Borelli, K. W.; Zhu, K.; Kalid, O. A structure-based virtual screening approach for discovery of covalently bound ligands. *J. Chem. Inf. Model.* **2014**, *54*, 1941–1950.

(17) Friesner, R. A.; Banks, J. L.; Murphy, R. B.; Halgren, T. A.; Klicic, J. J.; Mainz, D. T.; Repasky, M. P.; Knoll, E. H.; Shelley, M.; Perry, J. K.; Shaw, D. E.; Francis, P.; Shenkin, P. S. Glide: a new approach for rapid, accurate docking and scoring. 1. Method and assessment of docking accuracy. *J. Med. Chem.* **2004**, *47*, 1739–1749.

(18) Halgren, T. A.; Murphy, R. B.; Friesner, R. A.; Beard, H. S.; Frye, L. L.; Pollard, W. T.; Banks, J. L. Glide: a new approach for rapid, accurate docking and scoring. 2. Enrichment factors in database screening. *J. Med. Chem.* **2004**, *47*, 1750–1759.

(19) Kaiser, E.; Colescott, R. L.; Bossinger, C. D.; Cook, P. I. Color test for detection of free terminal amino groups in the solid-phase synthesis of peptides. *Anal. Biochem.* **1970**, *32*, 595–598.

(20) Smith, P. K.; Krohn, R. I.; Hermanson, G. T.; Mallia, A. K.; Gartner, F. H.; Provenzano, M. D.; Fujimoto, E. K.; Goeke, N. M.; Olson, B. J.; Klenk, D. C. Measurement of protein using bicinchroninic acid. *Anal. Biochem.* **1985**, *150*, 76–85.